UCRL-ID- 127718

ISLAY
Containment Data Report

T. Stubbs

R. Heinle

June, 1997

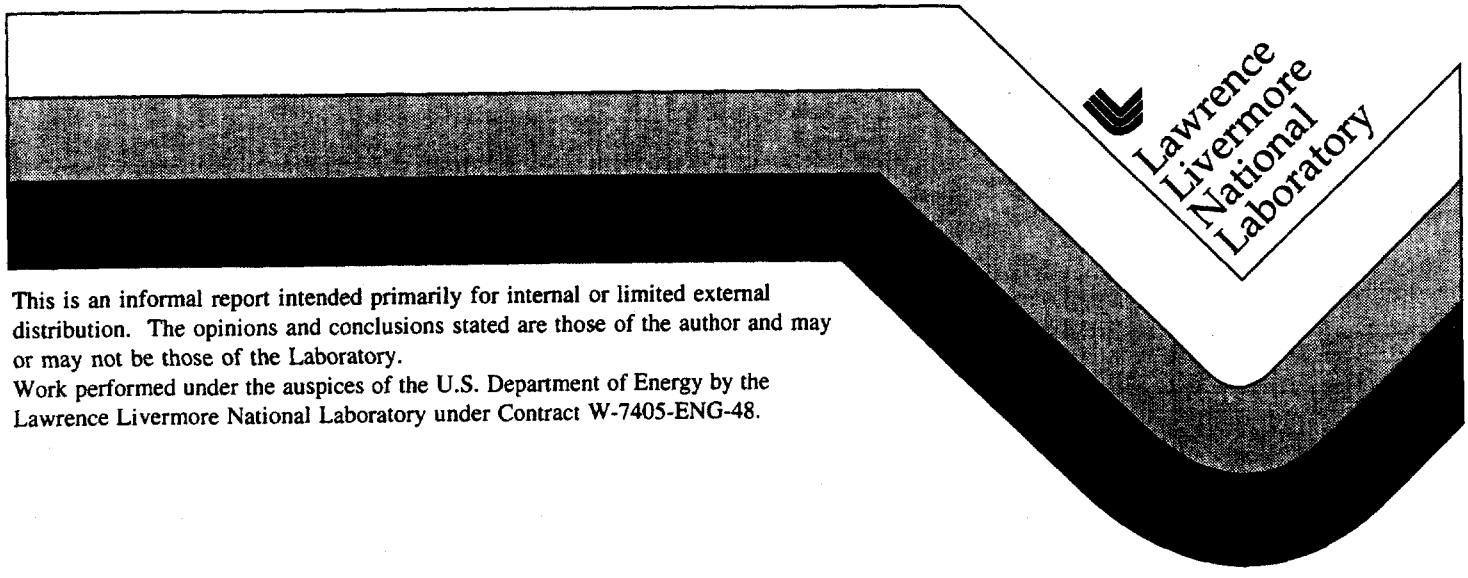

ISLAY Instrumentation Summary

Instrumentation	Fielded on this Event	Data Return	Present in this Report
Plug Emplacement	yes	yes	yes[a]
Radiation	yes	yes	yes
Pressure			
Stemming	yes	yes	yes
Challenge	no	-	-
Cavity	no	-	-
Atmospheric	no	-	-
Motion			
Free Field	no	-	-
Surface	yes	yes	yes
Plug	yes	yes	yes
Stemming	no	-	-
Surface Casing	no	-	-
Emplacement Pipe	yes	yes	yes
Hydroyield[b]	yes	yes	no
Collapse [c]	yes	yes	yes
Stress	no	-	-
Strain[d]	yes	yes	no
Other Measurements[e]	yes	yes	yes

(a) Description only.
(b) SLIFER or CORRTEX data; see reference 3.
(c) EXCOR or CLIPER in emplacement hole.
(d) Strain load on emplacement pipe, recorded on LSI-11 and not available.
(e) Internal emplacement pipe temperature and pressure.

Event Personnel

Containment Physics	
B. Hudson	LLNL
C. Olsen	LLNL
J. Kalinowski	EG&G/AVO
T. Stubbs	EG&G/AVO

Instrumentation	
L. Starrh	LLNL
M. Hatch	EG&G/AVO
L. Davies	EG&G/NVO
A. Moeller	EG&G/NVO

Contents

1. Event Description

1.1 Site

The ISLAY event was detonated in hole U2er of the Nevada Test Site as indicated in figure 1.1. The ISLAY device had a depth-of-burial (DOB) of 294 m in the Tunnel Beds Tuffs of area 2, about 160 m above the Paleozoic formation and 280 m above the standing water level, as shown in the geologic cross-sections of figures 1.2 and 1.3[1]. Stemming of the 2.44 m diameter emplacement hole followed the plan shown in figure 1.4. A log of the stemming operations was maintained by Holmes & Narver[2].

Detonation time was 07:31 PST on November 11 ,1981, and collapse progressed to the surface at about 70 minutes after the detonation resulting in a crater having a mean radius of 50.9 m and a maximum depth of 8.5 m.

No radiation arrivals were detected above ground and the ISLAY containment was considered successful.

1.2. Emplacement

There were four stemming plugs above the ISLAY event, each composed of rigid two-part- epoxy (TPE). The first (bottom) and third plugs were 3.3 m thick and the second plug was 6.86 m thick. Thickness of the top plug TPE was 5.2 m, about 3.1 m of which extended below the surface casing. Each of these plugs was overlain with a 1.8 m thick layer of soft "coal-tar epoxy" to act as a gas seal. A drag ring system was mounted to the emplacement pipe at the position of the second rigid plug and the emplacement pipe in the regions of the upper two plugs was coated with hydroseal to allow free motion of the pipe through these plugs. Stemming between the plugs consisted of layers of fines and coarse gravel. The top of the hole (above the top plug) was filled with surface-derived backfill to about 2.2 m below the ground level. See figure 1.4.

ISLAY included a mechanical PINEX experiment as part of the device diagnostics and, for this, the emplacement pipe was left open above the detector plate which was extracted to a receptacle above the ball valve closure on the top of the pipe. This receptacle was detached from the pipe shortly after the detonation and pulled to a location beyond the expected extent of the resulting crater. Below the detector plate, the pipe was sealed with a series of pressure domes.

1.3 Instrumentation

Figure 1.5 is a schematic layout of the instrumentation designed to monitor the containment performance of the ISLAY event.

Nine stations were fielded in the stemming to monitor pressure and radiation. The stemming region about 5 m beneath each of the four plugs contained pressure and radiation stations as well as the region about 8 m above each of the plugs except the top. Two additional elevations in the coarse stemming above and below the fines layer between the bottom and second plugs were also monitored for pressure and radiation.

The internal gas pressure and temperature of four of the five sealed sections of the emplacement pipe was monitored just below the corresponding pressure dome defining the section. Motion of the emplacement pipe was monitored at each of the four pressure and temperature stations, at the elevation of the deepest pressure dome, at the location of the neutron detector plate (defining the fifth sealed section) and near the top of the pipe below the ball valve. An additional station monitored pressure and radiation internal to the pipe near its top at a depth of about 15 m.

Standard LLNL vertical motion canisters, containing variable reluctance velocity and acceleration transducers, were emplaced in all four of the rigid stemming plugs and the ground surface, 15.24 m from SGZ. The recording trailer was instrumented with one vertical accelerometer.

Data from each of the above instruments were transmitted to the recording trailer by an analog system and recorded on magnetic tape.

Two CLIPER sensors, one attached to the instrumentation pendant and the other attached to the emplacement pipe and diagnostic canister were fielded to monitor cavity collapse and chimney formation.

Two "D-cable" systems were fielded to monitor the stemming emplacement and were recorded post-shot to sense collapse.

Strain (load) was monitored at a station on the emplacement pipe near its top. These data were recorded pre-shot on an LSI-11 computer and are not now available.

Results of the hydrodynamic yield measurements are reported elsewhere[3]

A history of the fielding operations of the instrumentation is outlined in reference 4. Further details of the instrumentation are given in reference 5.

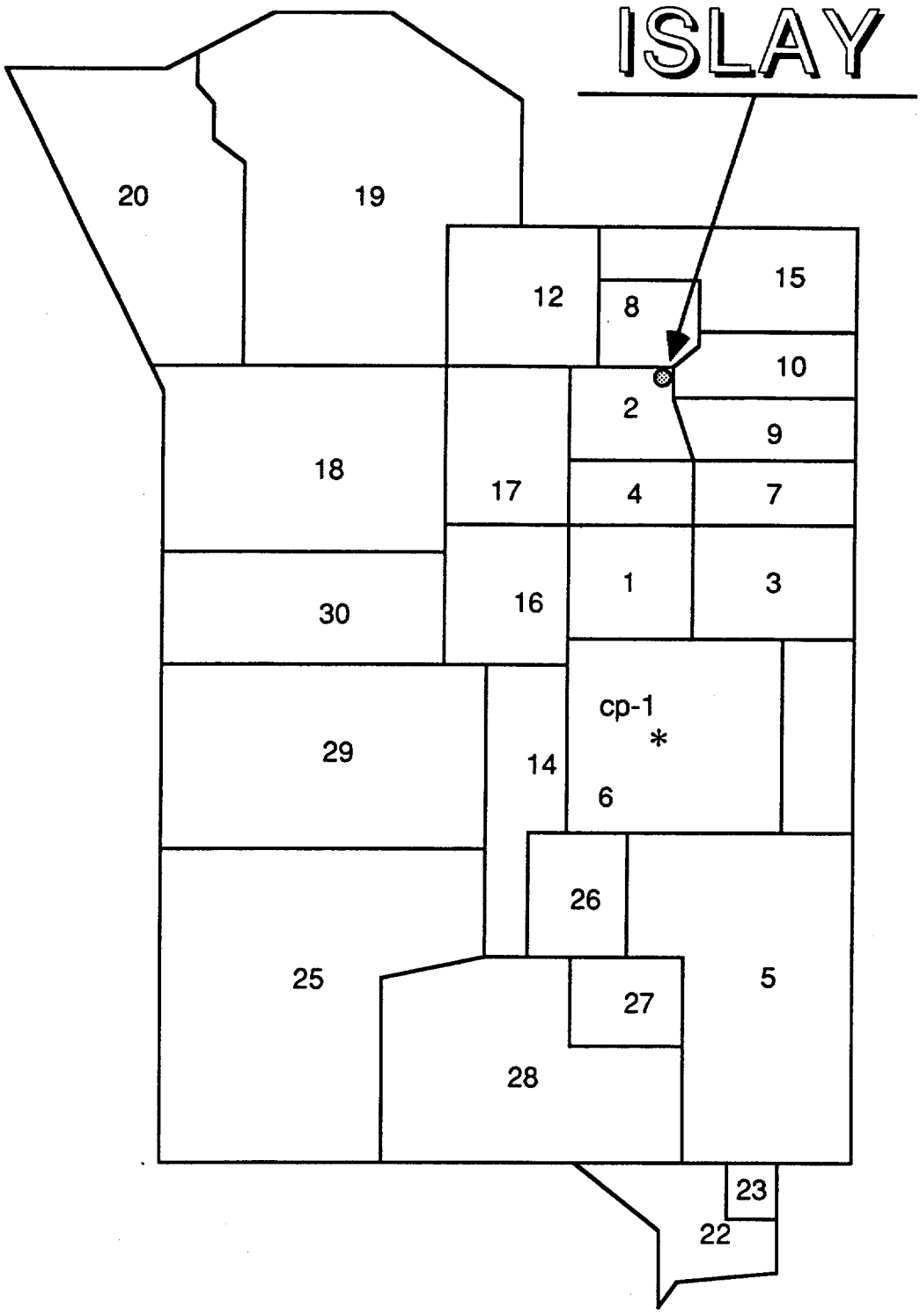

Figure 1.1 Map of the Nevada Test Site indicating the location of hole U2er.

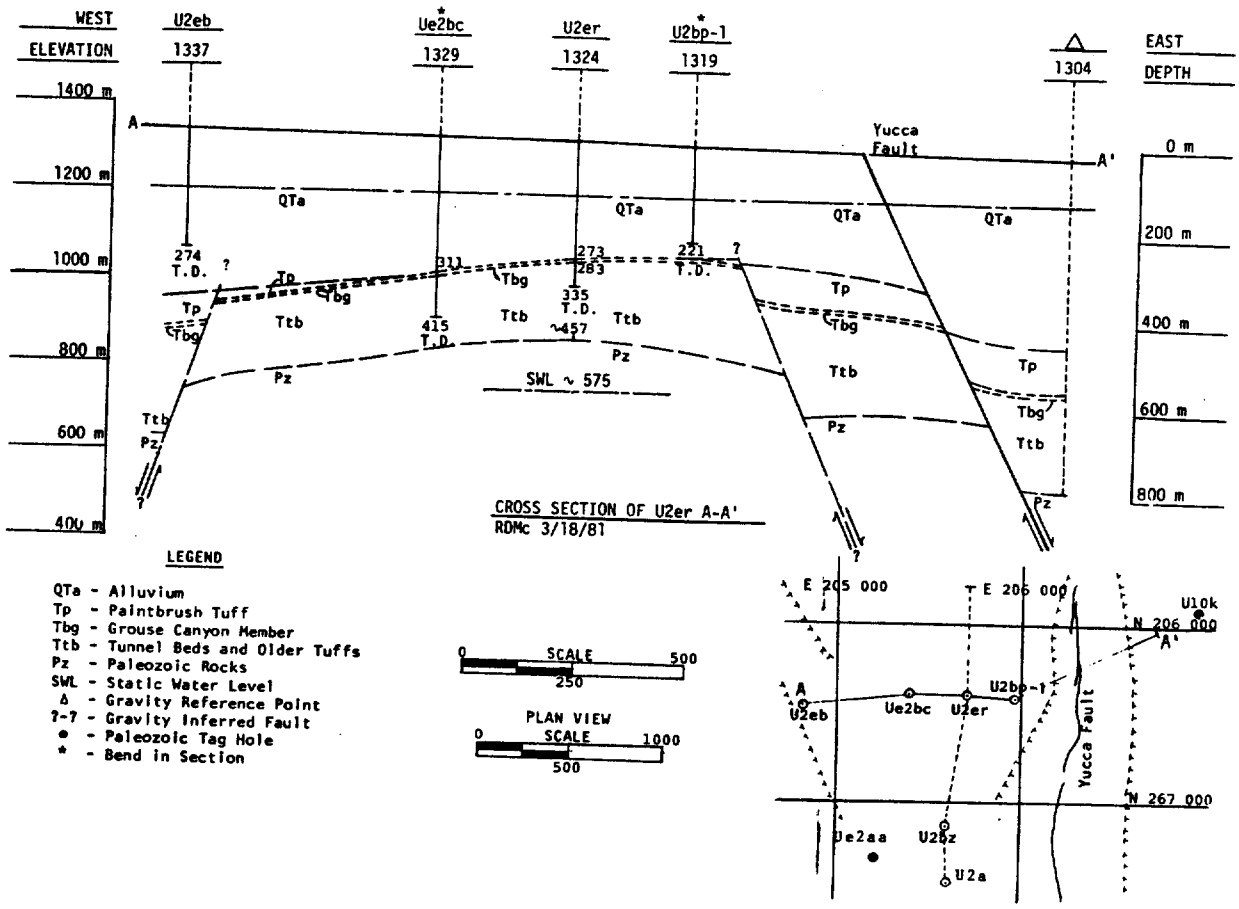

Figure 1.2 East-West geologic cross section through hole U2er.

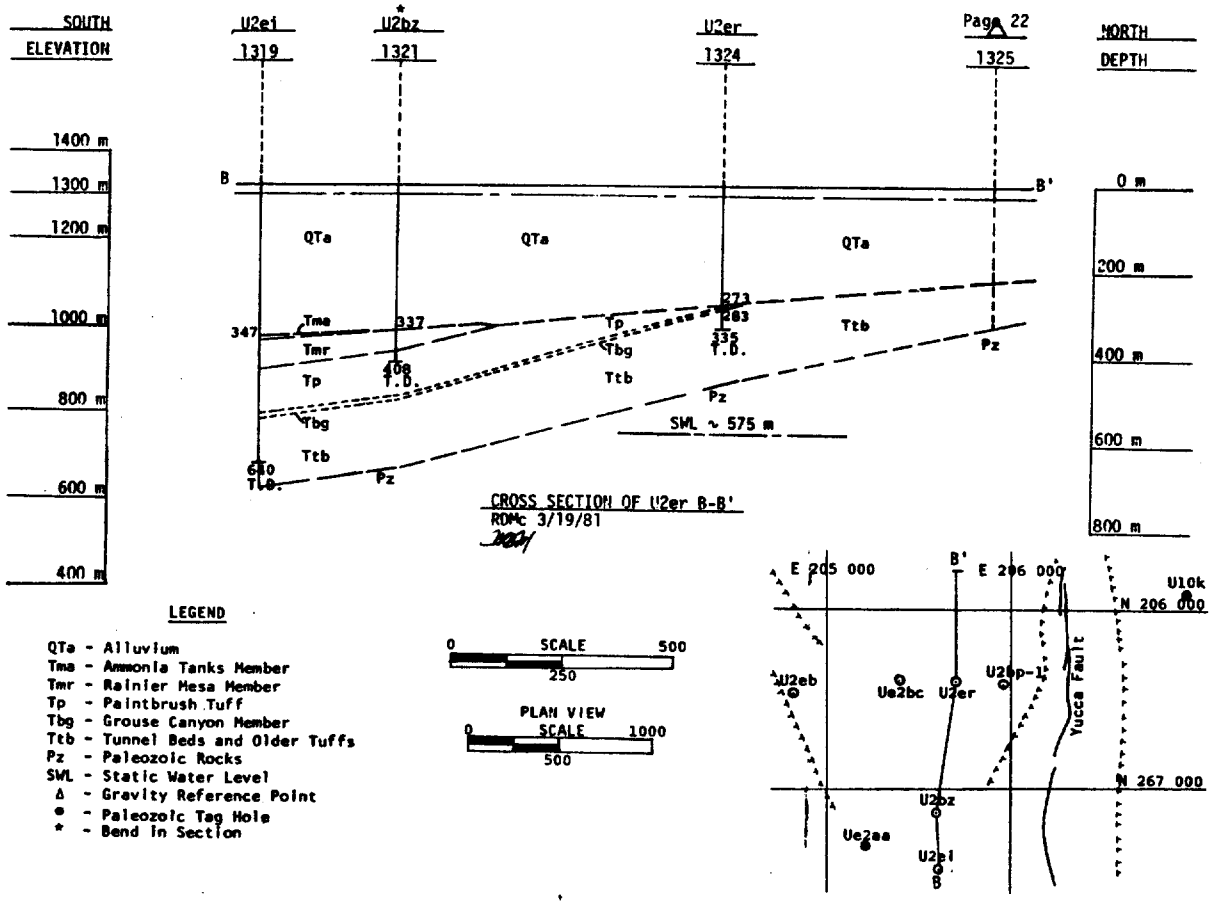

Figure 1.3 North-South geologic cross section through hole U2er.

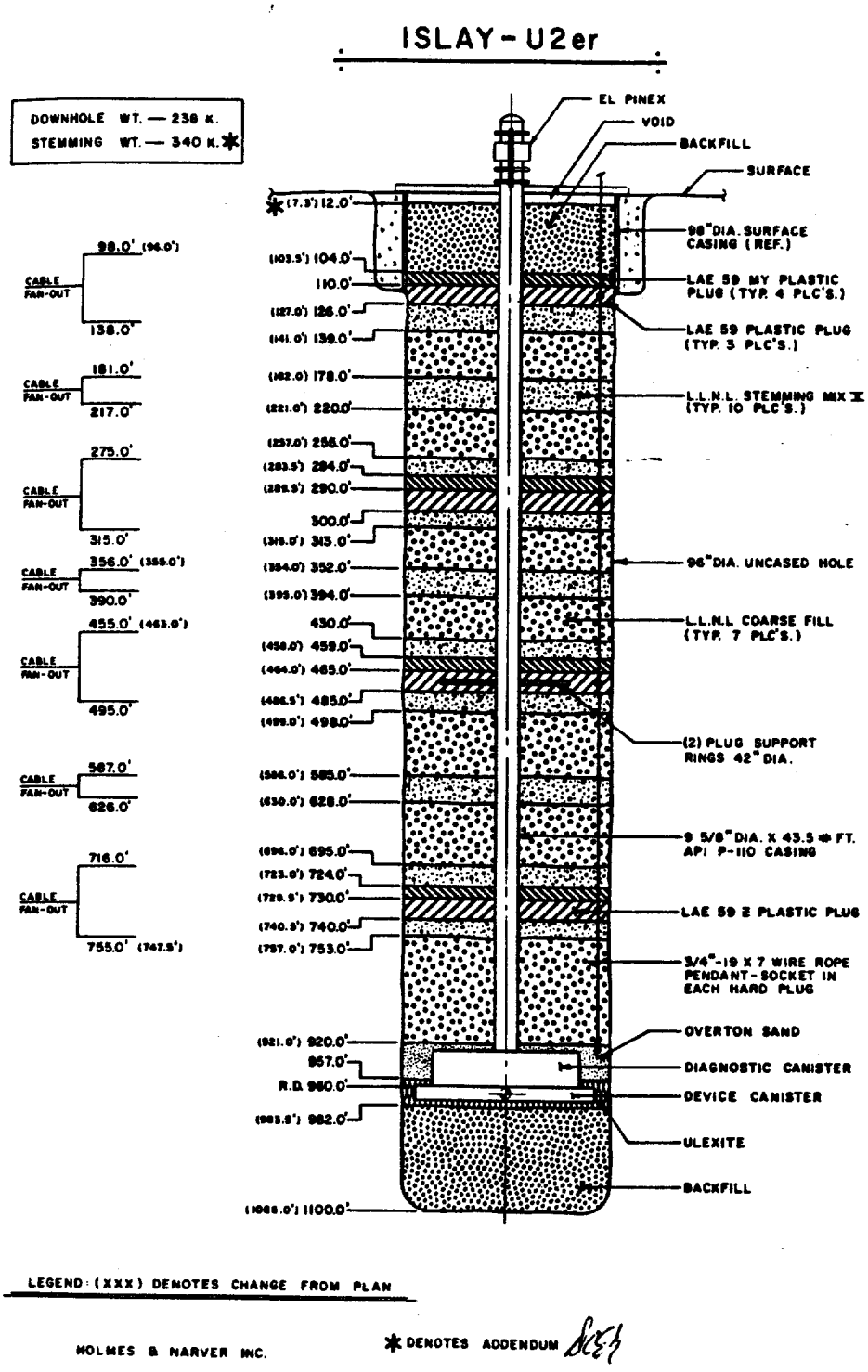

Figure 1.4 As-built stemming plan for the event ISLAY in Hole U2er.

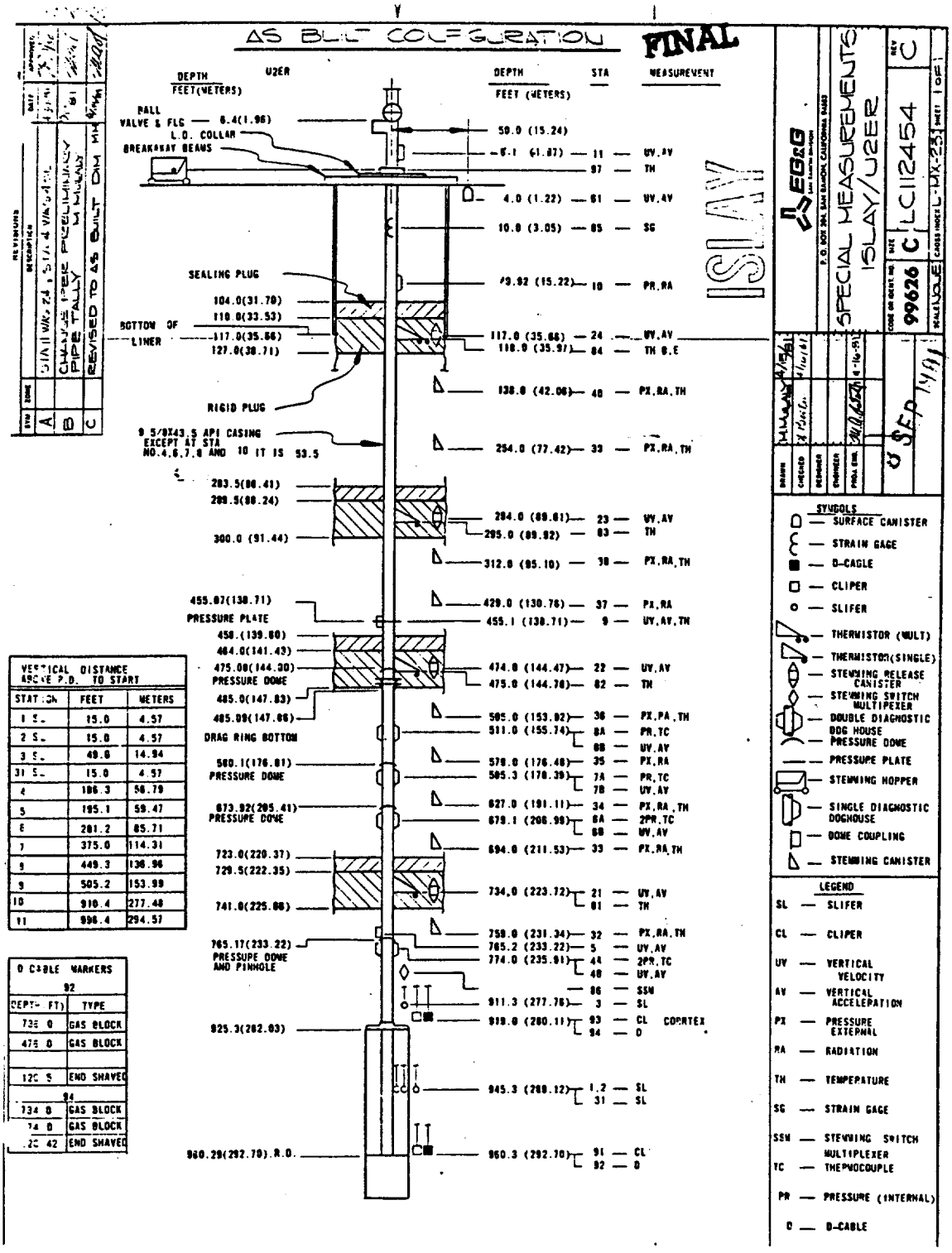

Figure 1.5 As-built containment instrumentation plan for the emplacement hole (U2er) on the ISLAY event.

2. Stemming Performance

2.1 Radiation and Pressure

Stemming pressure and radiation stations were fielded on the ISLAY event at nine locations as indicated in figure 1.5. The pressure and radiation wave forms from about 50 s before detonation until 4500 s after, recorded at all stemming stations, are shown in figures 2.1-2.9.

Figure 2.1 indicates an early arrival of both pressure and radiation at the region below the deepest rigid plug (station 32). The high radiation level and the pressure history suggest that the cavity gasses migrated to this level. The change in pressure without an accompanying change in radiation level seen at about 2000 s is likely due to a shift in stemming. A low-level radiation arrival is seen at about 200 s in station 33 above the deepest rigid plug (figure 2.2) indicating that the plug was a significant impedance to the cavity gas flow. Pressure histories from all stations above the deepest plug can be explained as the result of stemming or ground motion.

A hi-level radiation arrival occurring at about 850 s is seen at the bottom of the fines layer (station 34, figure 2.3) and no radiation arrivals are seen at any station above this. Since this radiation was about 4 orders-of-magnitude greater than the level seen at station 33 (at a deeper location), the source must have been other that percolation of the cavity gasses through the stemming. A possible scenario is the rupture of the emplacement pipe in the third sealed section at about the location of the bottom of the fines layer. This would also require compromise of the lower two pressure domes, allowing the cavity gasses to flow to that elevation. The late time of the arrival further suggests that the rupture may have also been a late time effect, if this scenario is correct. The lack of radiation seen at any station above this level indicates that the fines layer acted as an impedance to gas flow.

The radiation history of station 36 (figure 2.5) after collapse would suggest that this recording channel survived collapse. The level drops significantly below the ambient level of the source chip indicating that these data should be ignored beyond collapse time.

The pressure channel just below the top plug (station 40, figure 2.9) did, however, survive collapse and shows a characteristic pressure drop due to stemming fall at that time. The radiation channel begins a random, rapid oscillation between levels of 0.001 and 100 R/Hr at collapse, leading to the conclusion that it was lost at that time. The pressure history of station 40 is shown for the full recording time of greater that 6 hours in figure 2.10.

The first 20 s of the stemming pressure and radiation taken at stations 32 through 39 are shown in figures 2.11-2.18. Data from station 40 are shown for 250 s in figure 2.19.

Only the top three radiation detectors failed to show prompt radiation that is probably shine from the PINEX experiment in the emplacement pipe. Each of these three detectors was discharged by the EMP and took the first couple of seconds to recover. Station 40 (figure 2.19) required more than 150 s to recover, reducing the reliability of that transducer.

The peak of the prompt radiation was between 200 and 300 R/Hr at stations 32 through 35 (figures 2.11-2.14). All these stations were at elevations below the level of the pressure dome defining the top of the third sealed section of emplacement pipe. Across the formation coupling plug, the peak of the prompt radiation was down by about a factor of five (figures 2.15 and 2.16). A secondary radiation arrival was seen at station 32 at about 11 s (figure 2.11). This was likely due to cavity gas percolating into that region.

2.2 Motion

Explosion-induced histories of the motion measured in the stemming and on the ground surface during the ISLAY event are shown in figures 2.20–2.25. Only the acceleration channels are shown since, as discussed in reference 4, all of the velocity channels in the plugs and on the ground surface were compromised by an electrical grounding problem, presumably occurring at zero time. Characteristics of the associated motion and transducers are given in tables 2.1–2.3.

The drag ring system on the emplacement pipe may have induced motion that interfered with the ground motion signal at this station at early times (figure 2.21). Since the pipe was coated with hydroseal in the regions of the TPE plugs at elevations higher than the drag ring (around stations 23 and 24, figures 2.22 and 2.23), the pipe-induced motion at these higher stations was mitigated. The explosion-induced motion recorded in each of the rigid plugs and the ground surface was otherwise unremarkable.

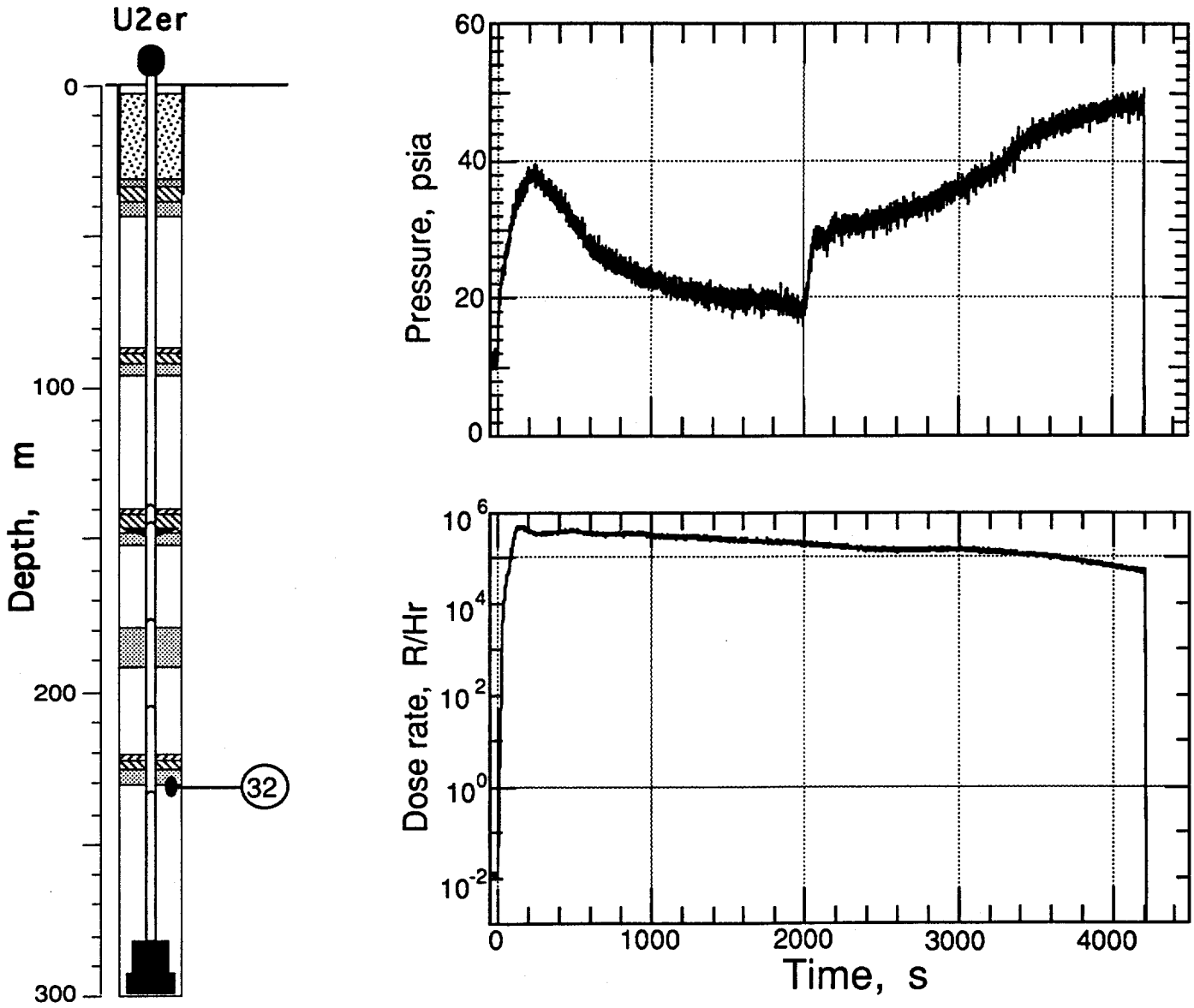

Figure 2.1 Pressure and radiation as monitored in the coarse stemming below the deep rigid plug at a depth of 231.3 m (station 32).

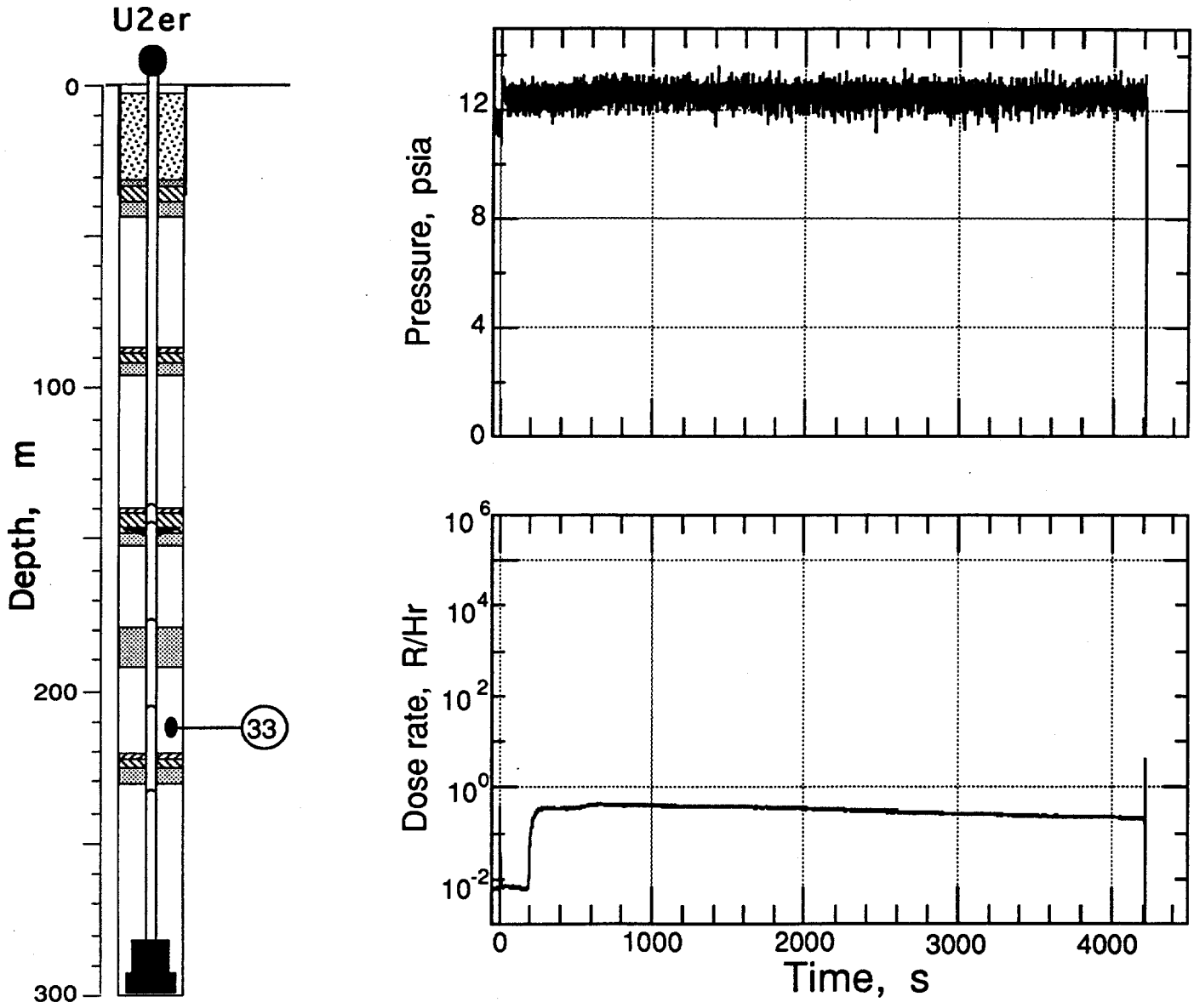

Figure 2.2 Pressure and radiation measured in the coarse stemming above the deep rigid plug at a depth of 211.5 m (station 33).

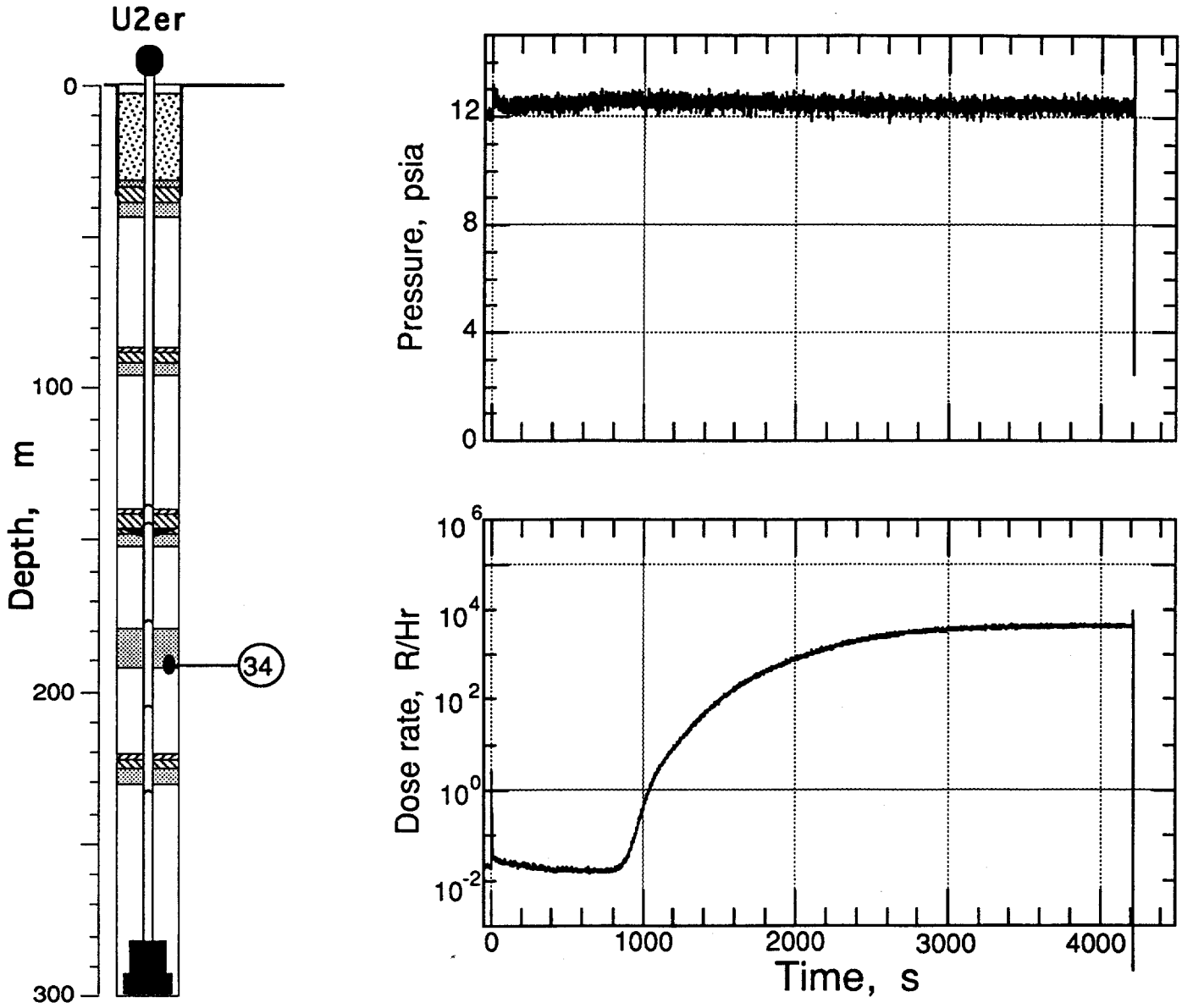

Figure 2.3 Pressure and radiation measured in the coarse stemming below the fines layer at a depth of 191.1 m (station 34).

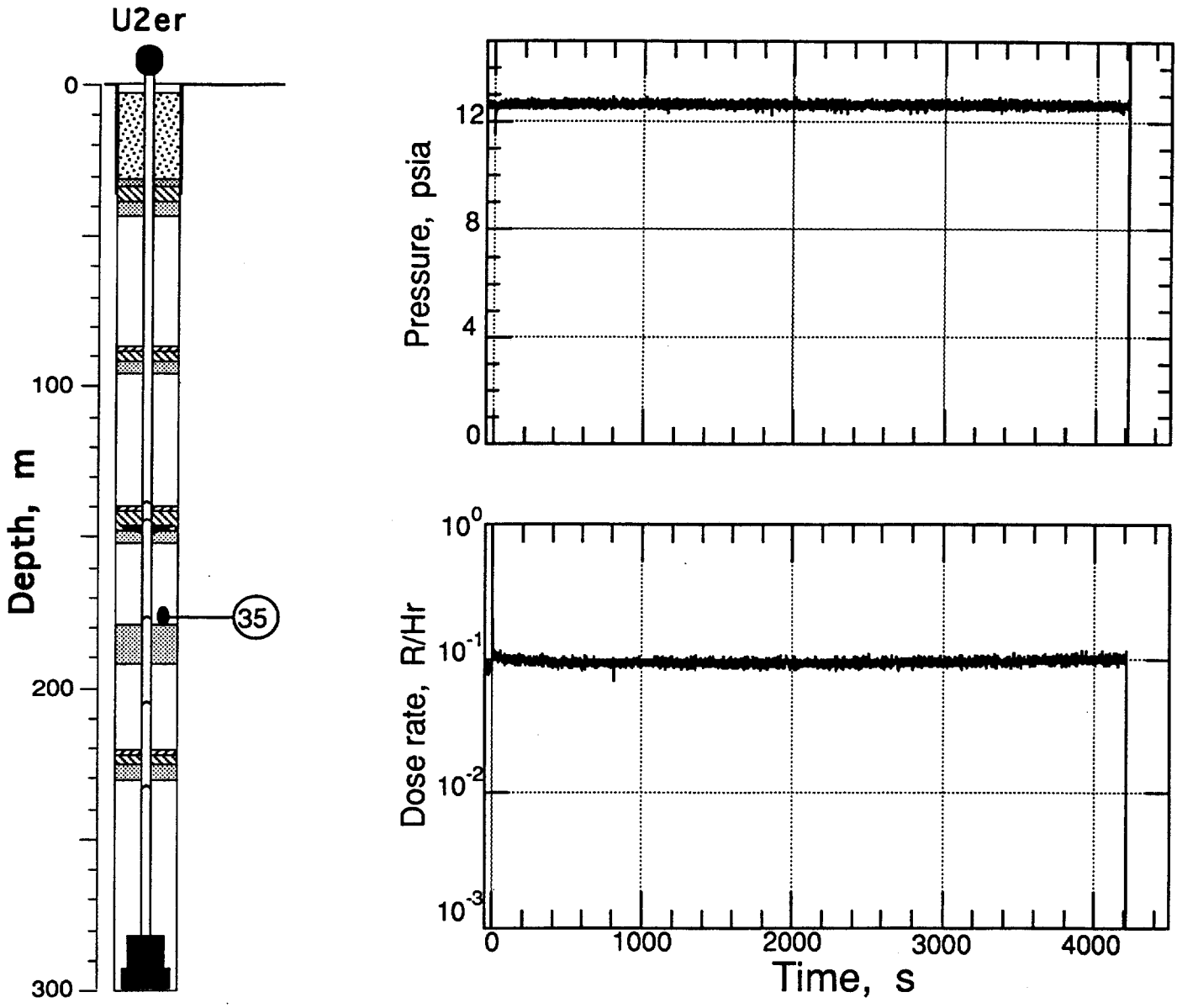

Figure 2.4 Pressure and radiation measured in the coarse stemming above the fines layer at a depth of 176.5 m (station 35).

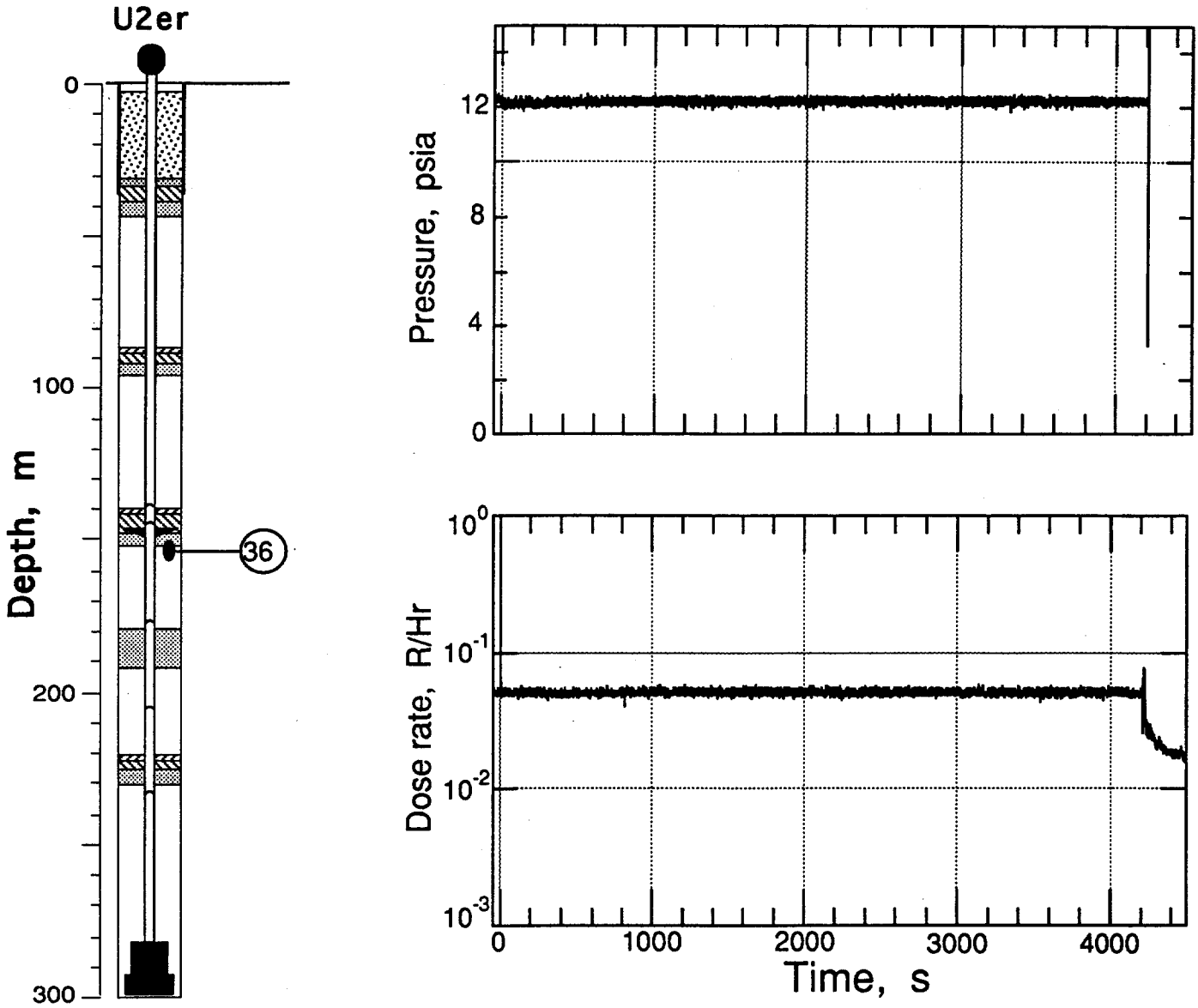

Figure 2.5 Pressure and radiation measured in the coarse stemming beneath the formation coupling plug at a depth of 153.9 m (station 36).

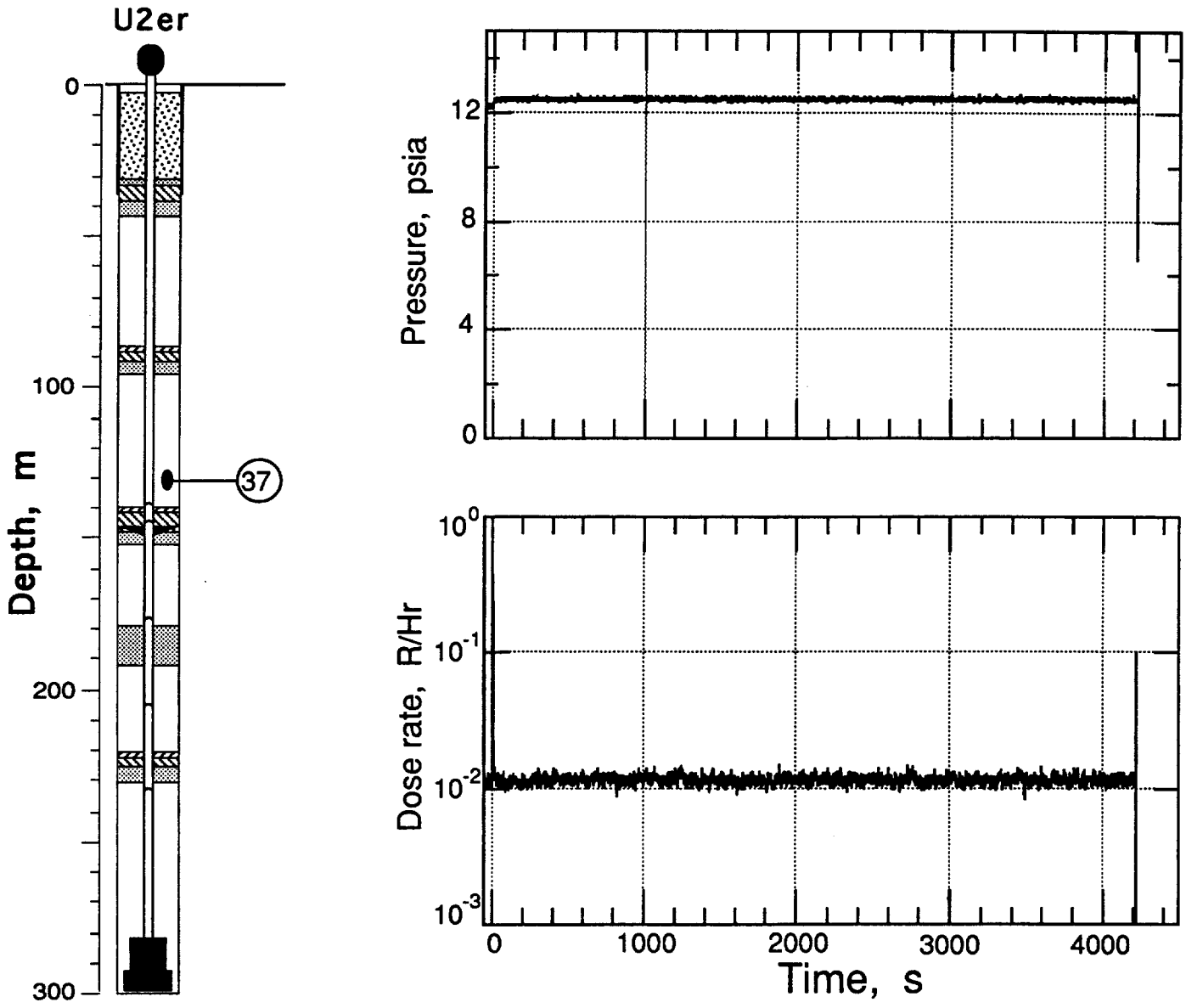

Figure 2.6 Pressure and radiation measured in the coarse stemming above the formation coupling plug at a depth of 130.8 m (station 37).

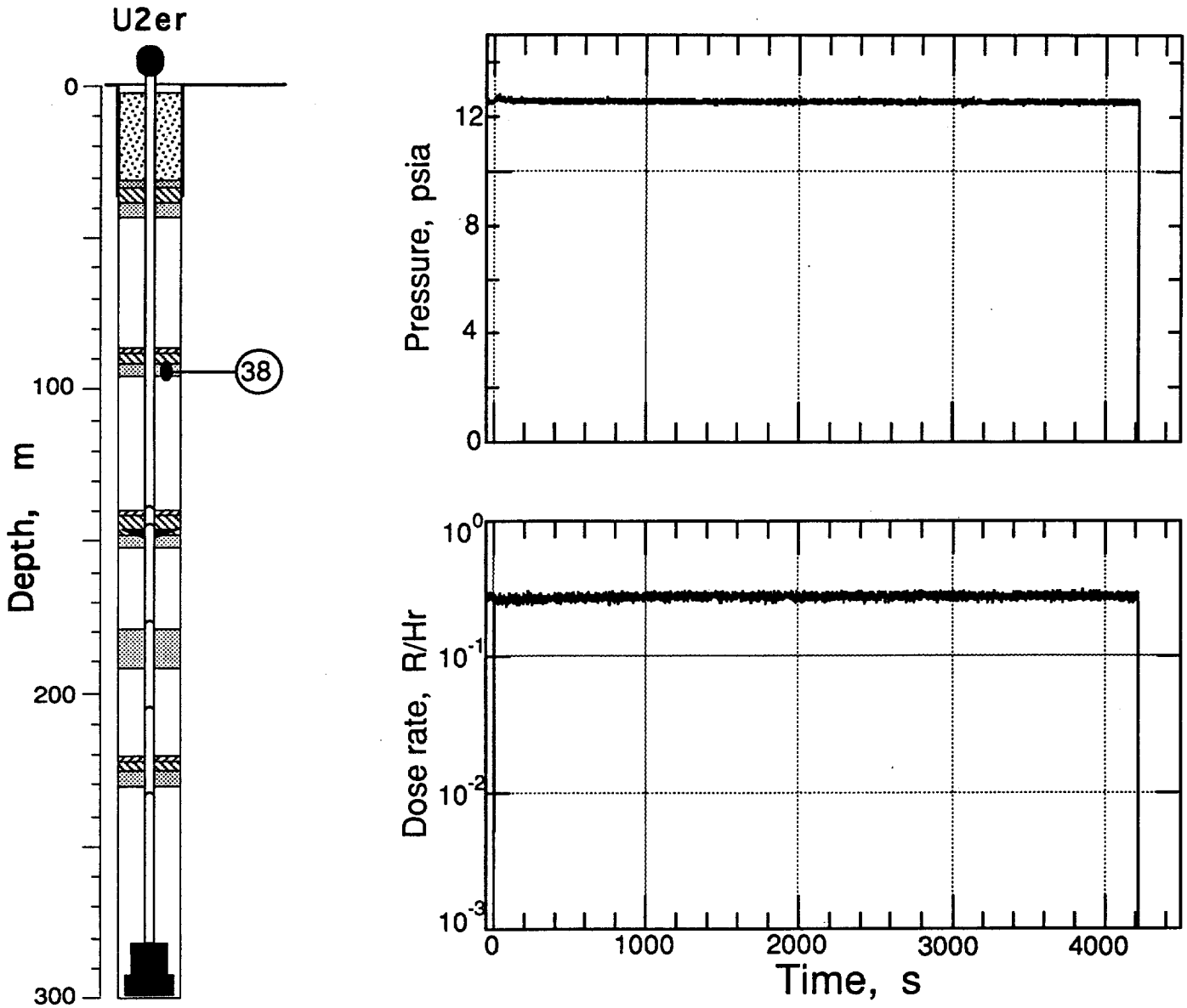

Figure 2.7 Pressure and radiation measured in the coarse stemming below the third rigid plug at a depth of 95.1 m (station 38).

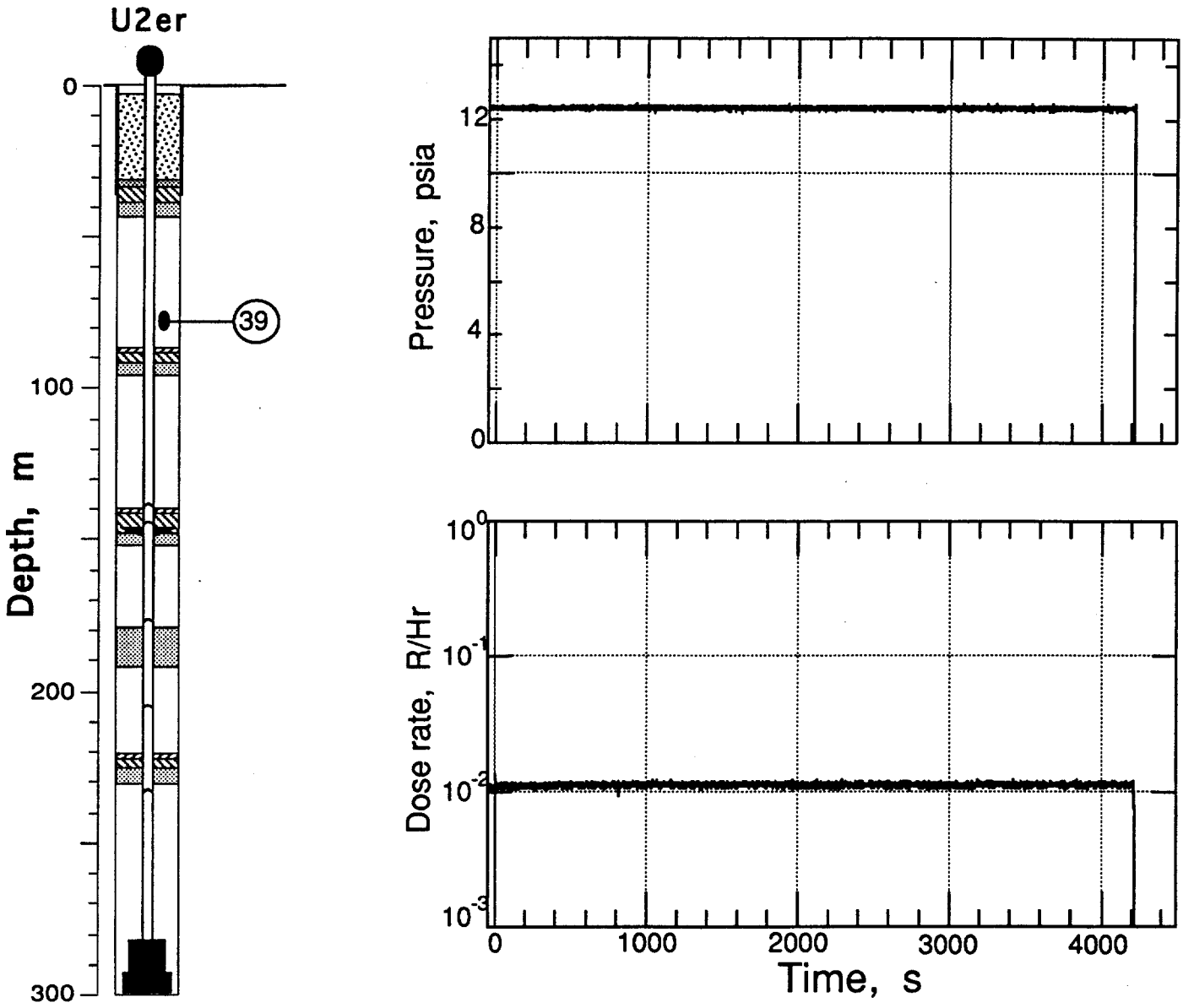

Figure 2.8 Pressure and radiation measured in the coarse stemming above the third rigid plug at a depth of 77.4 m (station 39).

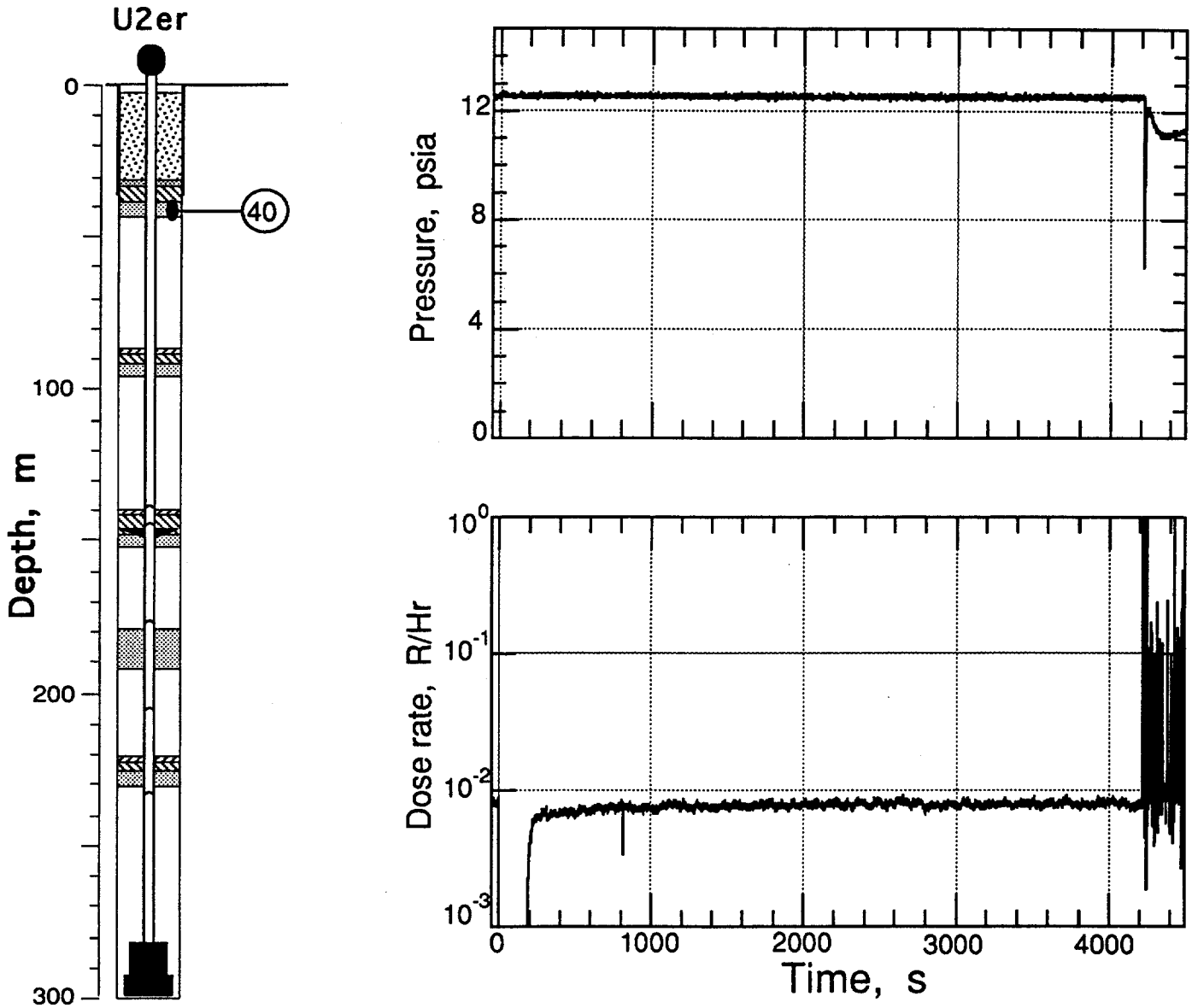

Figure 2.9 Pressure and radiation measured in the coarse stemming beneath the top plug at a depth of 42.1 m (station 40).

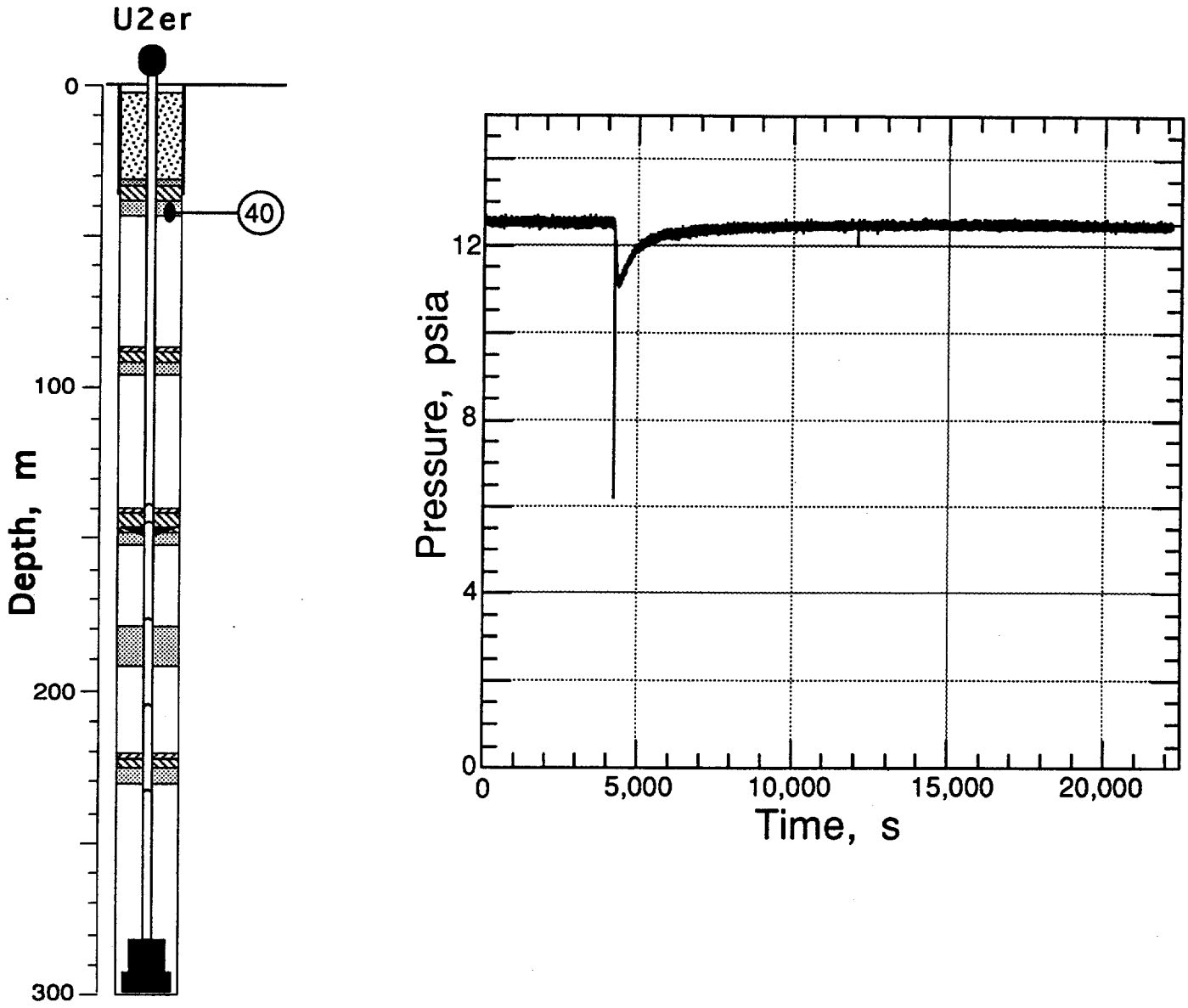

Figure 2.10 Pressure measured in the coarse stemming beneath the top plug at a depth of 42.1 m (station 40). The entire recording time of greater that 6 hours is shown.

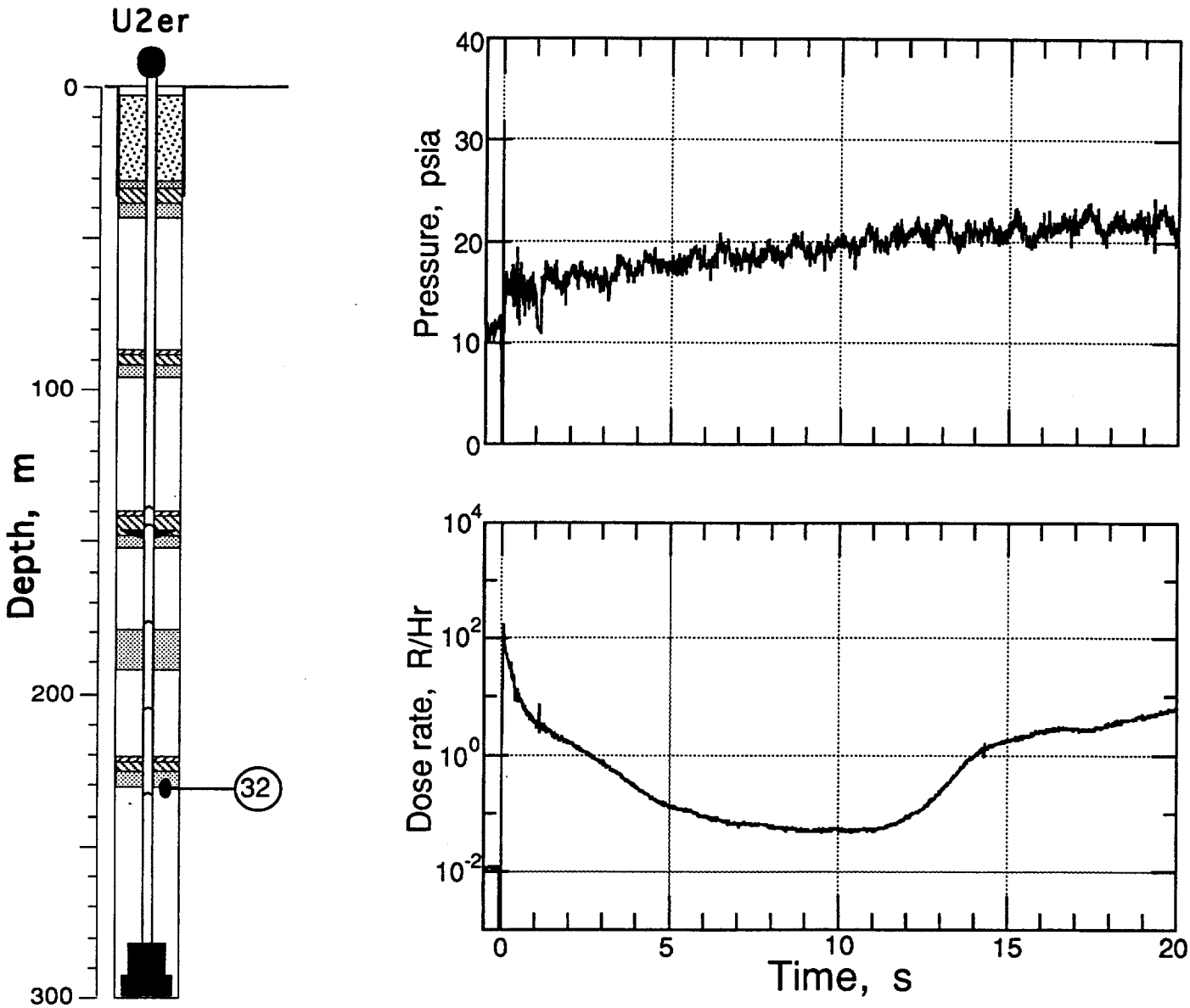

Figure 2.11 First 20 s of pressure and radiation as monitored in the coarse stemming below the deep rigid plug at a depth of 231.3 m (station 32).

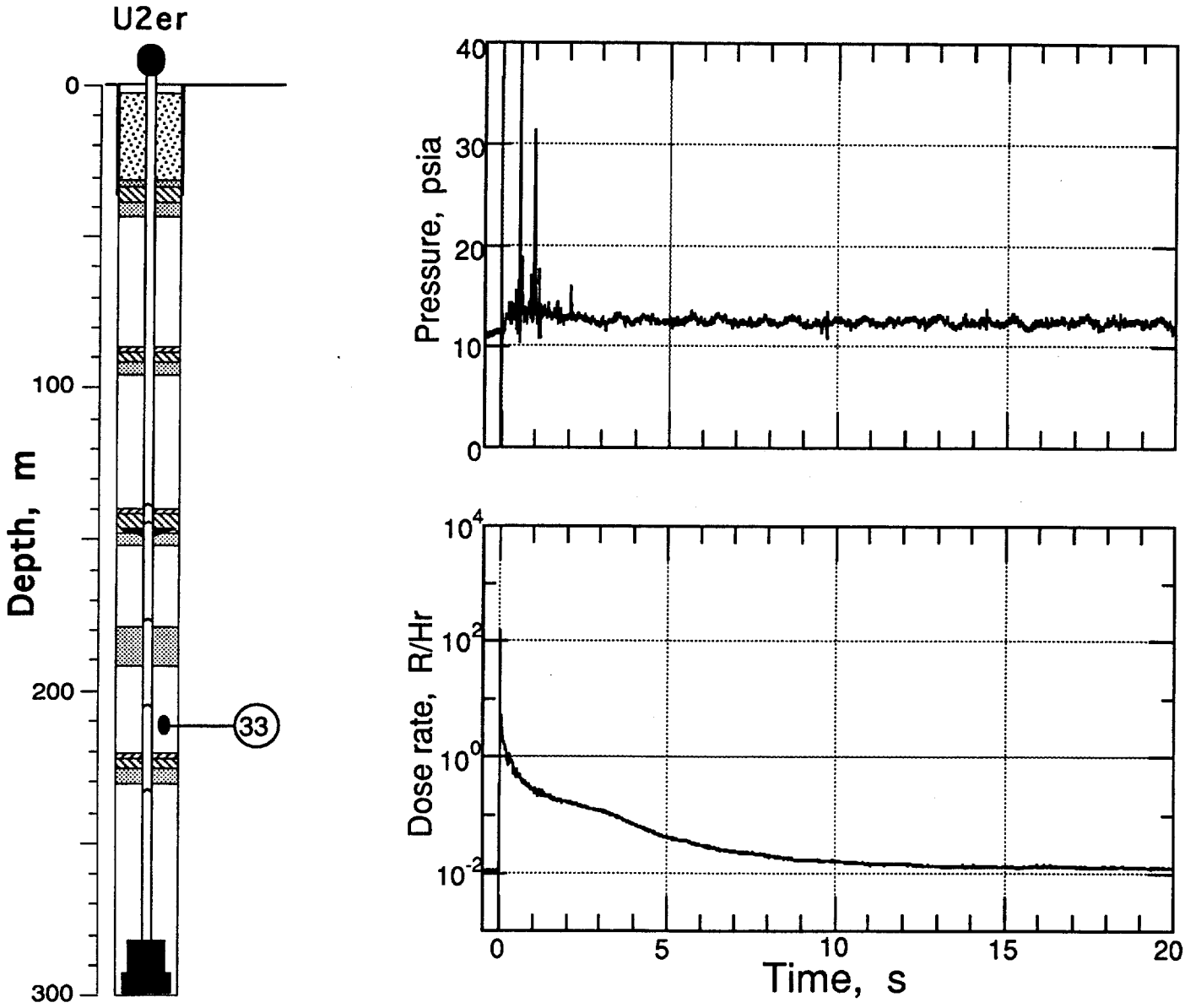

Figure 2.12 First 20 s of pressure and radiation measured in the coarse stemming above the deep rigid plug at a depth of 211.5 m (station 33).

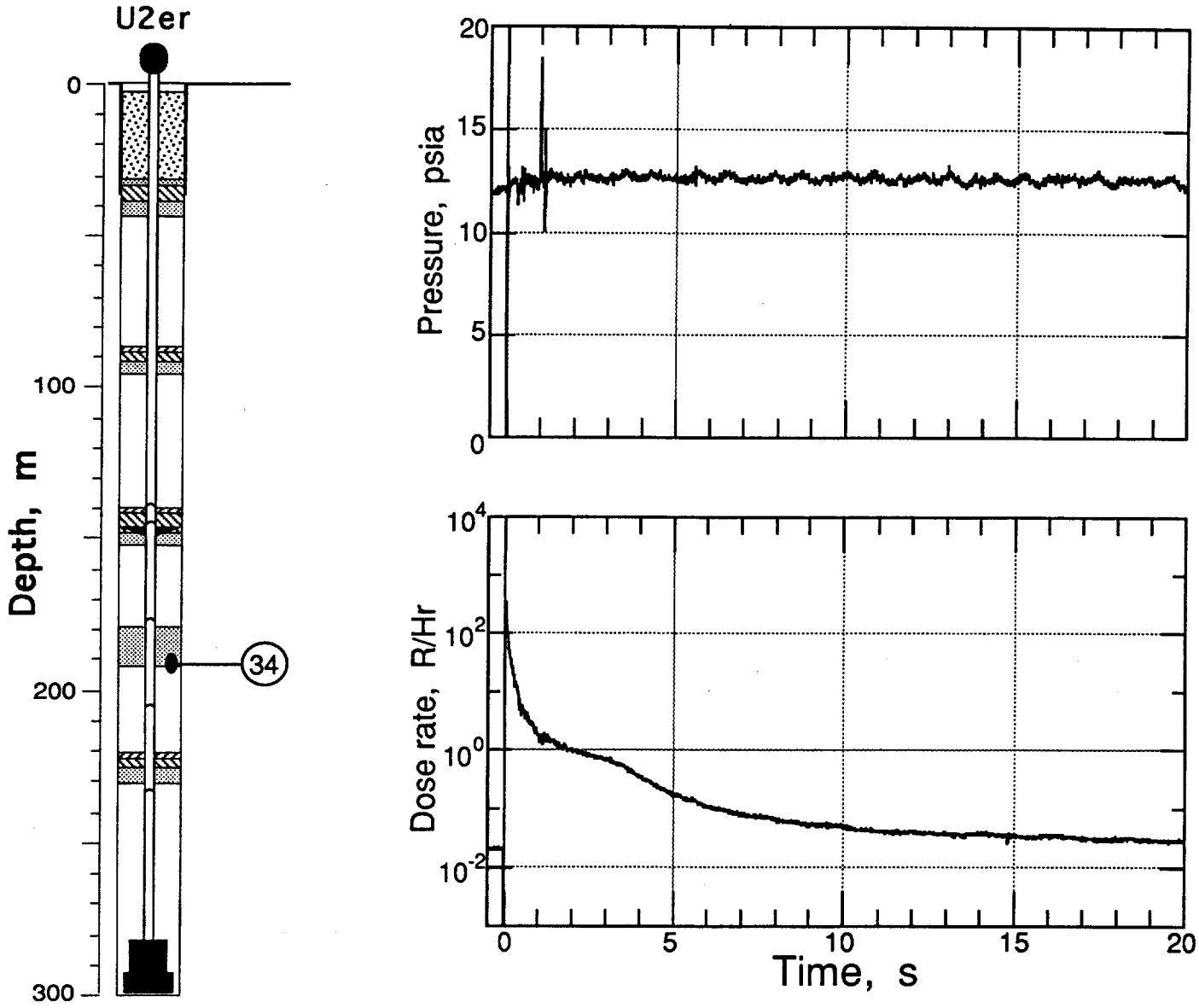

Figure 2.13 First 20 s of pressure and radiation measured in the coarse stemming below the fines layer at a depth of 191.1 m (station 34).

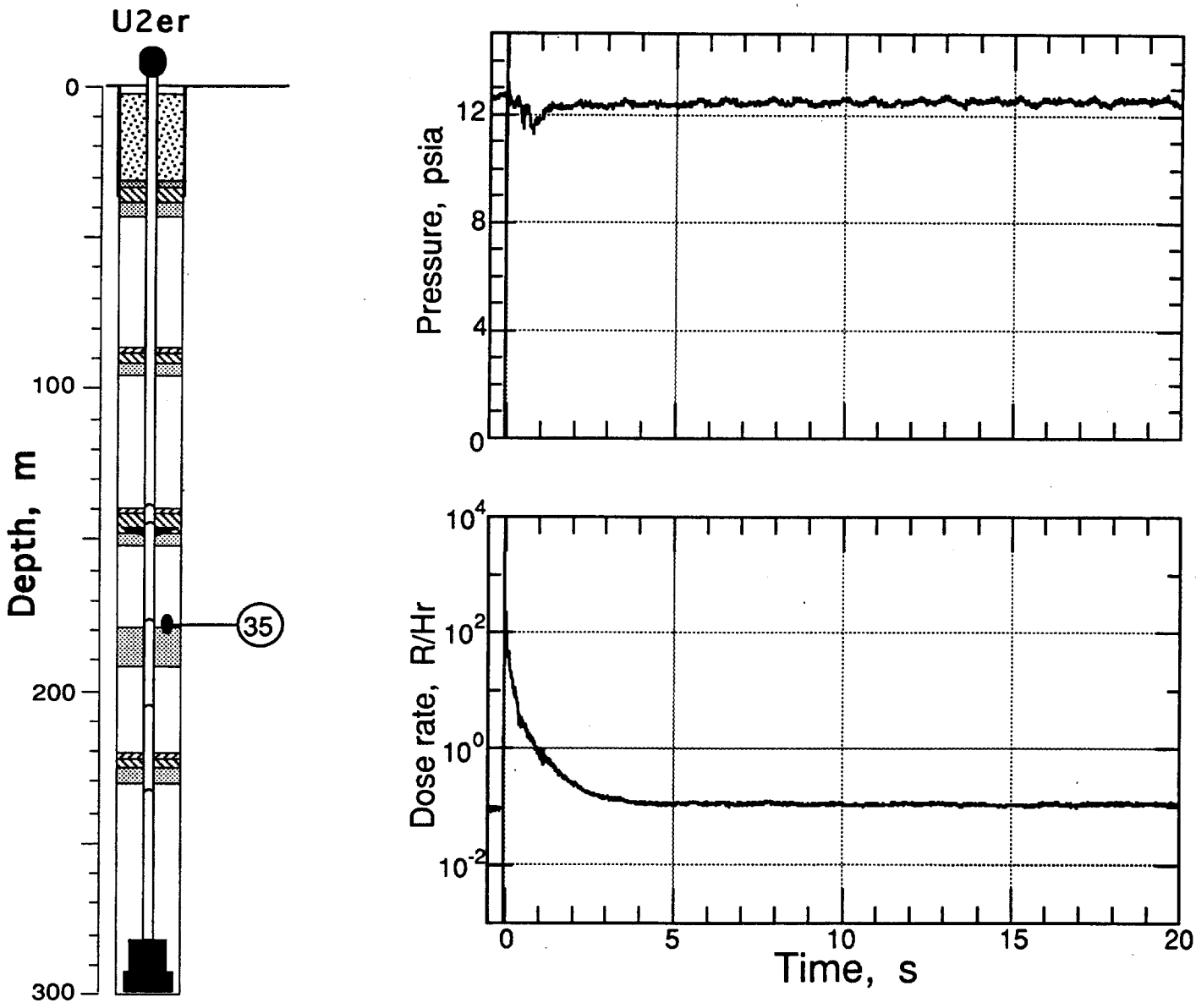

Figure 2.14 First 20 s of pressure and radiation measured in the coarse stemming above the fines layer at a depth of 176.5 m (station 35).

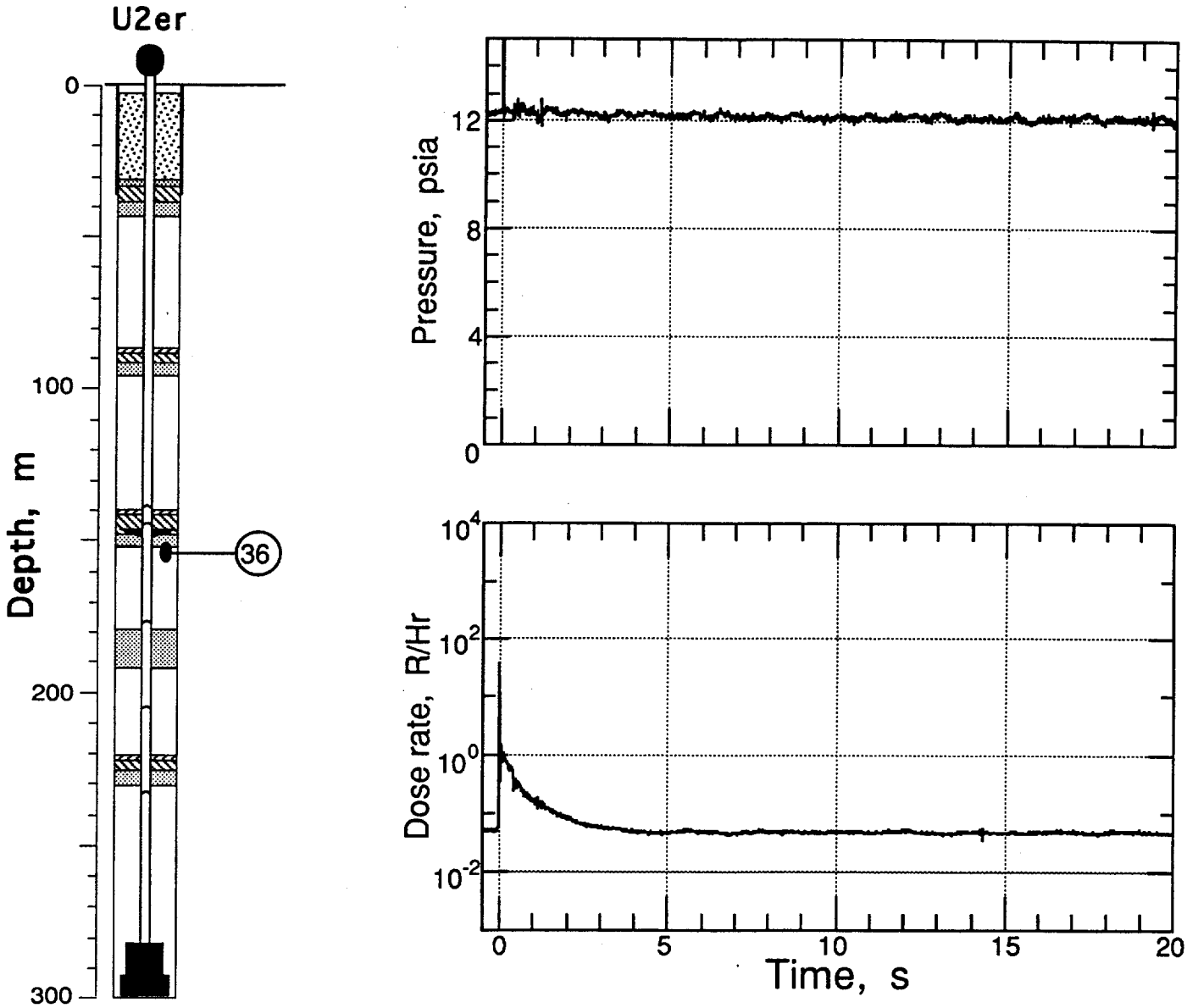

Figure 2.15 First 20 s of pressure and radiation measured in the coarse stemming beneath the formation coupling plug at a depth of 153.9 m (station 36).

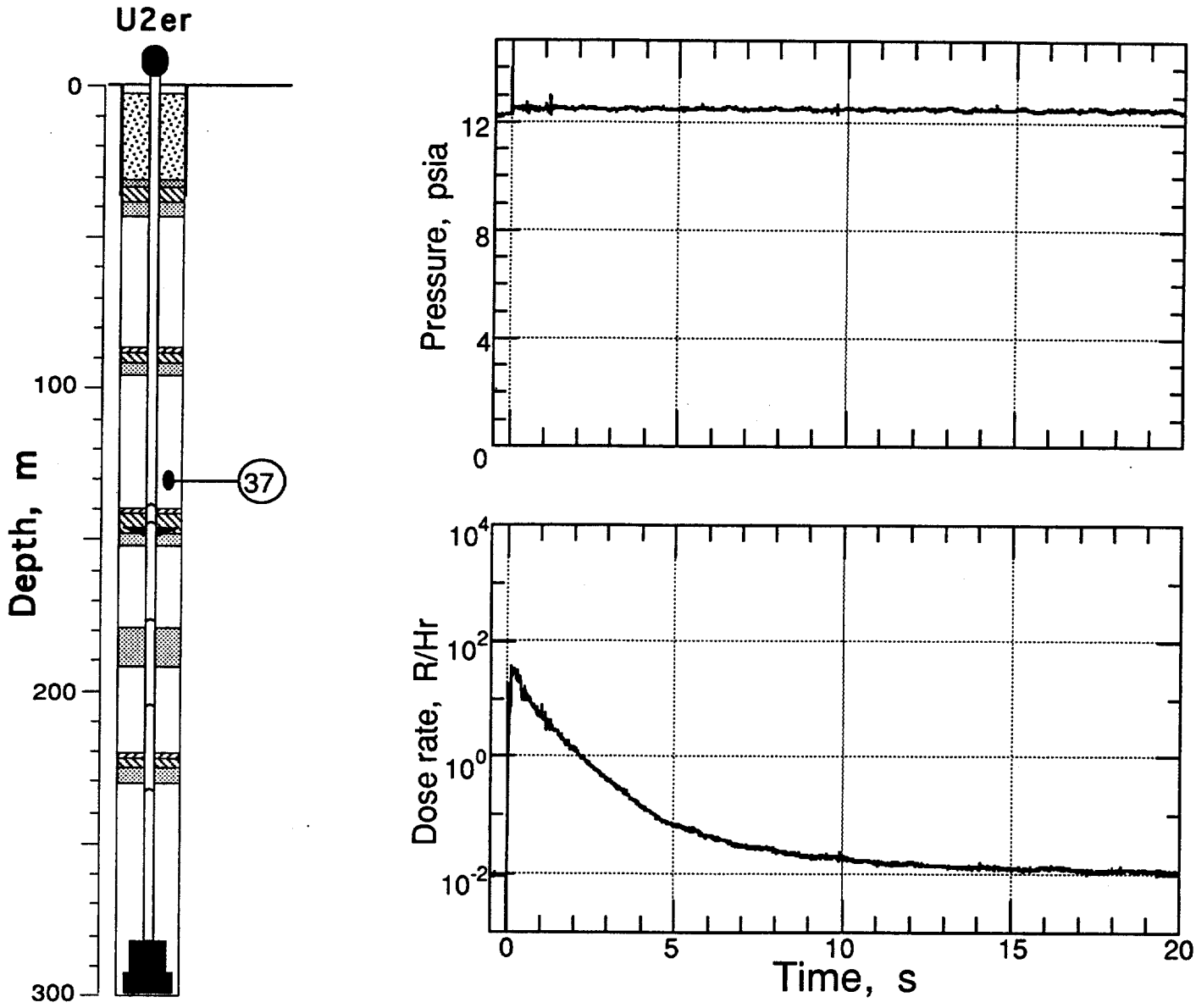

Figure 2.16 First 20 s of pressure and radiation measured in the coarse stemming above the formation coupling plug at a depth of 130.8 m (station 37).

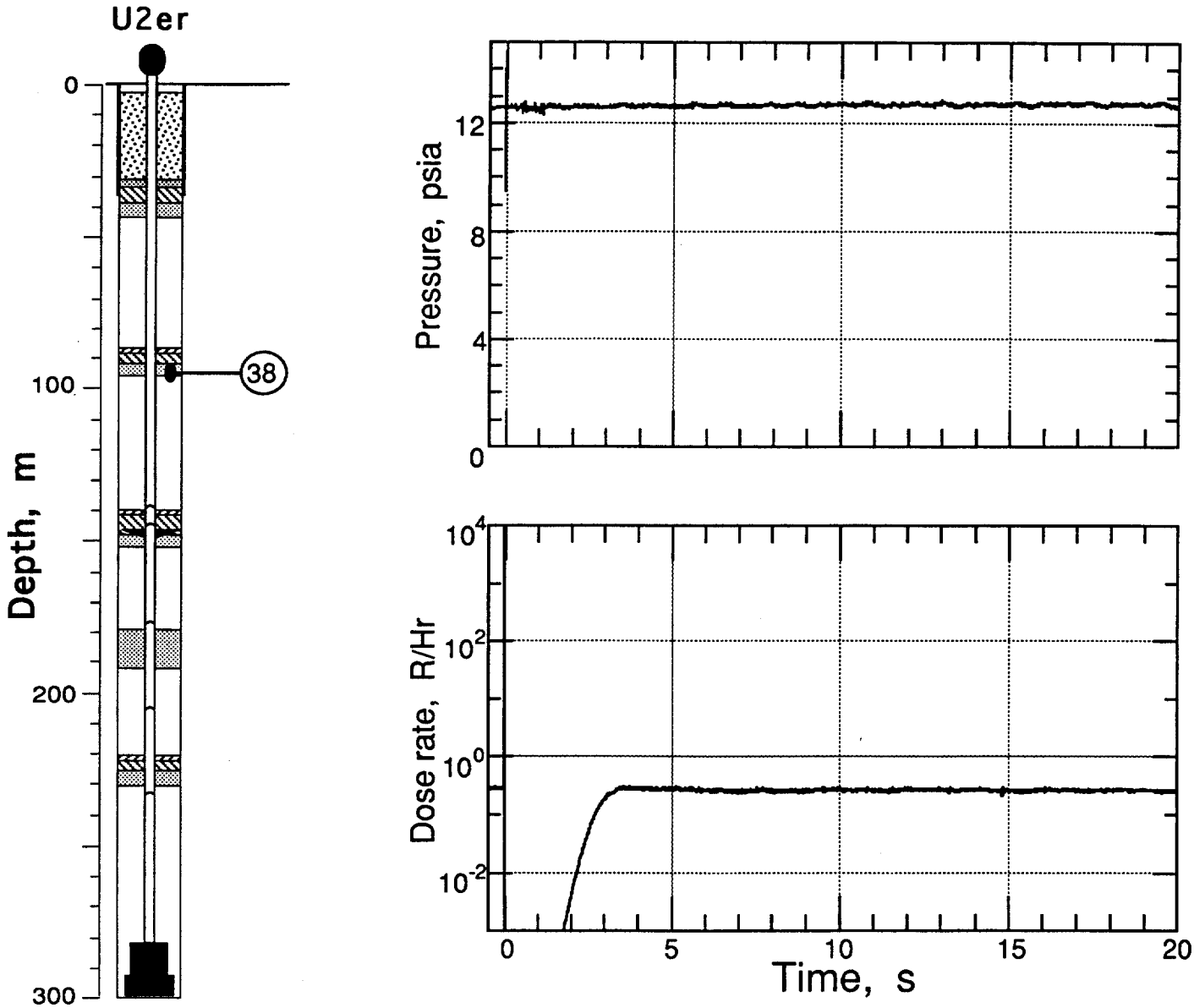

Figure 2.17 First 20 s of pressure and radiation measured in the coarse stemming below the third rigid plug at a depth of 95.1 m (station 38).

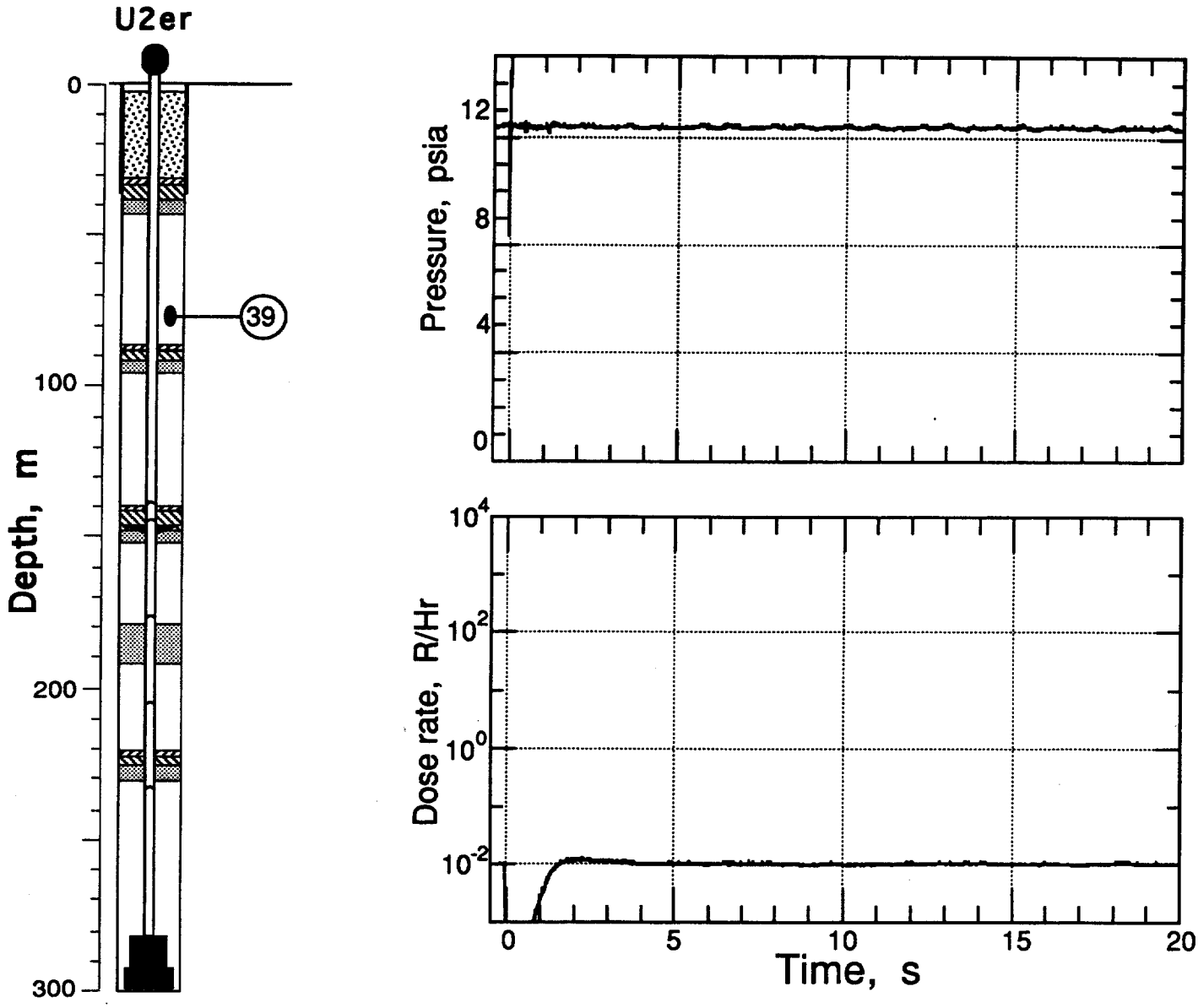

Figure 2.18 First 20 s of pressure and radiation measured in the coarse stemming above the third rigid plug at a depth of 77.4 m (station 39).

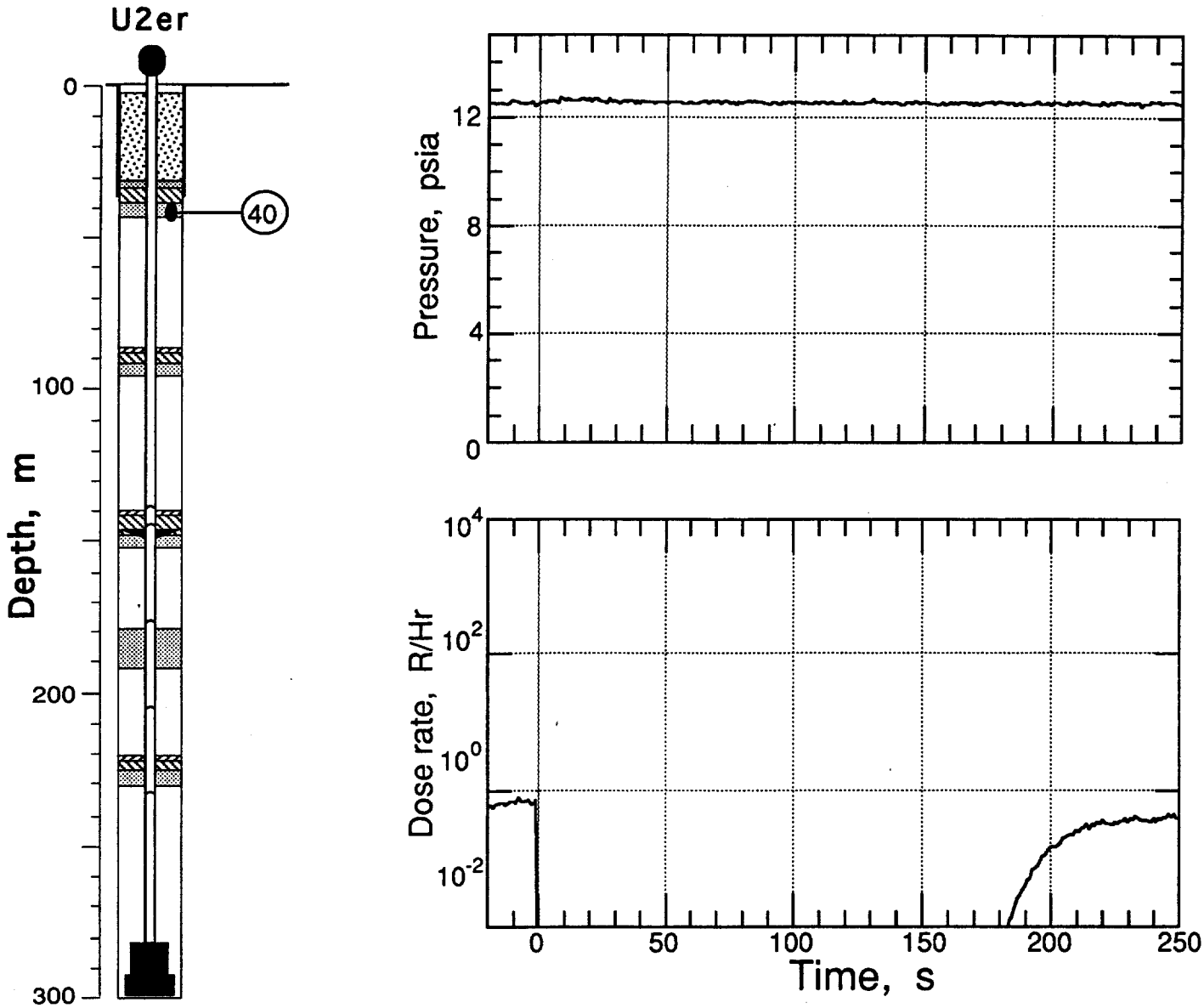

Figure 2.19 First 250 s of pressure and radiation measured in the coarse stemming beneath the top plug at a depth of 42.1 m (station 40).

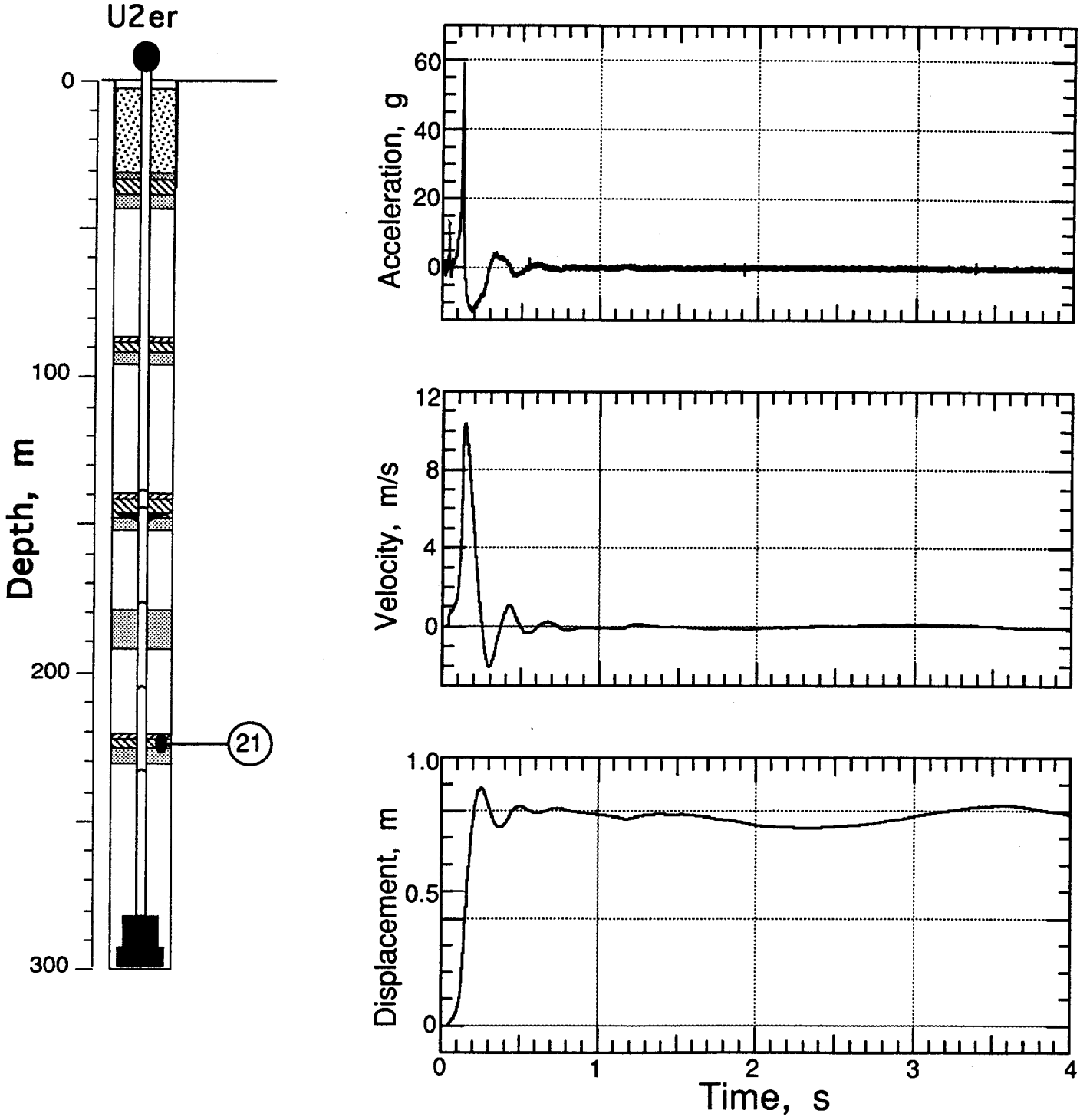

Figure 2.20 Explosion-induced vertical motion of the bottom rigid plug (station 21, at a depth of 223.7 m). All motion is derived from the accelerometer channel.

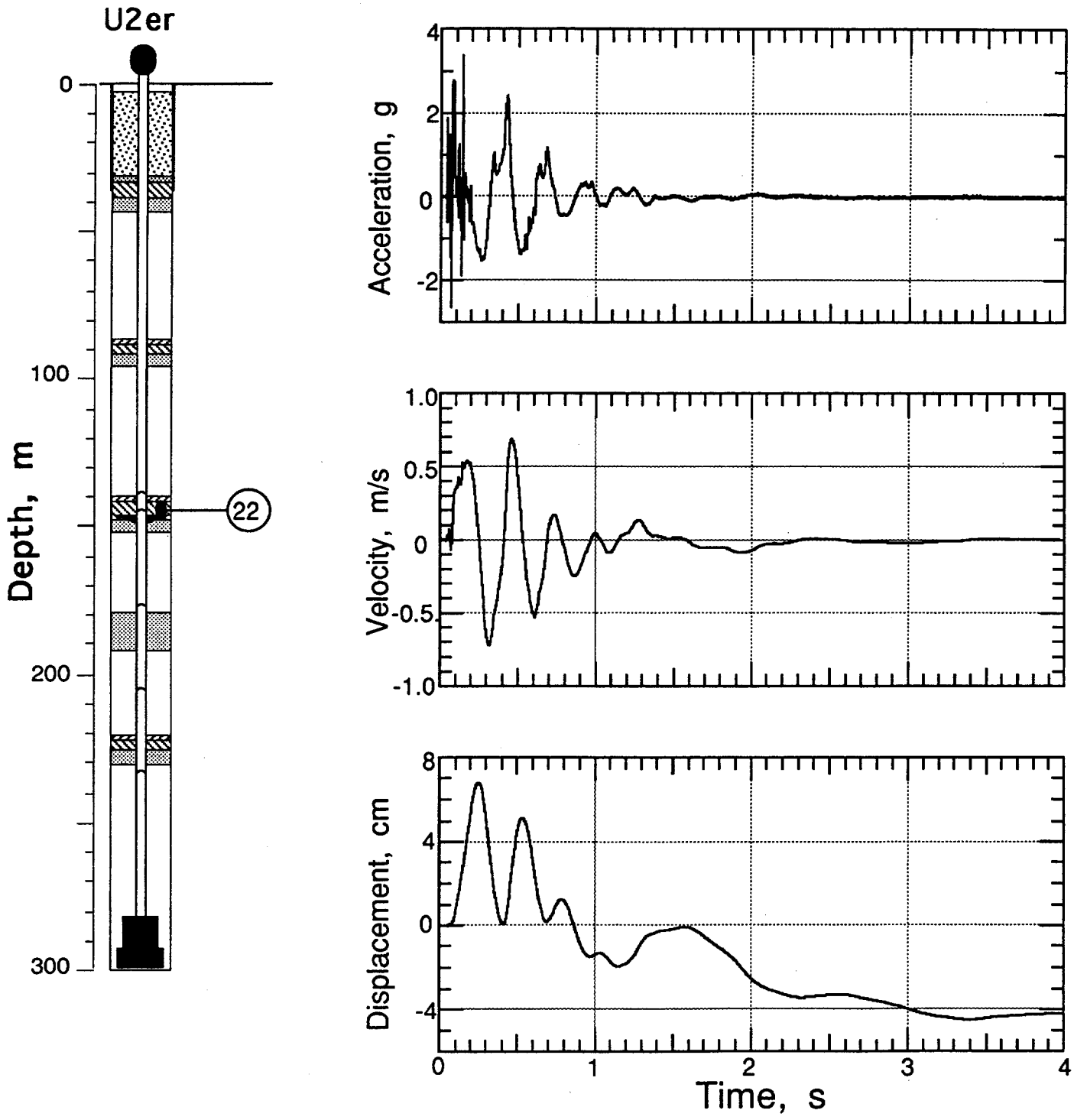

Figure 2.21 Explosion-induced vertical motion of the second rigid plug (station 22, at a depth of 144.6 m). All motion is derived from the accelerometer channel. The acceleration at early time shows strong motion induced by the emplacement pipe and the drag ring.

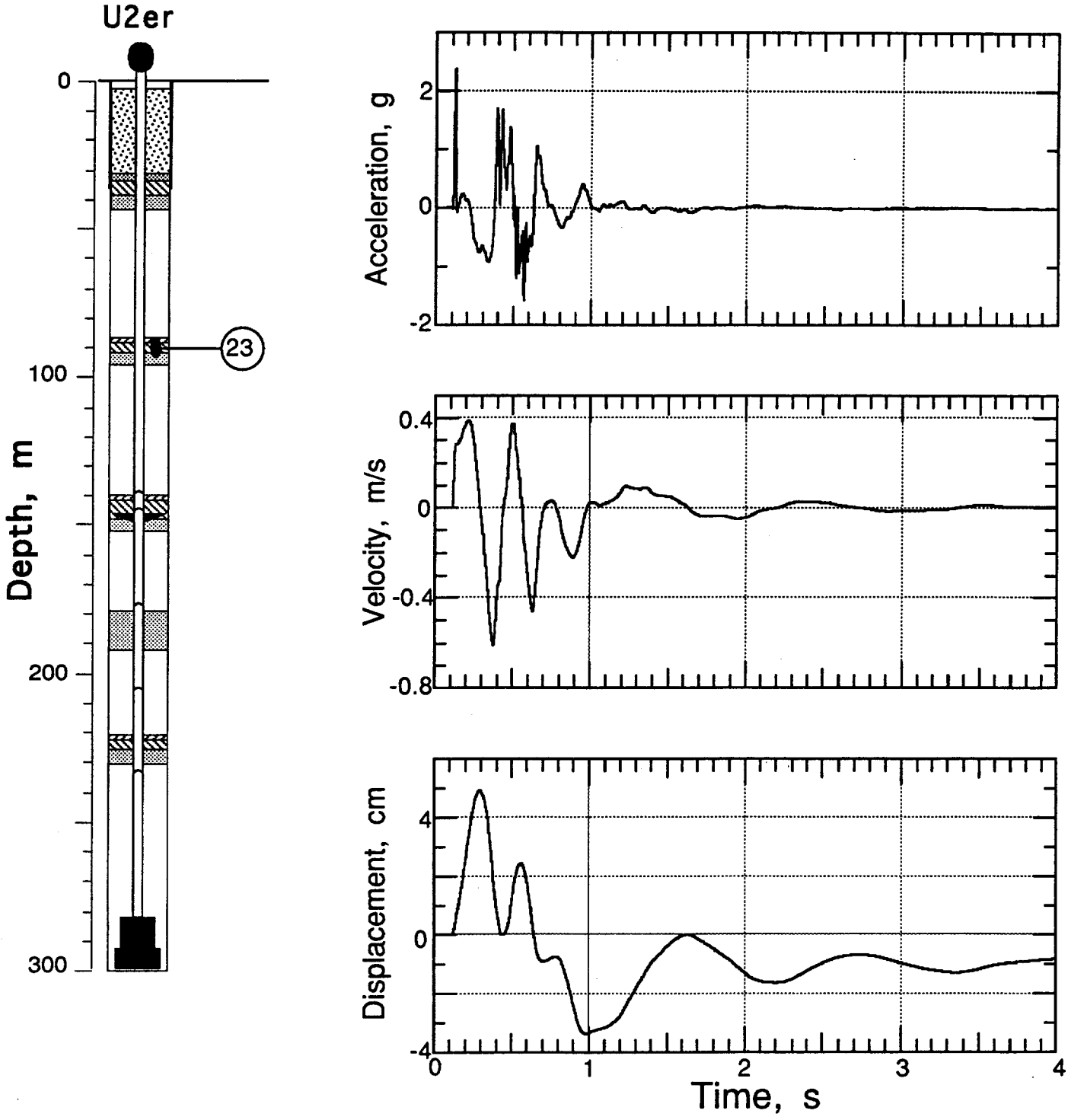

Figure 2.22 Explosion-induced vertical motion of the third rigid plug (station 23, at a depth of 89.6 m). All motion is derived from the accelerometer channel.

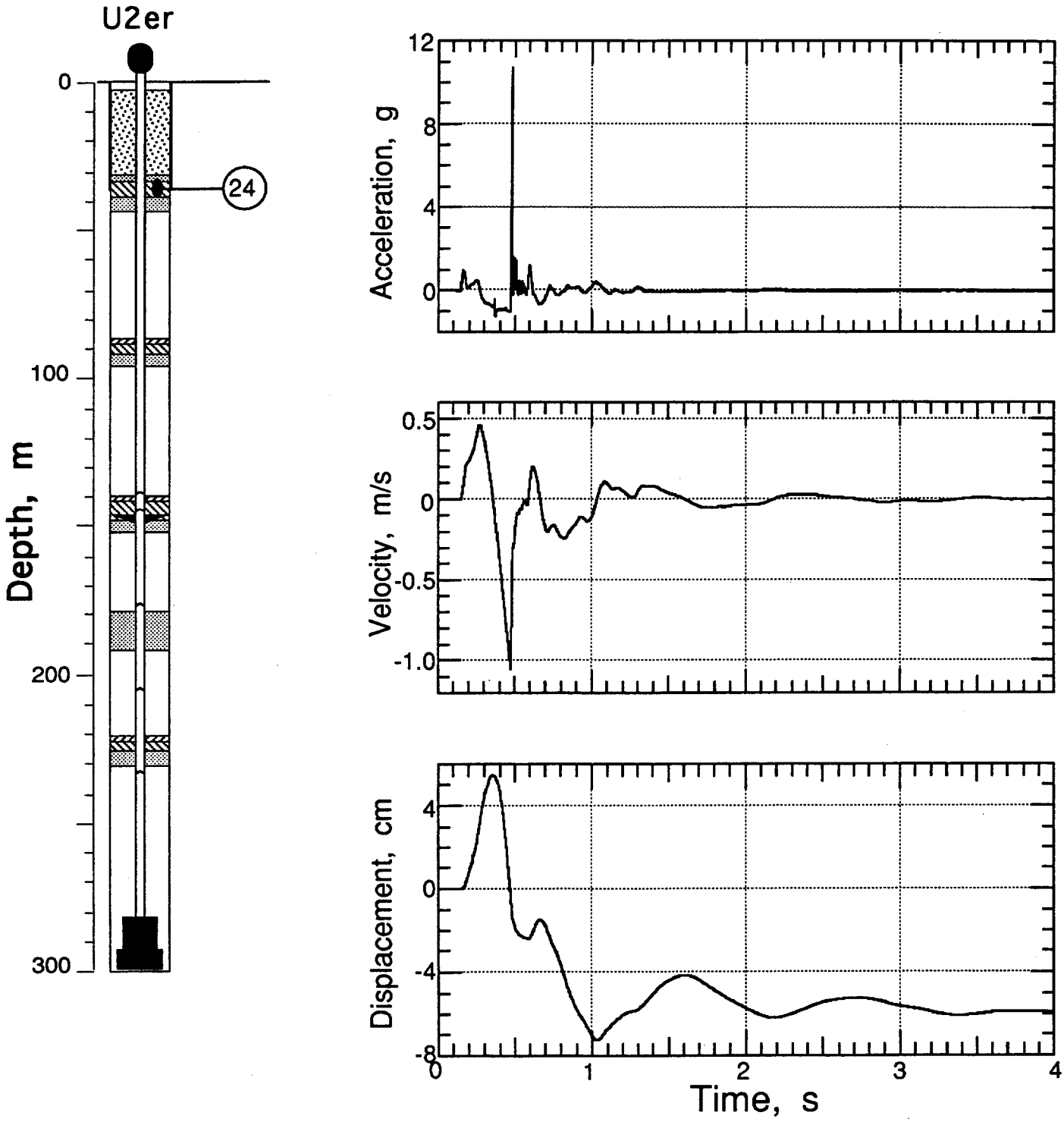

Figure 2.23 Explosion-induced vertical motion of the top plug (station 24, at a depth of 35.7 m). All motion is derived from the accelerometer channel.

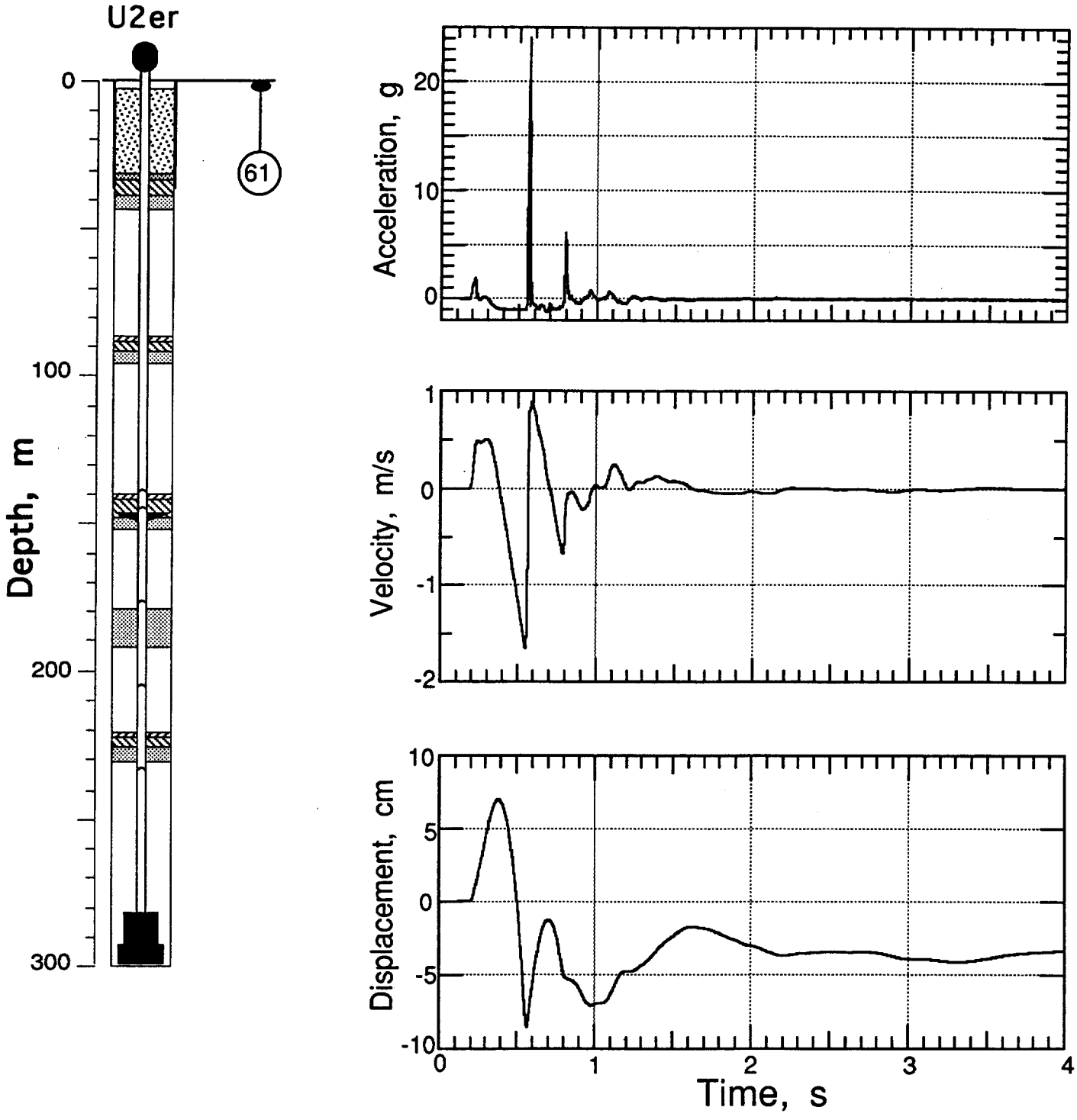

Figure 2.24 Explosion-induced vertical motion of the ground surface at a depth of 0.9 m and horizontal range of 15.24 m (station 61). All motion is derived from the accelerometer channel.

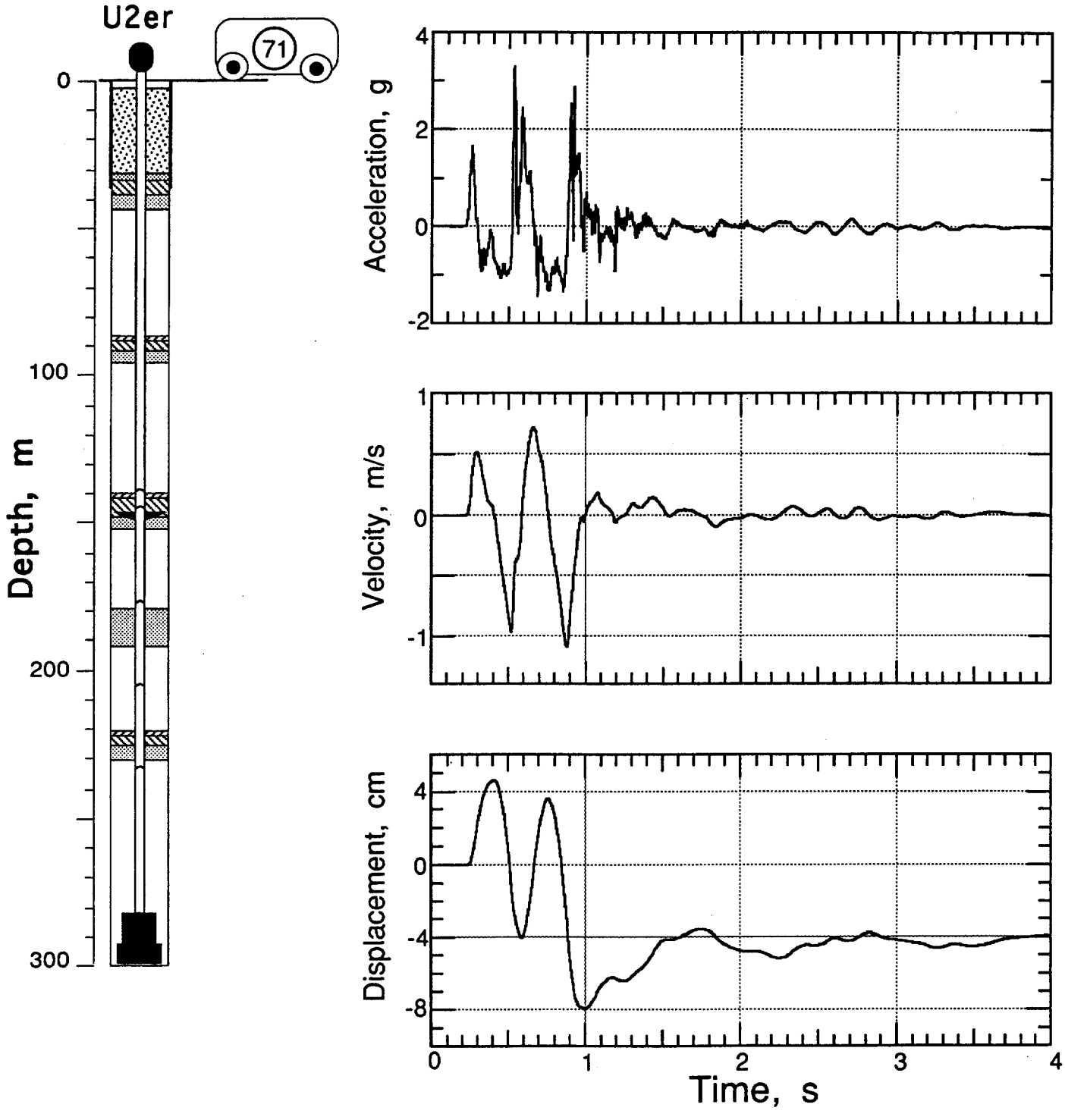

Figure 2.25 Explosion-induced vertical motion of the recording trailer.

Table 2.1 Summary of Containment-Related Motion

Gauge	Slant Range (m)	Arrival Time (ms)	Acceleration Peak (g)	Velocity Peak (m/s)	Displacement Peak (cm)	Displacement Residual (cm)
4av	58.1	11.6[a]	-515[a]	-3[a]	(b)	(b)
4uv		11.4[a]	-	-5.8[a]	(b)	(b)
5av	60.8	(c)	-	-	-	-
5uv		(c)	-	-	-	-
6av	87.0	17.5[a]	-220[a]	-1.6[a], 12.0	38.5	20
6uv		18[a]	-	-1.9[a], 10.1	43.5	37
7av	115.6	(c)	-	-	-	-
7uv		21[a]	-	-1.5[a], 7.6	10	8
8av	138.3	27.7[a]	-41[a]	-0.5[a], 1.2	2	1
8uv		28[a]	-	-0.8[a], 1.3	-1.1[d]	-1.7[d]
9av	155.3	37	3	0.51	6.0	2
9uv		37	-	0.53	6.4	(b)
11av	295.9	160	1.6	0.45	2.4	-1.5
11uv		160	-	0.44	2.2	-5.1
21av	70.3	36.3[a]	12.5[a],57	10.3	88	80
21uv		(e)	-	-	-	-
22av	149.5	32[a]	-0.6[a], 2.6	0.54	6.8	-4
22uv		(f)	-	-	-	-
23av	204.4	110	2.4[a]	0.39	4.9	-1
23uv		(f)	-	-	-	-
24av	258.3	150	0.9, 10.7[g]	0.46	5.4	-5.8
24uc		(f)	-	-	-	-
6 1av	294.4	185	1.8, 24[g]	0.51	7.0	-3.5
61uv		(f)	-	-	-	-
71av	330[h]	215	1.6, 3.3[g]	0.51	4.6	-4

(a) First motion (precursor or from pipe).
(b) Could not estimate this value.
(c) This channel not functioning.
(d) Uncorrectable baseline drift.
(e) This channel lost at ZIP.
(f) Channel lost: NATEL multiplexer failure.
(g) Slap-down.
(h) Approximate; station mounted in recording trailer.

Table 2.2 Containment-Related Accelerometer Characteristics

Gauge	Natural Frequency (Hz)	Damping Ratio	System Range (g's)
4av	1175	0.67	4000
5av	1720	0.65	4000
6av	1575	0.64	2000
7av	1250	0.65	500
8av	1300	0.60	300
9av	1300	0.65	300
11av	680	0.75	100
21av	1350	0.65	400
22av	440	0.75	30
23av	191	0.65	6
24av	329	0.65	20
61av	580	0.55	30
71av	220	0.65	10

Table 2.3 Containment-Related Velocimeter Characteristics

Gauge	Natural Frequency (Hz)	Time to 0.5 Amplitude (s)	Calibration Temperature (°F)	Operate Temperature (°F)	System Range (m/s)
4uv	3.81	84	73.4	73.39	275
5uv	3.81	89	73.3	74.13	275
6uv	3.64	110	73.4	75.61	150
7uv	3.76	91	73.7	80.15	150
8uv	3.84	61	73.6	75.98	100
9uv	3.40	12.42	74.3	81.06	12
11uv	3.74	9.57	74.02	74.13	6
21uv	3.85	31	73.70	101.05	80
22uv	3.50	20.1	75.51	90.73	12
23uv	3.45	11.7	74.95	111.06	6
24uv	3.42	11.99	73.92	115.26	6
61uv	3.40	12.67	75.1	78.90	6

3 Collapse phenomena

3.1 Motion

Collapse-induced histories of the stemming motion measured on the ISLAY event are shown in figures 3.1-3.6. Station 21 (figure 3.1) is shown for completeness: the motion data are clearly invalid, giving only timing of signal loss. The oscillations between the NATEL groups of VCO's introduced noise in the velocimeter channels, reducing their reliability. The velocity gauge data are, never the less, shown in figures 3.2-3.6 along with the corresponding accelerometer data. Notable is the onset of collapse at station 22, the formation coupling plug (figure 3.2). This occurs at about 4211 s, the same time as it occurs at station 11, the top of the emplacement pipe (figure 3.5). Strongly suggested is that the emplacement pipe remained a solid unit between the formation coupling plug and the surface and fell as a unit with the formation. Comparing figures 3.4 and 3.5, the top of the emplacement pipe reached nearly its full downward excursion (greater than 4 m) before the top plug began to move.

Collapse reached the ground surface 4213 s after detonation with slap-down occurring about 2 s later. See figure 3.6.

3.2 Radiation and Pressure

Pressure and radiation histories recorded during the 20 s of the collapse activity are shown in figures 3.7 - 3.14. All stations below the formation coupling plug show a drop in pressure indicating a stemming fall preceding the loss of signal. The loss of signal was abrupt at all stations above the formation coupling plug with the exception of the station just below the top plug (which survived collapse - station 40, figure 3.14). This suggests cable breakage, possibly due to the movement of the emplacement pipe before the stemming moved.

An change in radiation corresponding in time to the decrease in pressure is seen at all stations below the formation coupling plug with the greatest change being seen at the stations at or below the fines layer (figures 3.7-3.9).

Progression of the collapse is shown in figure 3.15 by the position of the broken ends of the CLIPER cable and pressure histories. Pressure records show the position of the onset of collapse to move uniformly up the hole to the elevation of the formation coupling plug. Above this, the signals that were lost were apparently lost by a mechanism other than stemming fall. The CLIPER record is surprising in that it should have broken with the instrumentation cables with which it was mounted.

CLIPER station 91, mounted on the emplacement pipe and diagnostics canister, gave no usable information.

D-cable information is not in a form that is usable to investigate the progression of the cavity collapse.

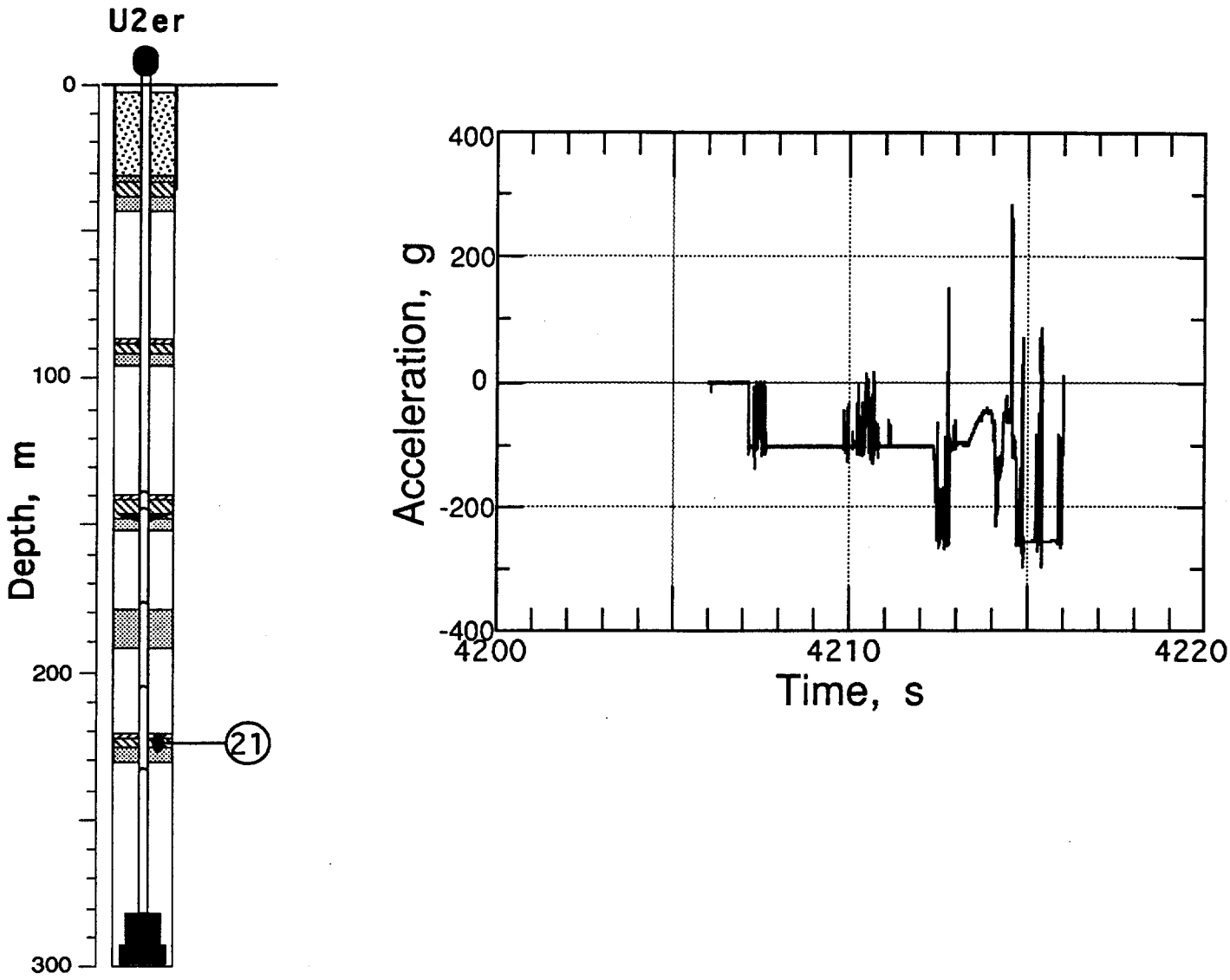

Figure 3.1 Collapse-induced vertical motion of the bottom rigid plug (station 21, at a depth of 223.7 m).

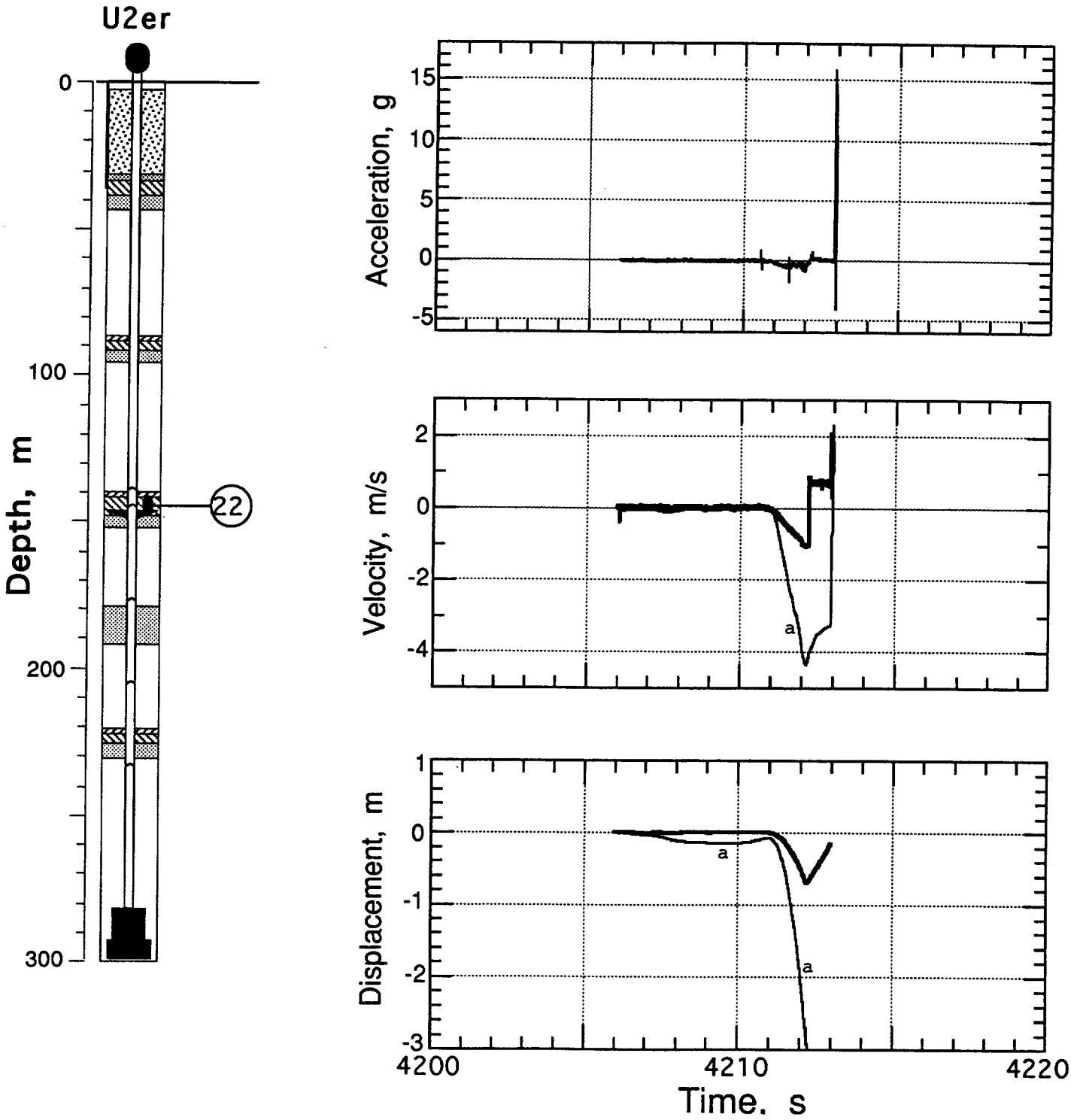

Figure 3.2 Collapse-induced vertical motion of the second rigid plug (station 22, at a depth of 144.6 m). The acceleration at early time shows strong motion induced by the emplacement pipe and the drag ring. Traces annotated with "a" are derived from the accelerometer data.

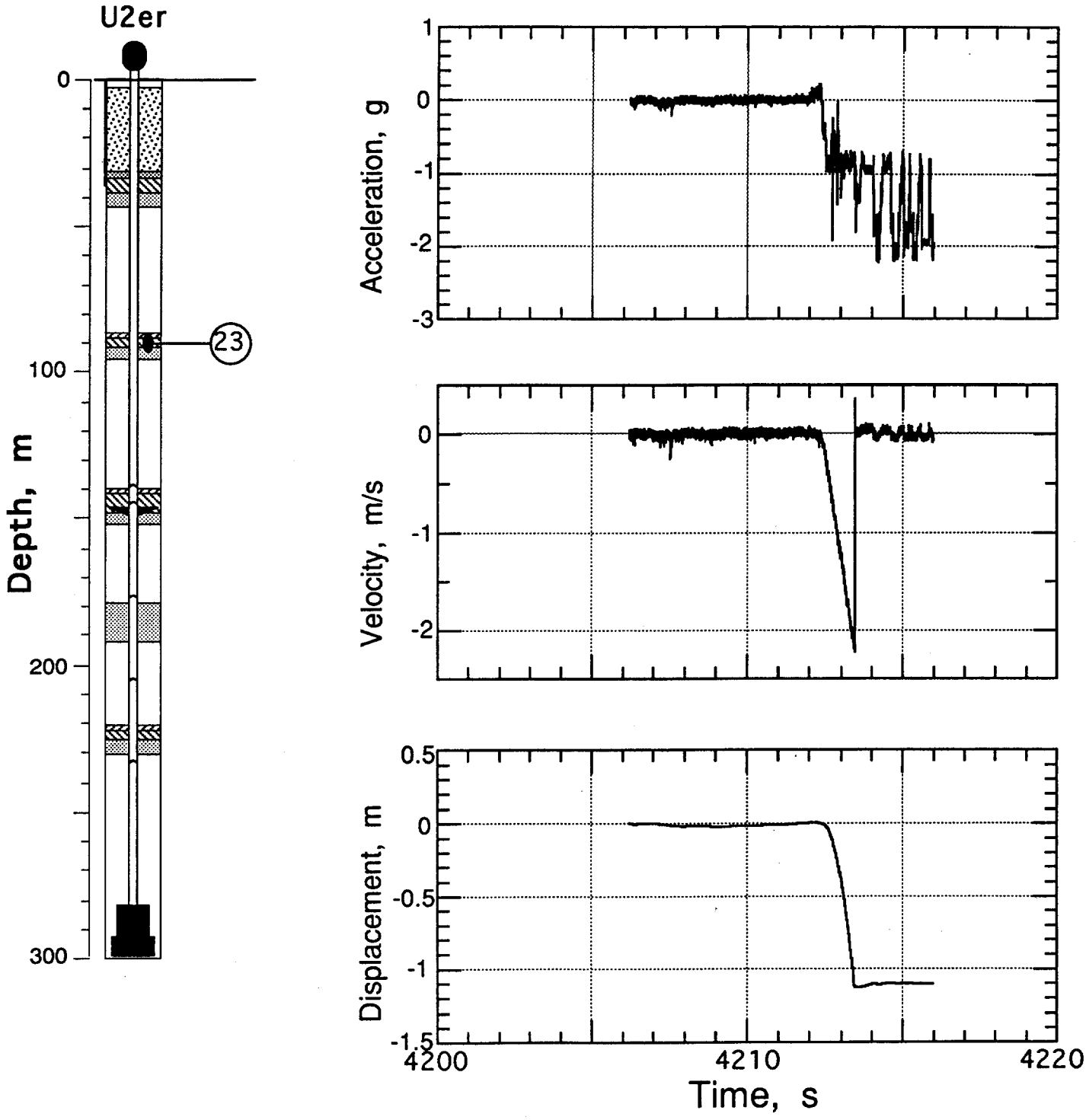

Figure 3.3 Collapse-induced vertical motion of the third rigid plug (station 23, at a depth of 89.6 m). All motion is derived from the accelerometer channel. Electronic cycling between the VCO groups is evident in the noise following collapse. Displacement is derived from the velocity gauge data only.

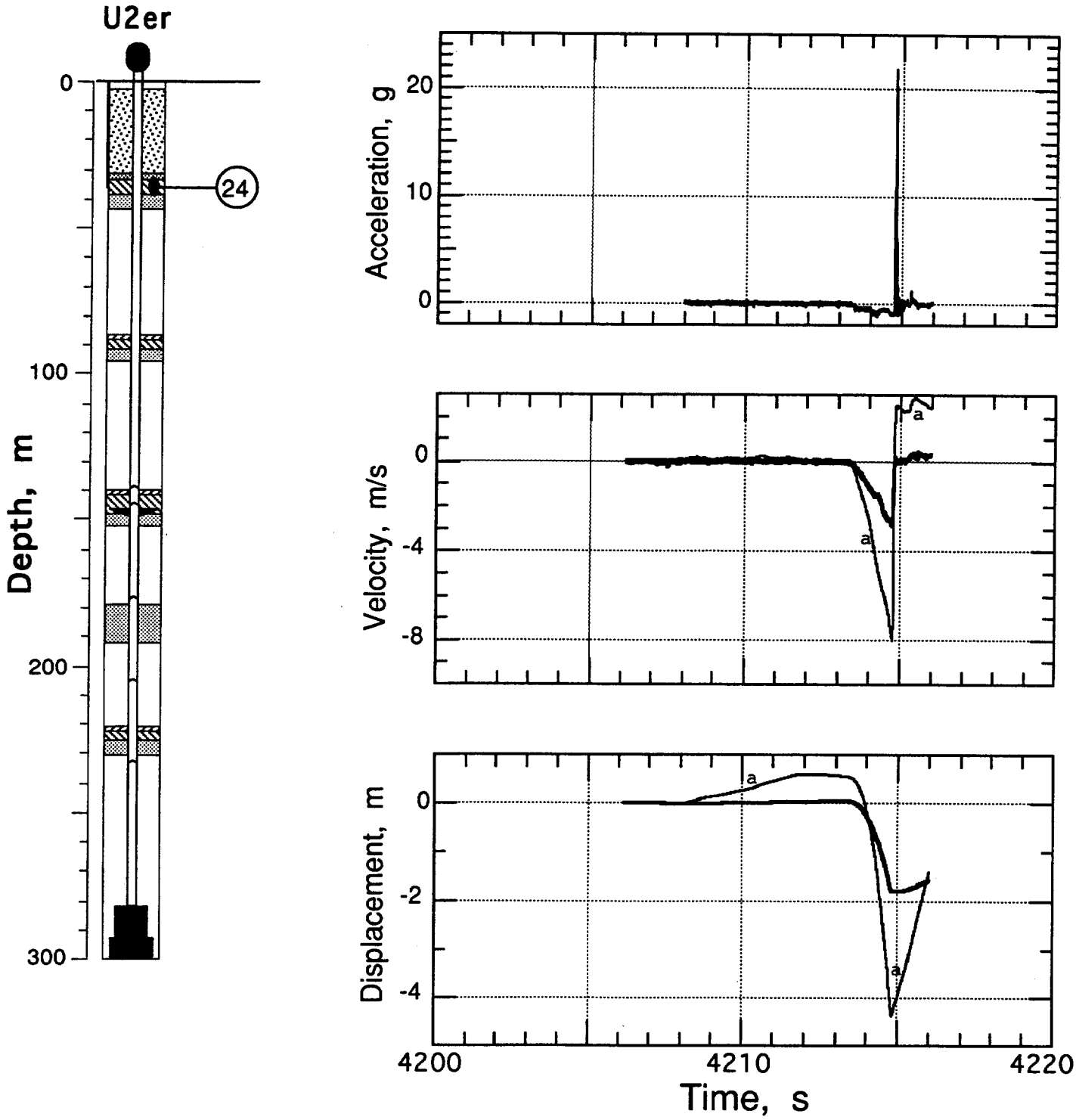

Figure 3.4 Collapse-induced vertical motion of the top plug (station 24, at a depth of 35.7 m). All motion is derived from the accelerometer channel. Traces annotated with "a" are derived from the accelerometer data.

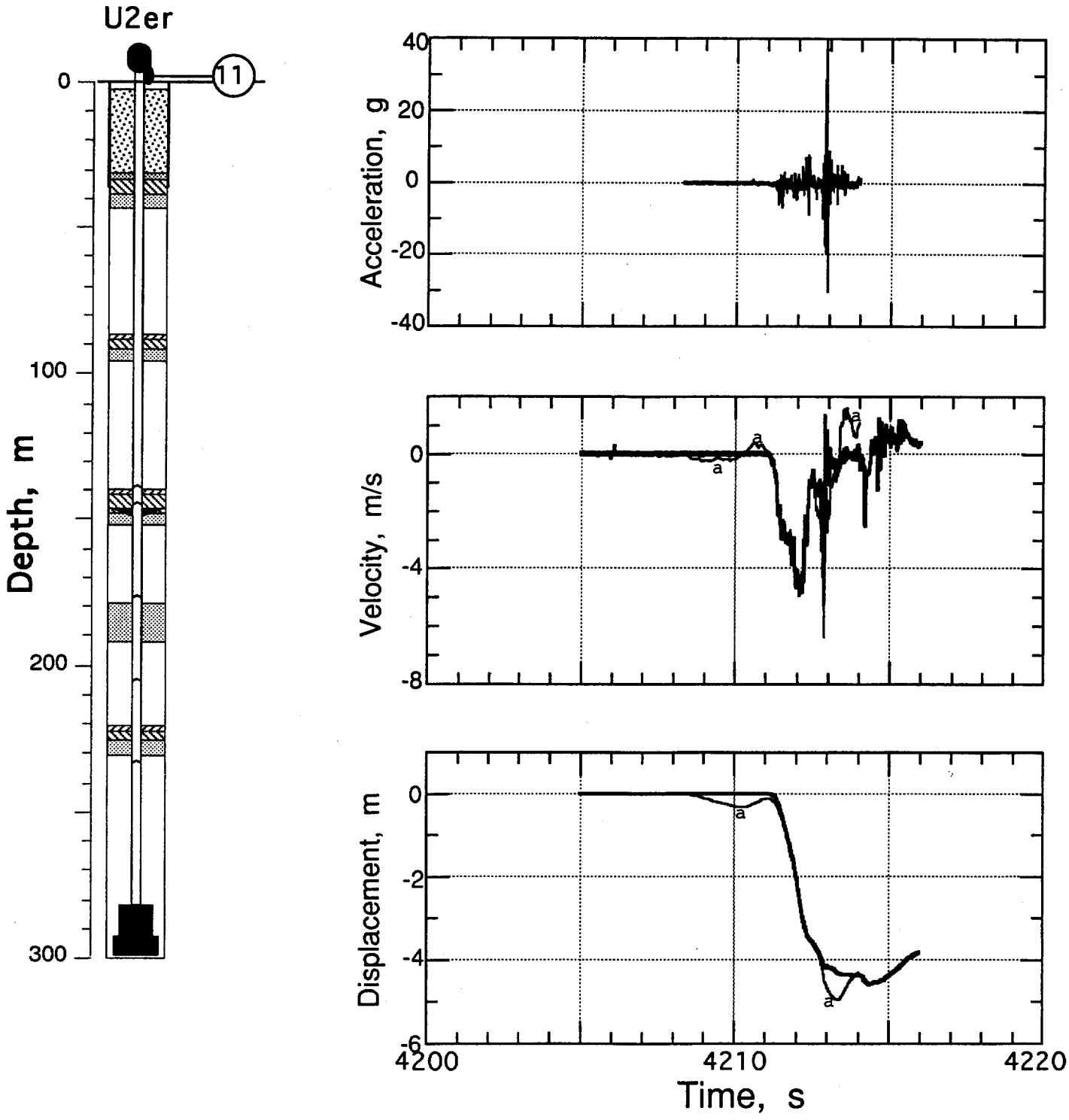

Figure 3.5 Collapse-induced vertical motion of the emplacement pipe (station 11, on the pipe 1.9 m above ground level but below the ball valve). Traces annotated with "a" are derived from the accelerometer data.

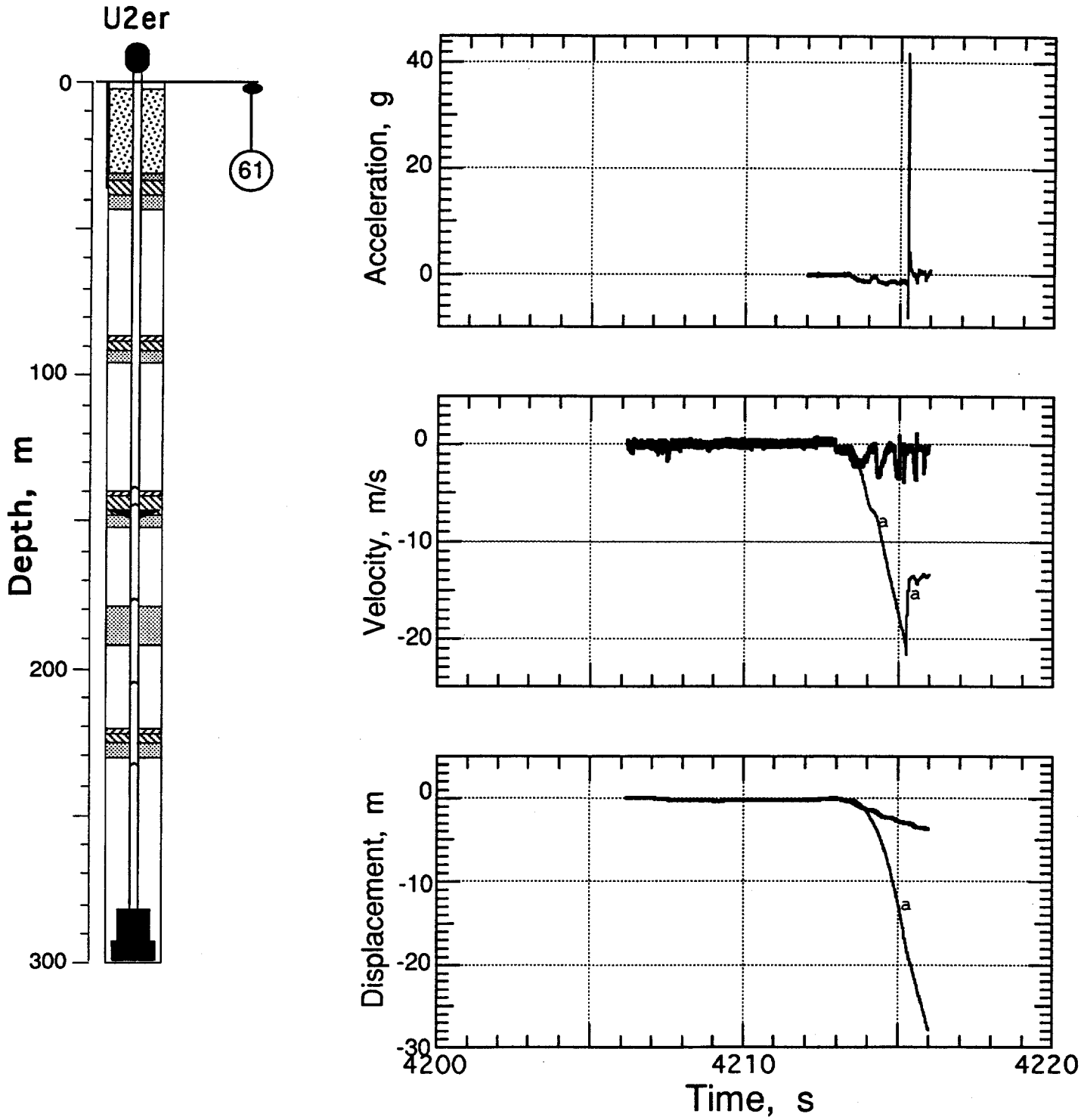

Figure 3.6 Collapse-induced vertical motion of the ground surface at a depth of 0.9 m and horizontal range of 15.24 m (station 61). Electronic cycling between the VCO groups is evident in the noise following collapse. Traces annotated with "a" are derived from the accelerometer data.

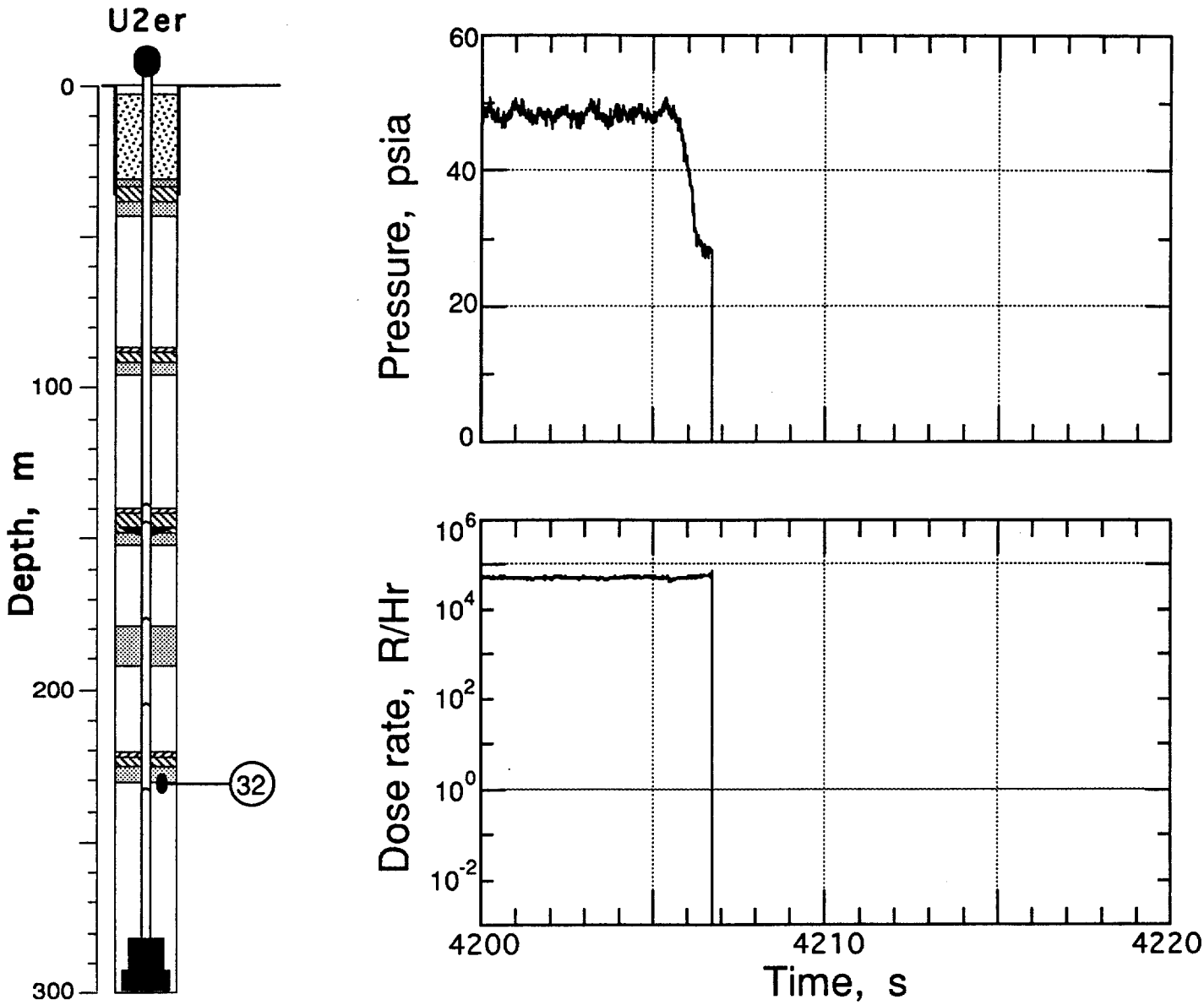

Figure 3.7 Collapse epoch pressure and radiation as monitored in the coarse stemming below the deepest rigid plug (station 32 at a depth of 231.3 m).

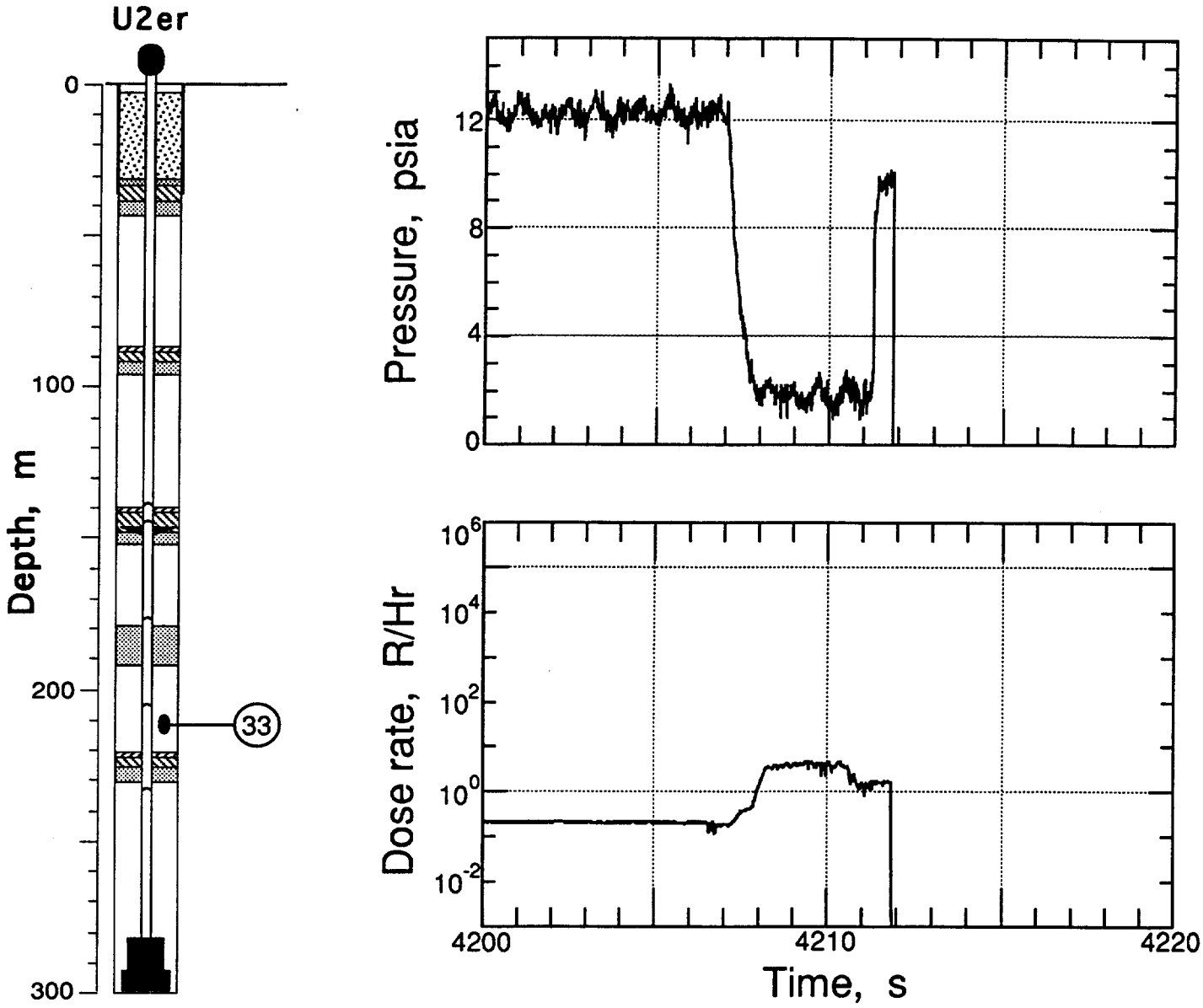

Figure 3.8 Collapse epoch pressure and radiation as monitored in the coarse stemming above the deepest rigid plug (station 33 at a depth of 211.5m).

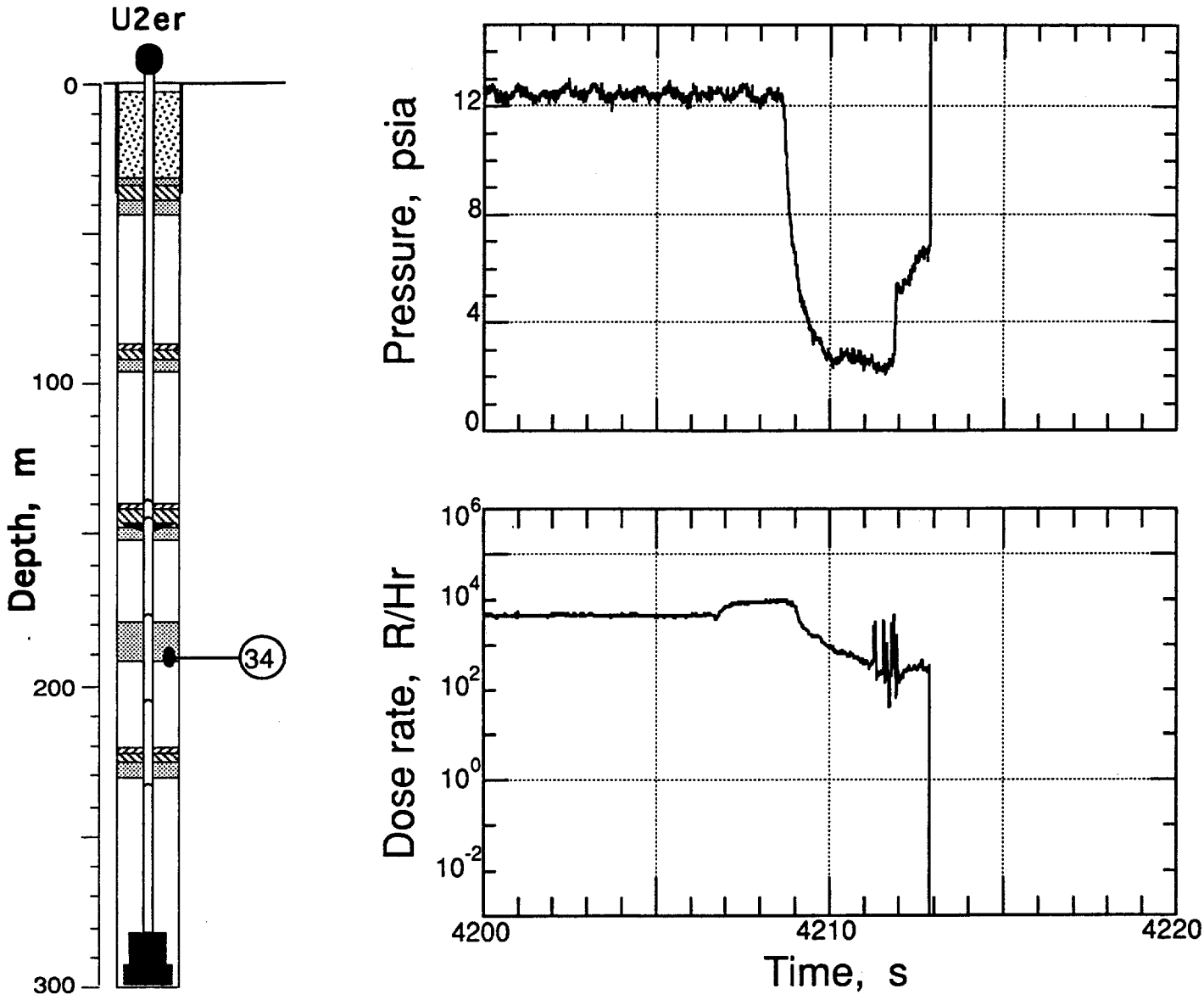

Figure 3.9 Collapse epoch pressure and radiation measured in the coarse stemming below the fines layer (station 34 at a depth of 191.1 m).

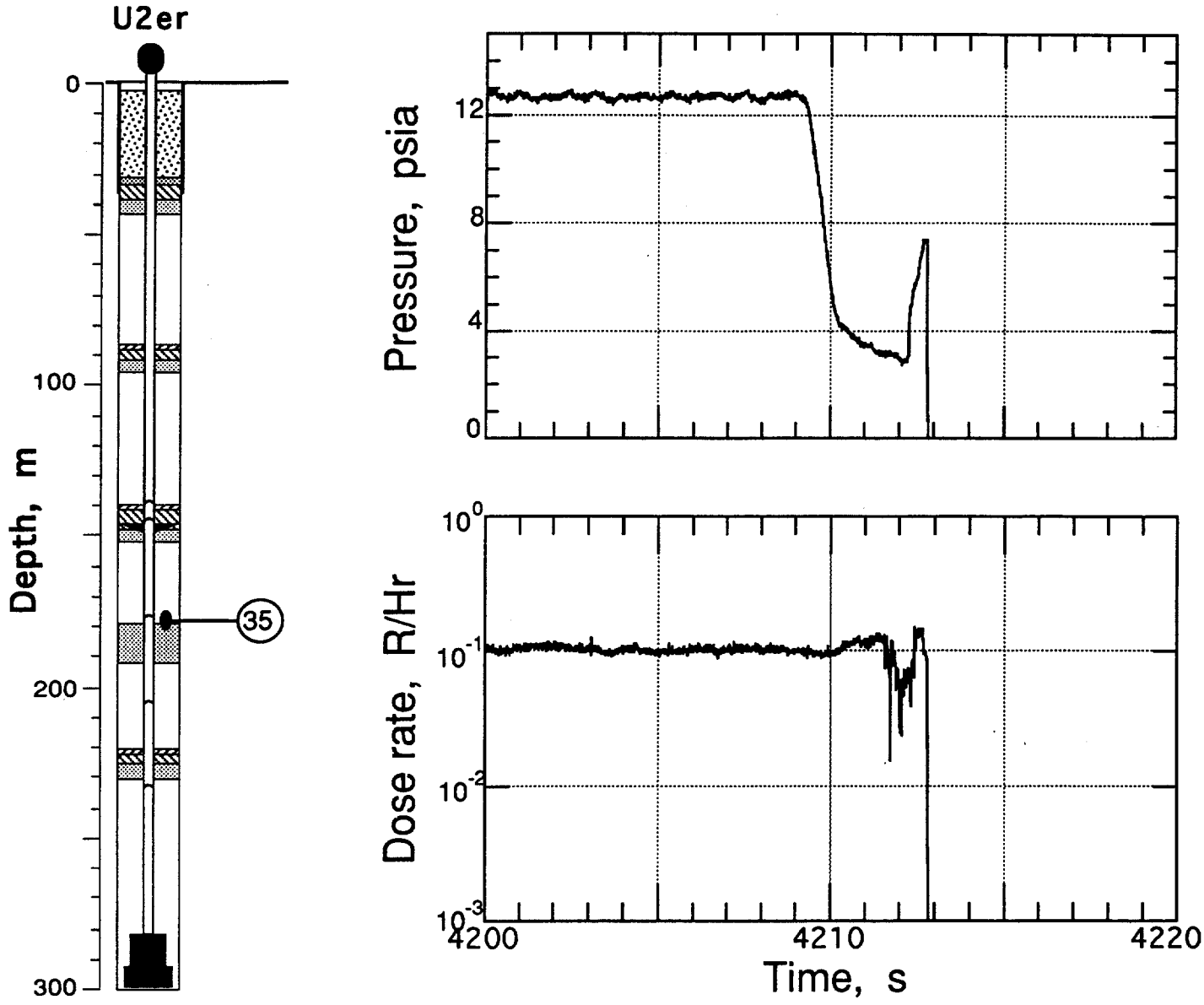

Figure 3.10 Collapse epoch pressure and radiation measured in the coarse stemming above the fines layer (station 35 at a depth of 176.5 m).

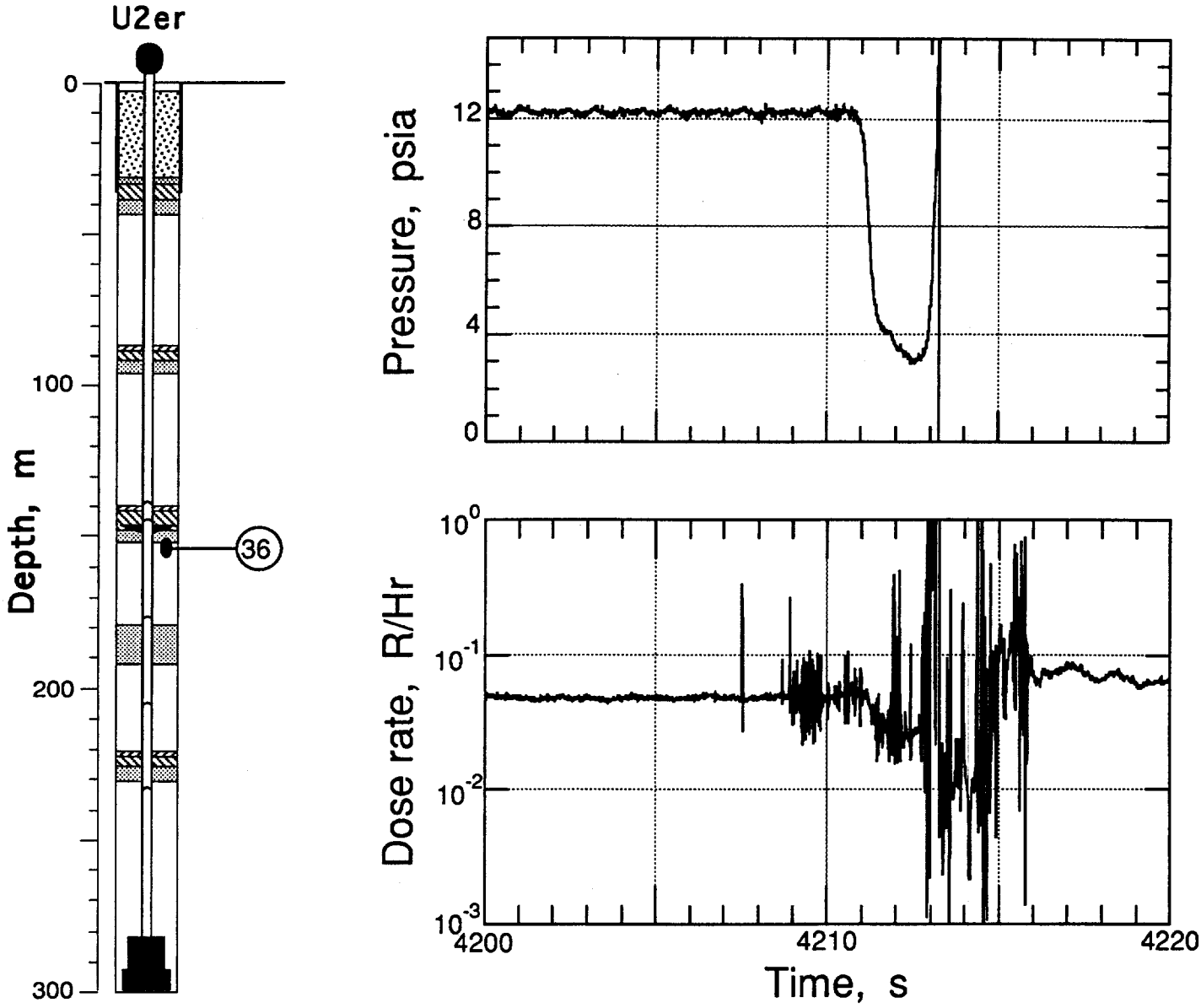

Figure 3.11 Collapse epoch pressure and radiation measured in the coarse stemming beneath the formation coupling plug (station 36 at a depth of 153.2 m).

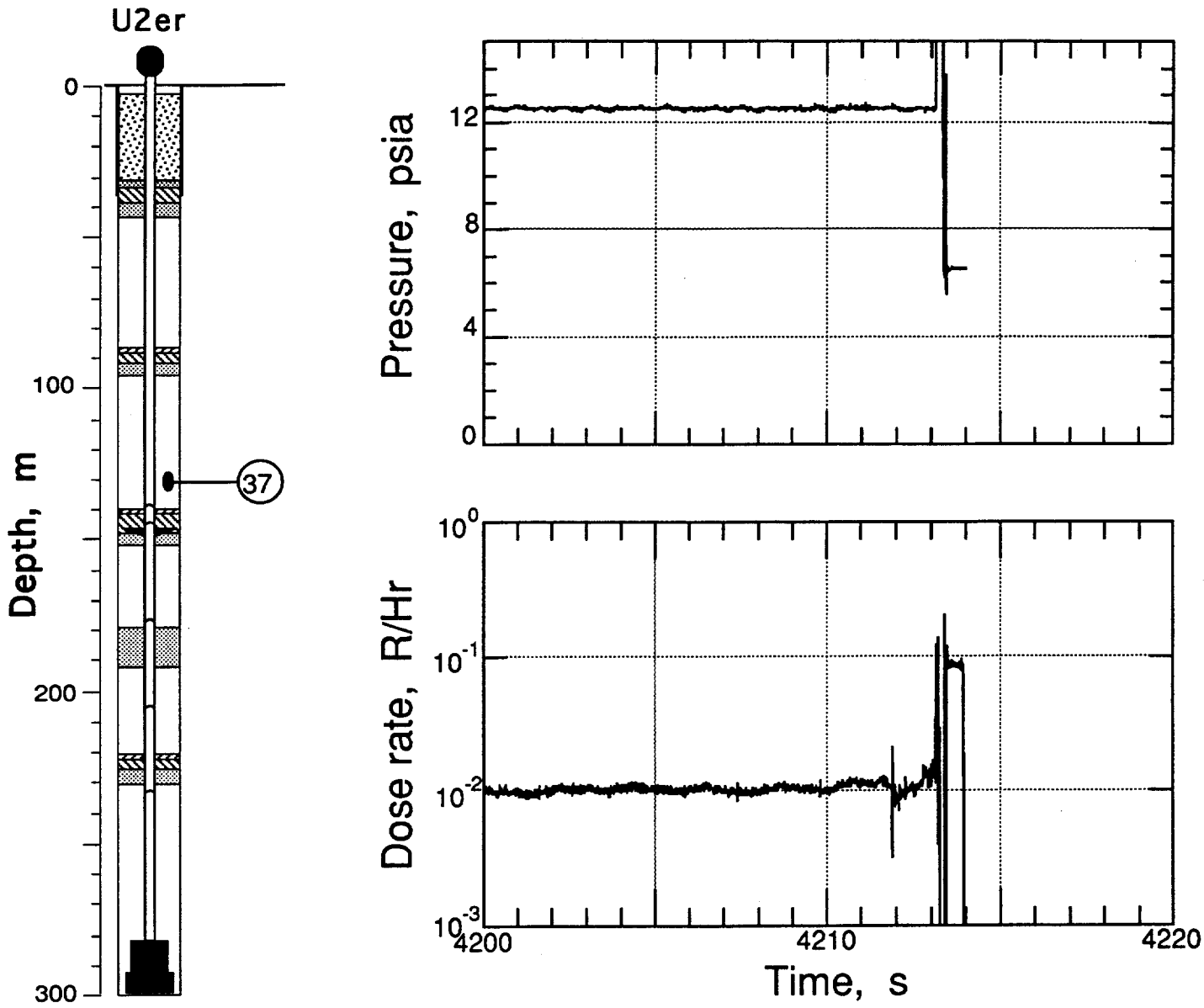

Figure 3.12 Collapse epoch pressure and radiation measured in the coarse stemming above the formation coupling plug (station 37 at a depth of 130.7 m).

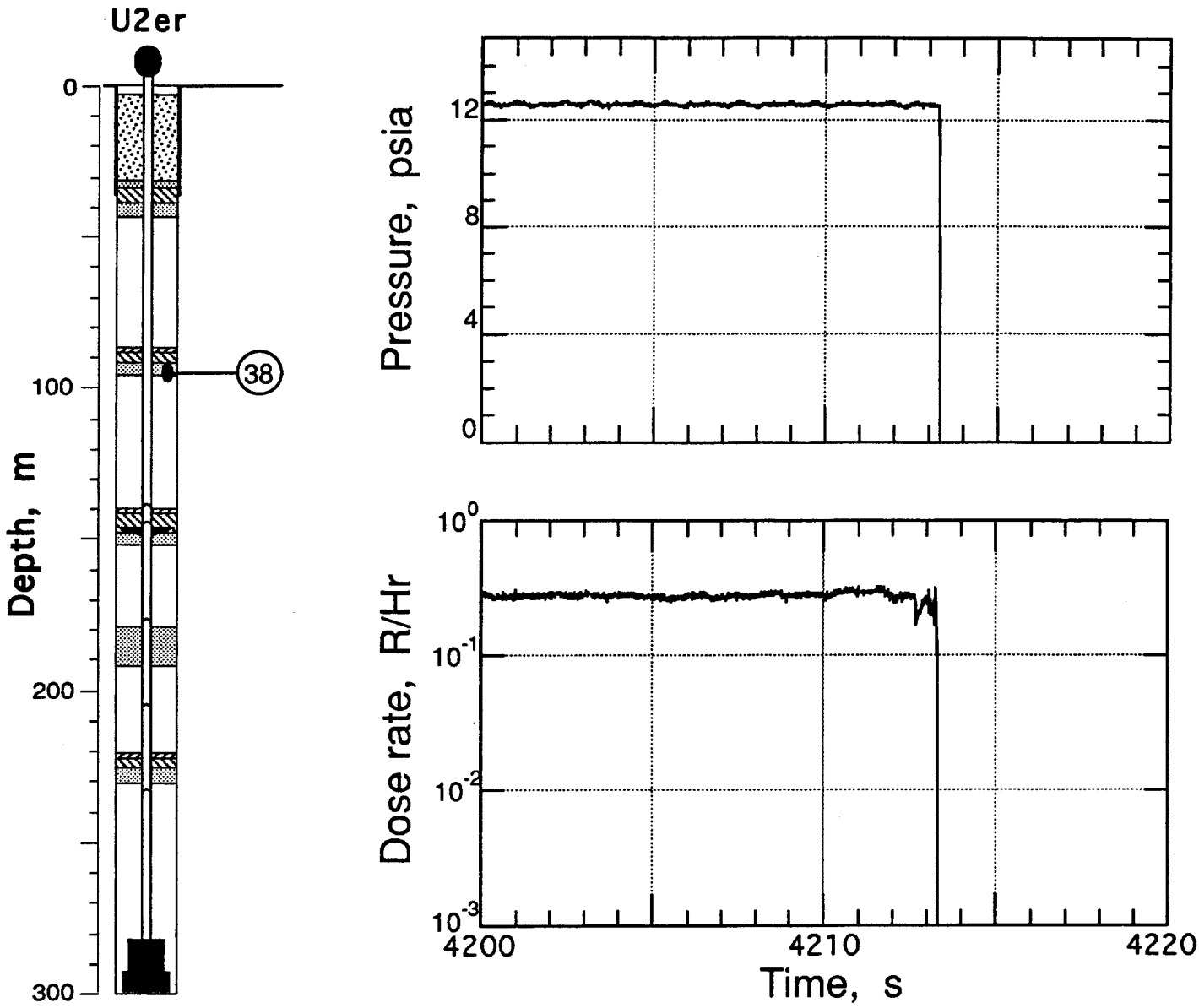

Figure 3.13 Collapse epoch pressure and radiation measured in the coarse stemming below the third plug (station 38 at a depth of 95.1 m).

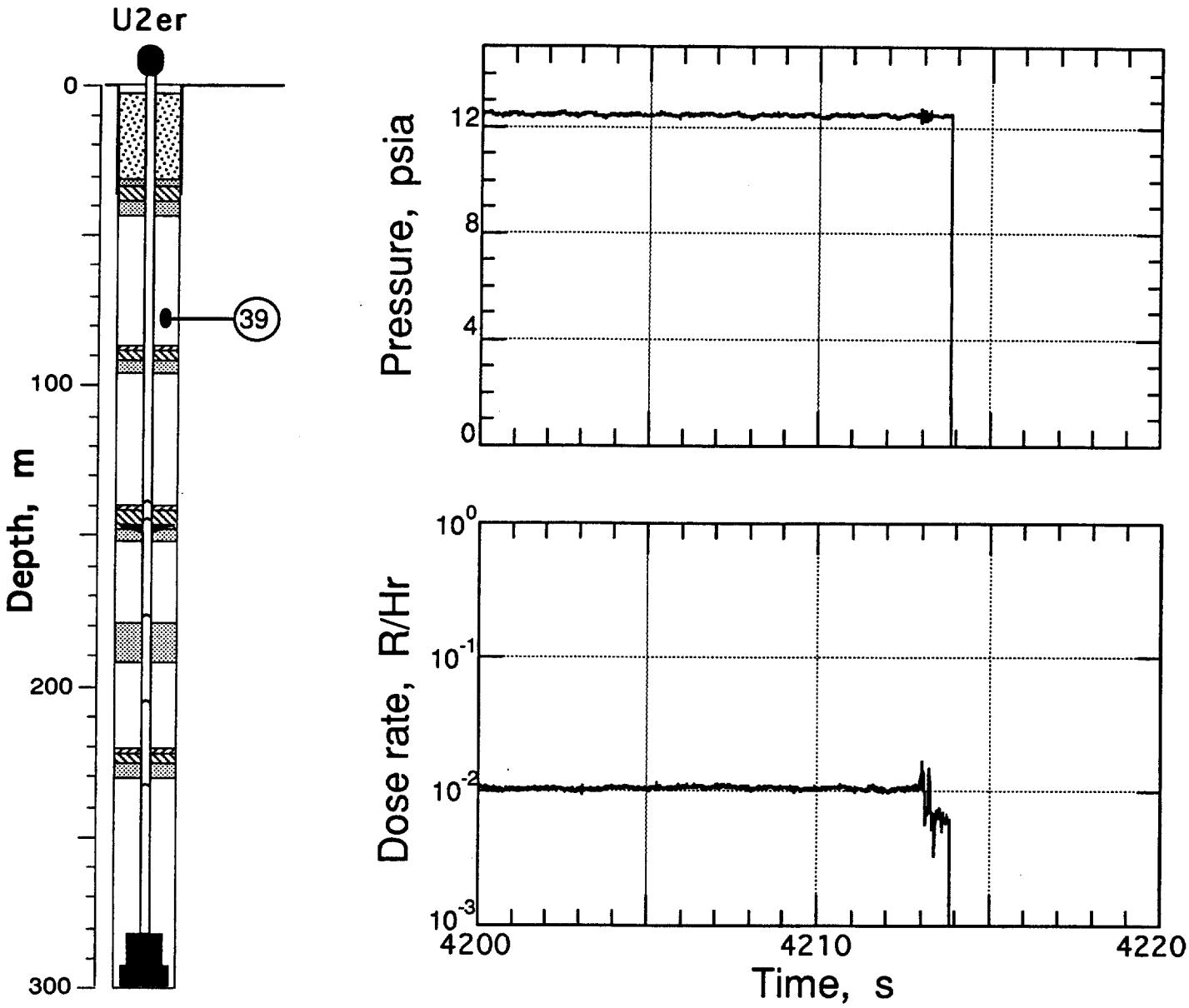

Figure 3.14 Collapse epoch pressure and radiation measured in the coarse stemming above the third plug (station 39 at a depth of 77.4 m).

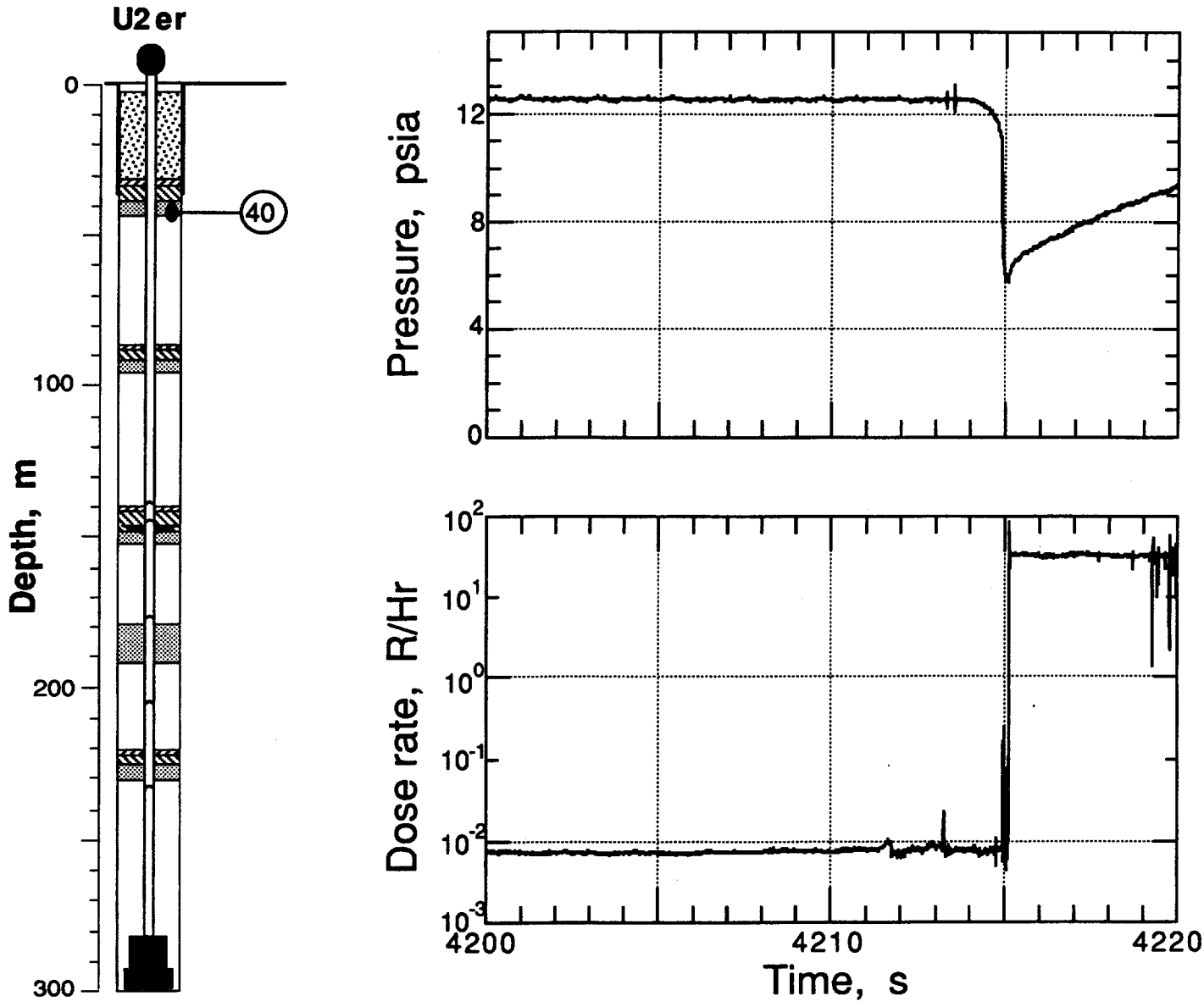

Figure 3.15 Collapse epoch pressure and radiation measured in the coarse stemming beneath the top plug (station 40 at a depth of 42.1 m).

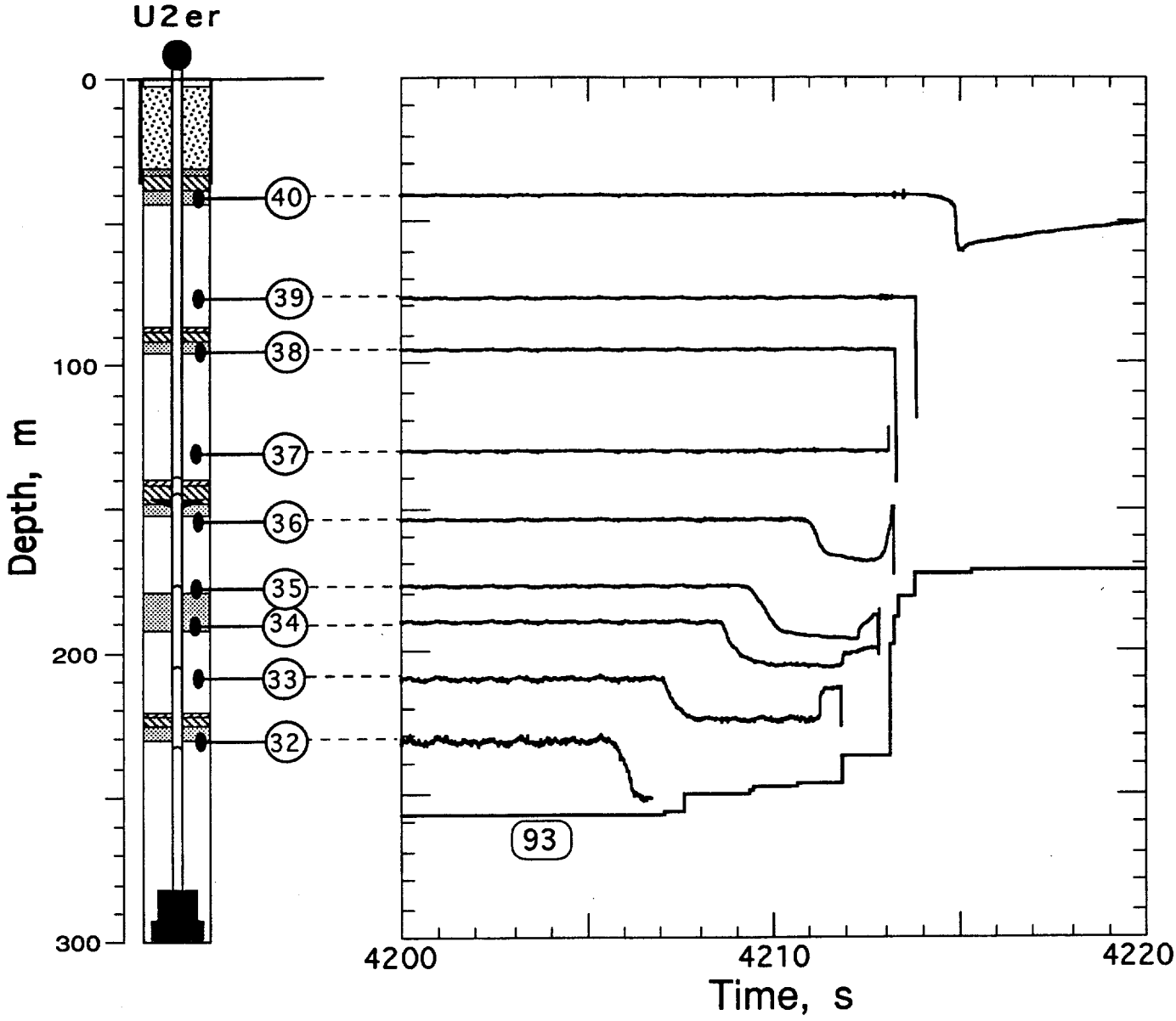

Figure 3.16 Progression of collapse as shown by the position of the break in the CLIPER cable on the instrumentation pendant (station 93). Also shown are representative pressure wave forms. Pressure histories at stations below the formation coupling plug indicate a stemming fall before cable station loss while above that plug, the loss of signal is suggestive of a cable breakage at the time of the drop of the formation coupling plug. For magnitudes of the pressure drops see figures 3.7-3.14.

4 Measurements on the Emplacement Pipe

4.1 Motion

Vertical motion of the emplacement pipe was monitored at elevations below each of the four deepest pressure domes below the formation coupling plug. Three additional motion stations were fielded on the pipe at the location of the deepest pressure dome, the detector plate and near the top of the pipe below the ball valve. Motion histories obtained at these locations are shown in figures 4.1-4.7. Peak motion values and transducer characteristics are given in tables 3.1-3.3.

Just below the deepest pressure dome (station 4, figure 4.1) and at it (station 5, figure 4.2) there was little correlation between the histories measured by the velocity gauge and accelerometer after the first 20 ms suggesting that the pipe, or at least the gauge mounts, were compromised at early time. Motion at all other stations on the pipe below the formation coupling plug (figures 4.3-4.5) indicate good correlation between acceleration and velocity at early times (prior to 0.2 s) but divergence at later times.

Station 9, on the pipe at the elevation of the detector plate (figure 4.6) closely matches the motion of station 22 (figure 2.21) indicating that the drag rings force the motion of the pipe to be the same as that of the formation coupling plug. It does not, however, match that of the pipe at station 8 (figure 4.5).

To insure that the line-of-sight for the neutron PINEX experiment remained open during emplacement, the pipe was supported from the top by break-away beams. The motion of the top of the pipe (station 11, figure 4.7) included noise contributions from the break-away beams and a major downward motion from the release of tension at about 20 ms.

4.2 Pressure, Temperature, and Radiation

Five sections of the emplacement pipe were sealed by pressure domes intended to retard and retain the gas pressure generated by the device. The top pressure dome included a recoverable neutron detector which was drawn up through the pipe beyond the ball valve which was then closed shortly after the shot. Each of the four deepest sealed sections was internally monitored for pressure and temperature and the resulting data are shown in figures 4.8-4.11.

Stations 4 and 6 just below the first and second pressure domes, respectively, (figure 4.8 and 4.9) were both instrumented with high and low sensitivity pressure gauges. The detected pressure was too low to be accurately measured by the low sensitivity sensors and it appears that only station 4 detected gas flow in the pipe. The temperature change in station 4 may have been due gas stagnation at the first pressure dome. A slight pressure jump of about 0.28 bar (4 psi) lasted for about 1.2 s at station 6 and there was no accompanying temperature change .

Station 7, just below the third pressure dome and above the fines layer (figure 4.10) shows a pressure rise of about 3 psi for the first 200 s and then a drop of about 8 psi in pressure beginning about 3000 s terminating with collapse. This suggests that the pipe section below the third pressure dome may have been in communication with the surrounding stemming, confirming the pipe rupture referred to in section 2.1.

Station 8, just below the formation coupling plug (figure 4.11) shows a slight downward drift in both pressure and temperature. No conclusions are made about these data.

The emplacement pipe was also instrumented for internal pressure and radiation at a station 11 in the top section at a depth of about 15 m. Histories of these measurements are shown in figure 4.12. No change from ambient background values are seen.

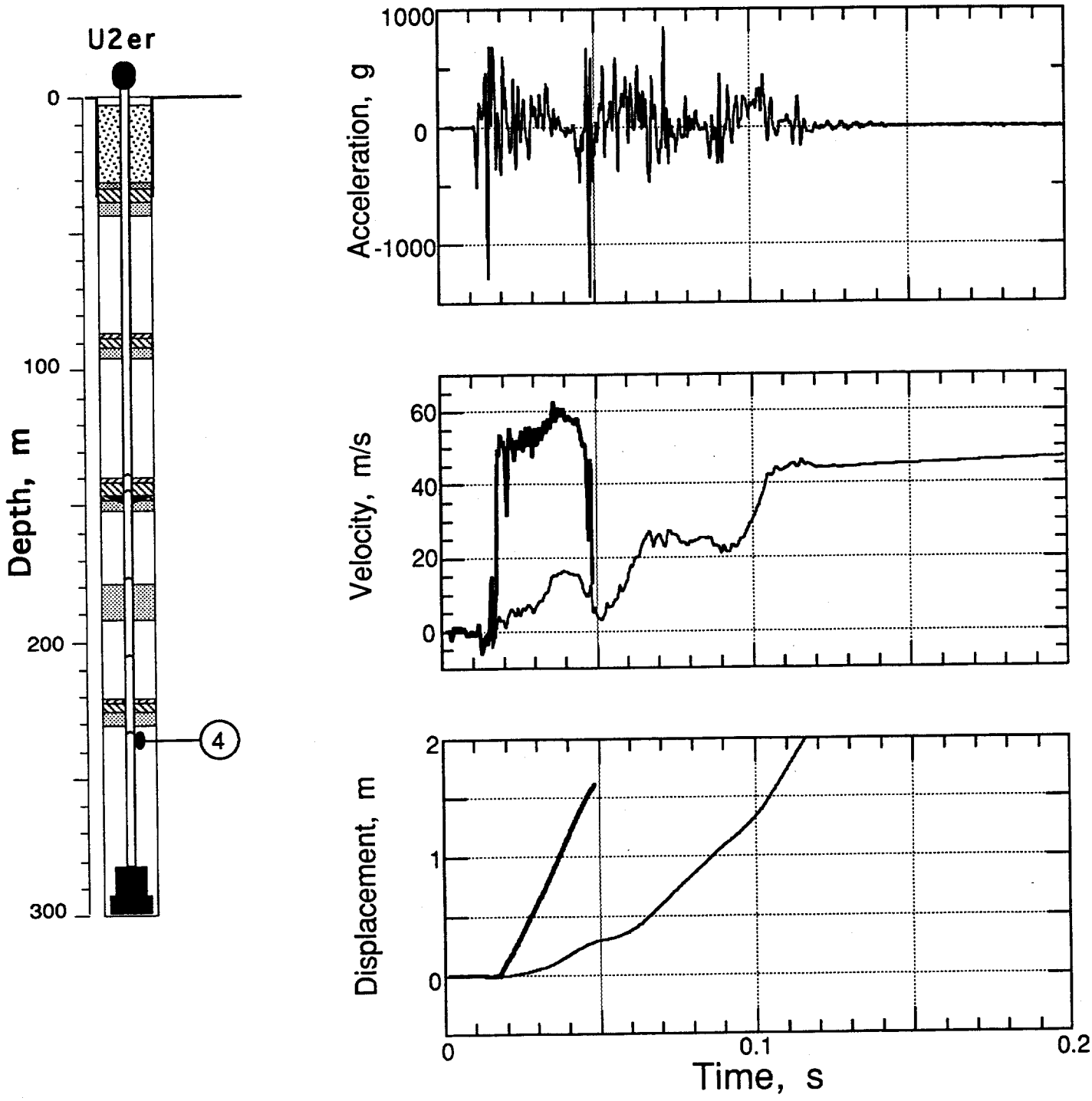

Figure 4.1 Vertical motion recorded on the emplacement pipe 2.7 m below the first pressure dome above the diagnostics canister (station 4 at a depth of 235.9 m). Heavy traces are the histories derived from the velocity gauge.

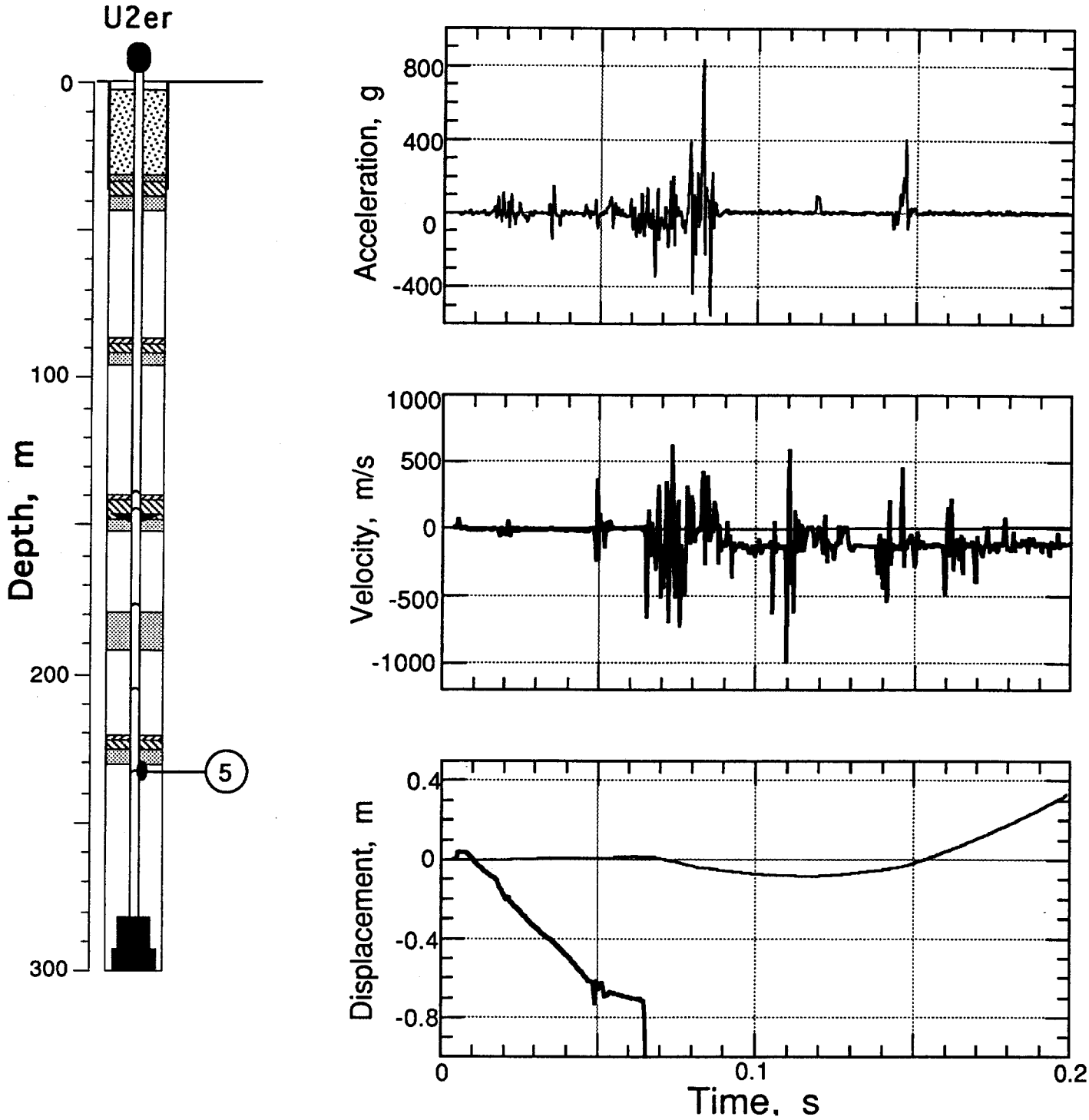

Figure 4.2 Vertical motion recorded on the emplacement pipe at the first pressure dome above the diagnostics canister (station 5 at a depth of 233.2 m). Heavy traces are the histories derived from the velocity gauge.

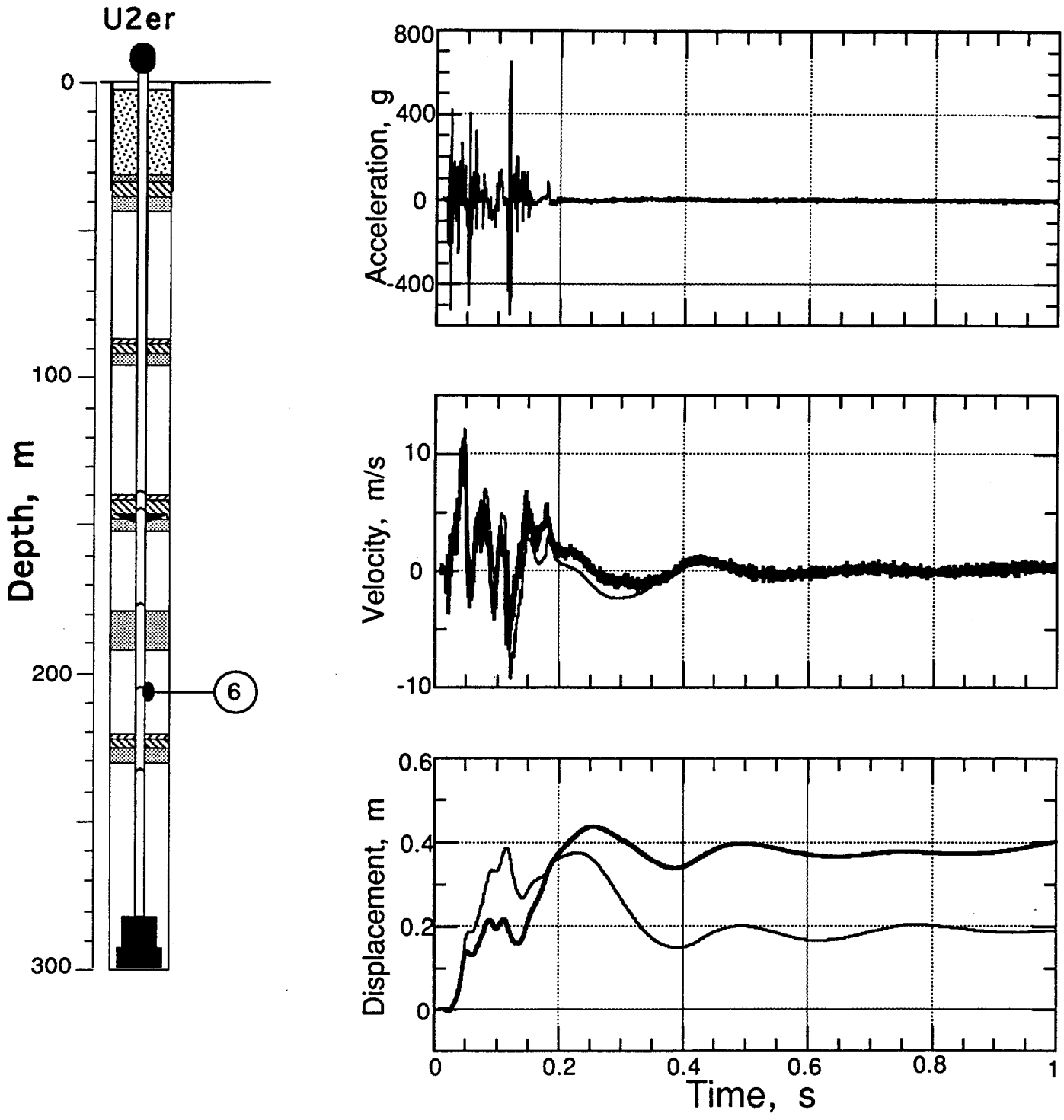

Figure 4.3 Vertical motion recorded on the emplacement pipe 1.6 m below the second pressure dome above the diagnostics canister (station 6 at a depth of 207.0 m). Heavy traces are the histories derived from the velocity gauge.

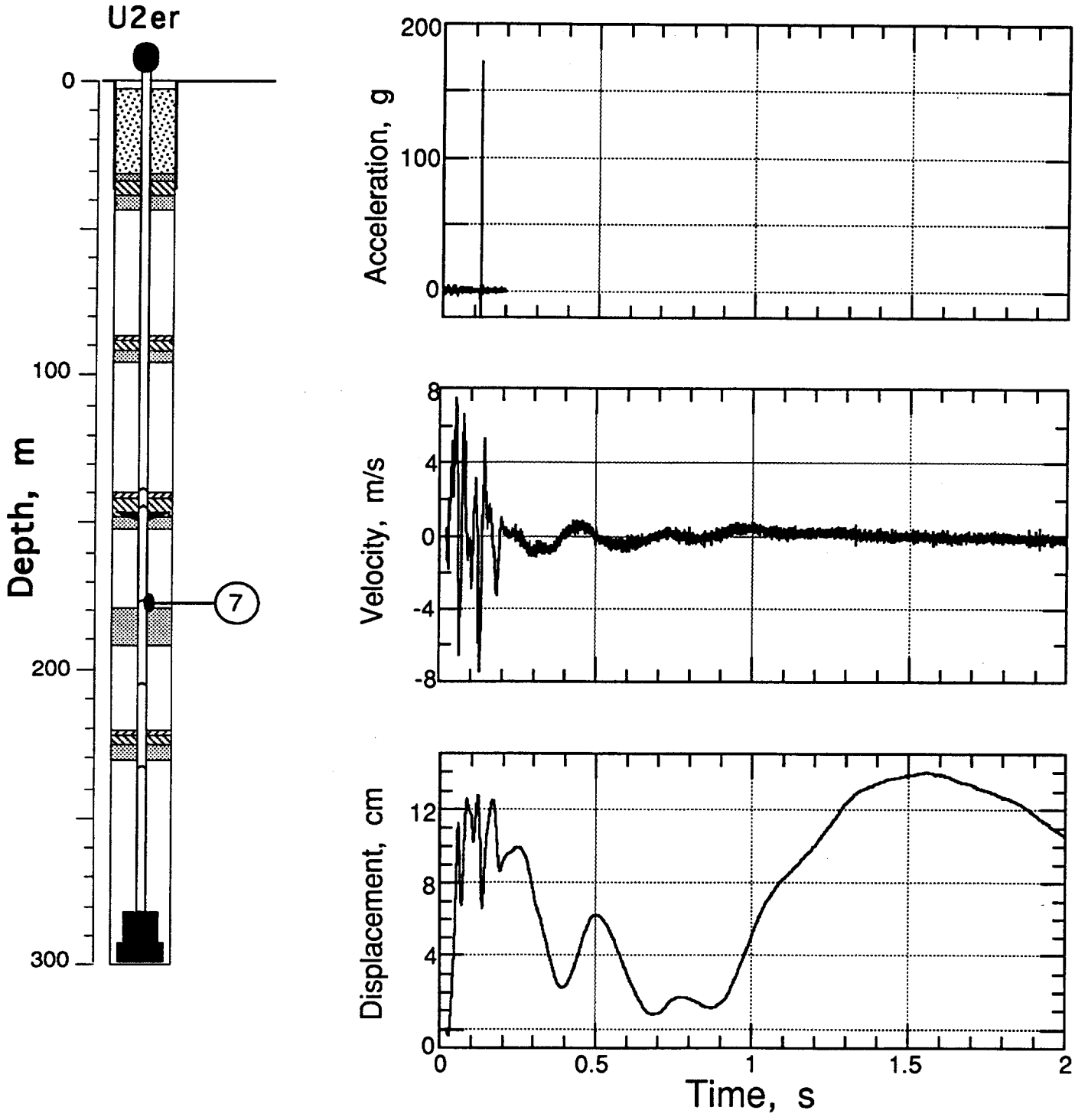

Figure 4.4 Vertical motion recorded on the emplacement pipe 1.6 m below the third pressure dome above the diagnostics canister (station 7 at a depth of 178.4 m). The accelerometer at this location failed pre-shot and is shown for completeness.

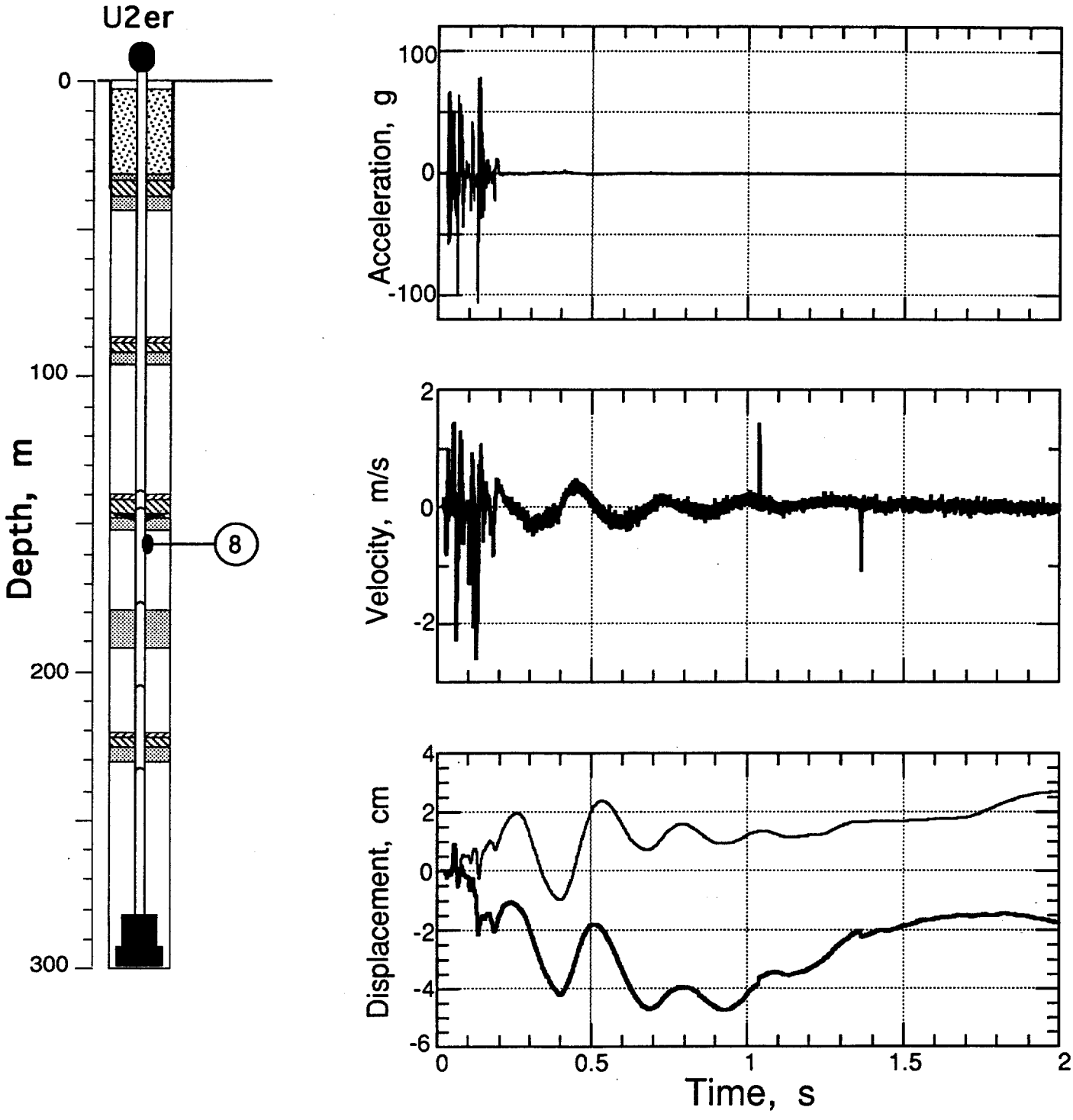

Figure 4.5 Vertical motion recorded on the emplacement pipe 10.9 m below the fourth pressure dome above the diagnostics canister (station 8 at a depth of 155.7 m). Heavy traces are the histories derived from the velocity gauge.

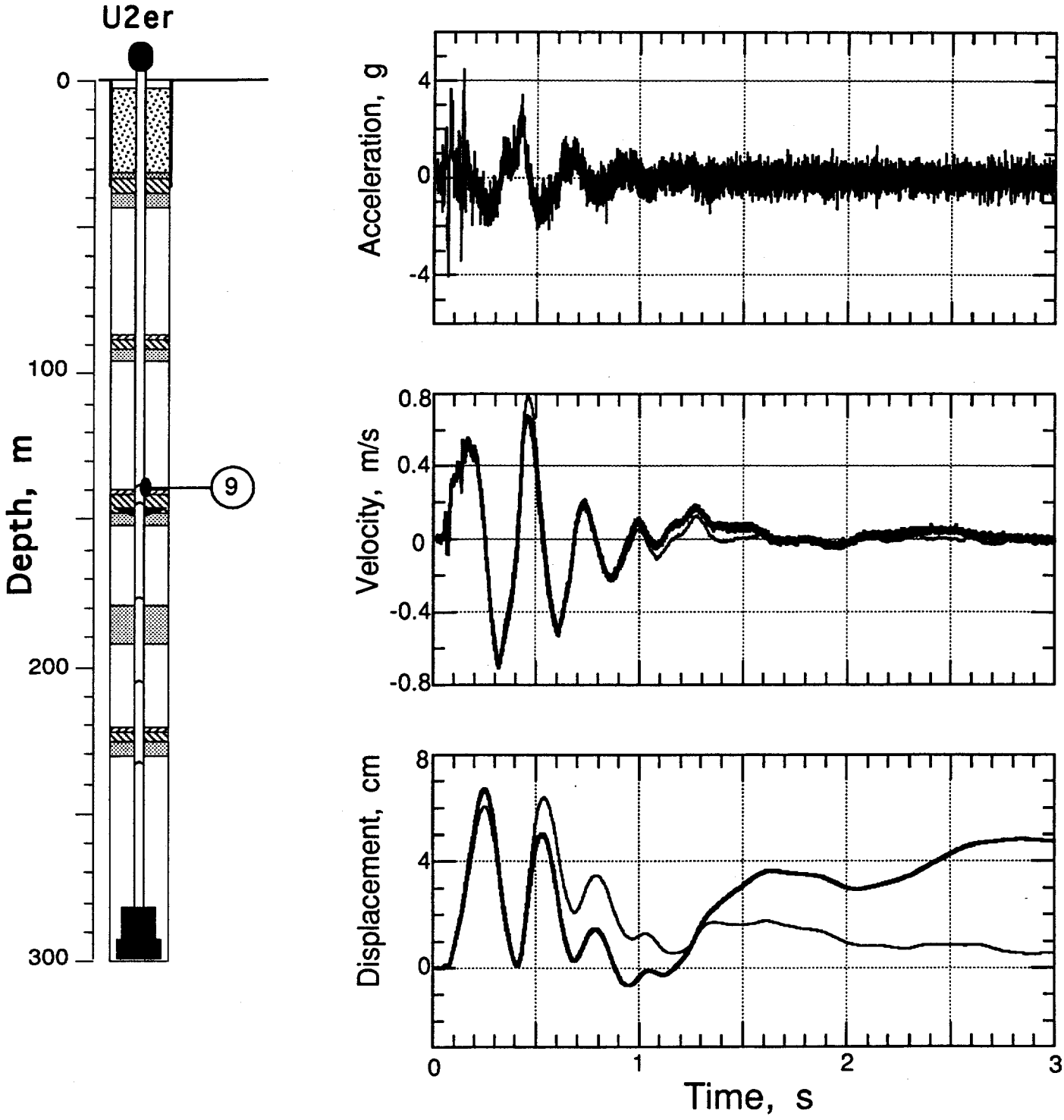

Figure 4.6 Vertical motion recorded on the emplacement pipe at the detector plate above the formation coupling plug (station 9 at a depth of 138.7 m). Heavy traces are the histories derived from the velocity gauge.

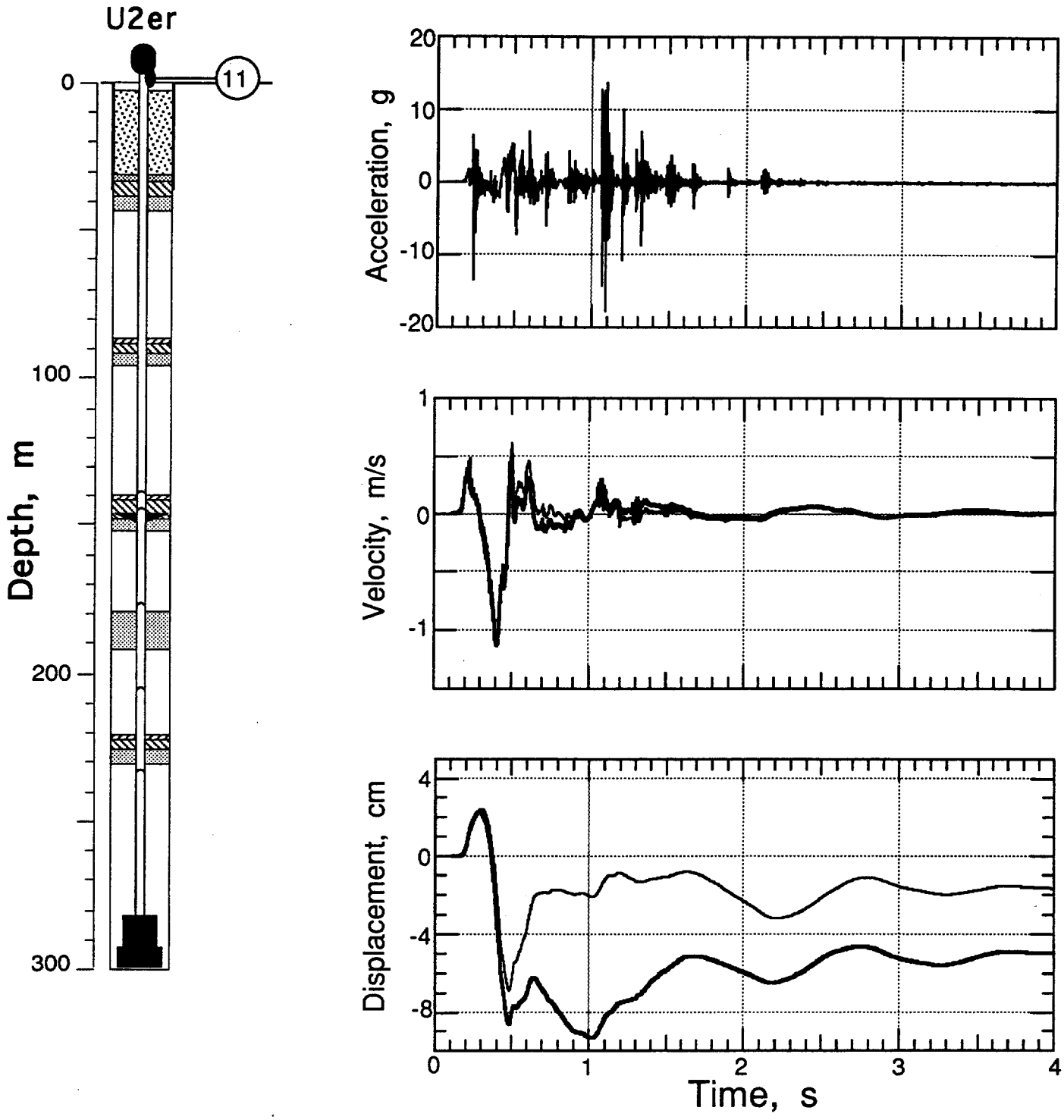

Figure 4.7 Vertical motion recorded on the emplacement pipe 1.9 m above ground and below the ball valve (station 11). Heavy traces are the histories derived from the velocity gauge.

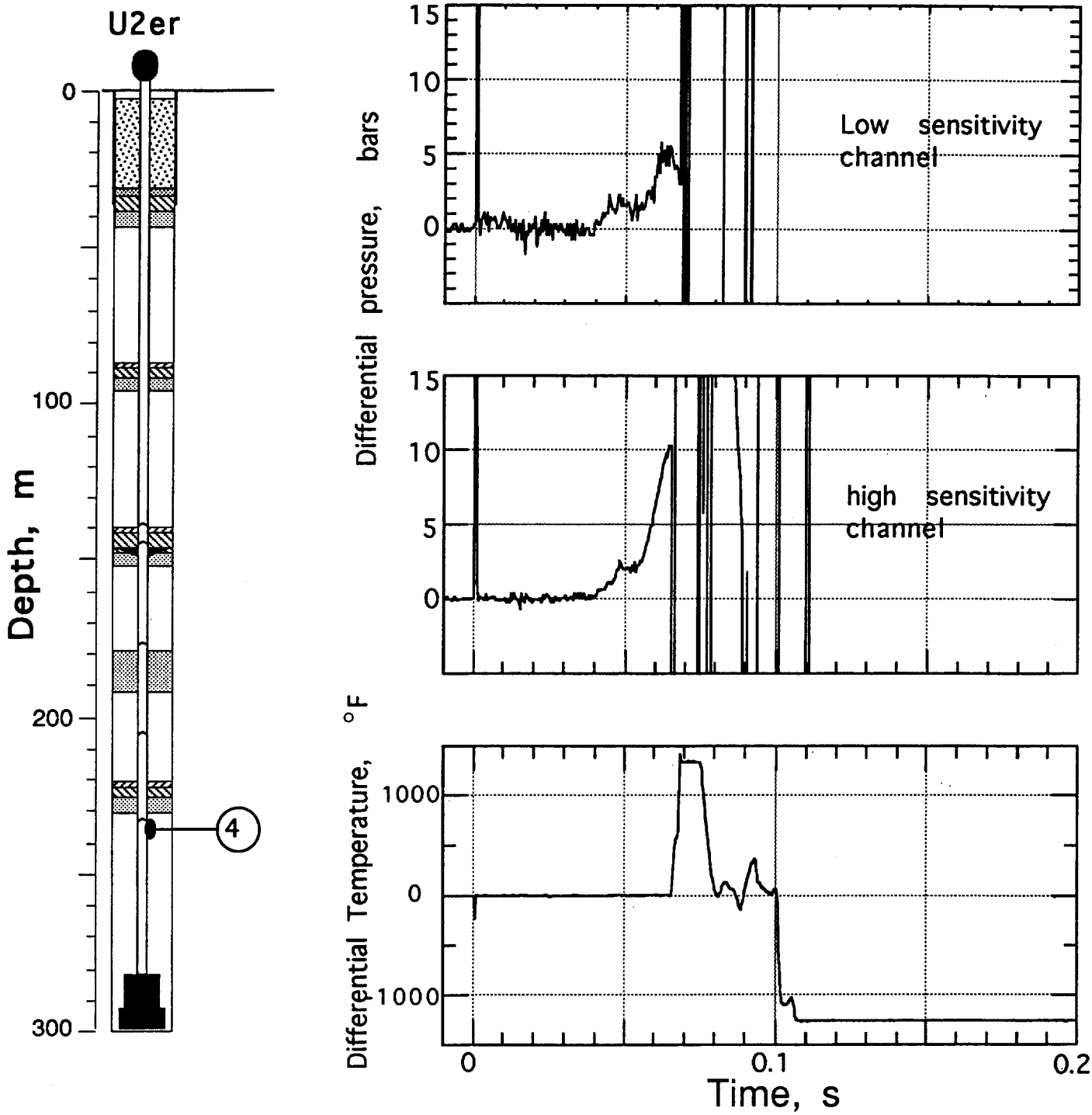

Figure 4.8 Pressure and temperature recorded in the emplacement pipe 2.7 m below the first pressure dome above the diagnostics canister (station 4 at a depth of 235.9 m). The low sensitivity pressure channel had a system range of 690 bars while the high sensitivity channel had a range of 210 bars.

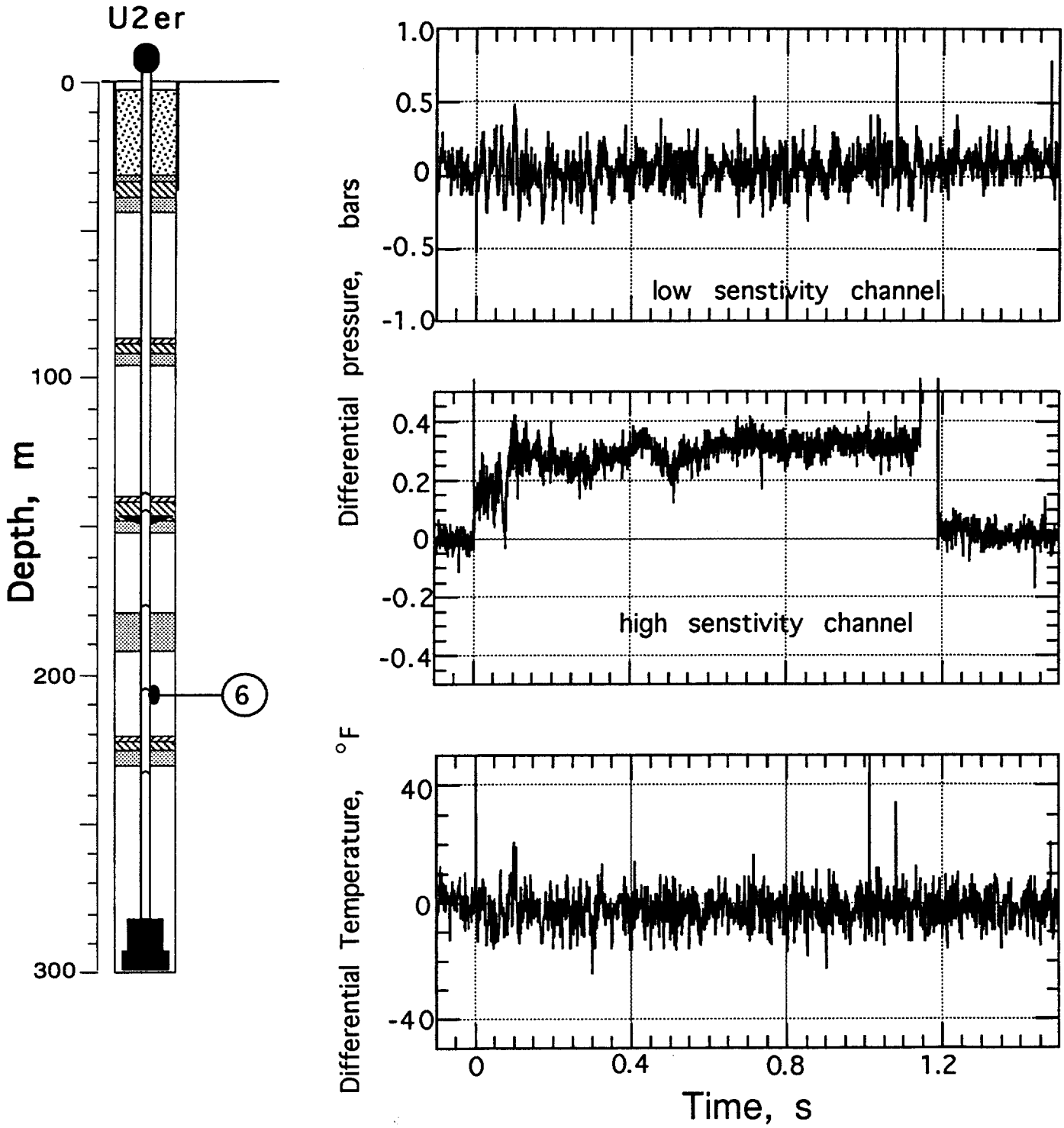

Figure 4.9 Pressure and temperature recorded in the emplacement pipe 1.6 m below the second pressure dome above the diagnostics canister (station 6 at a depth of 207.0 m). The low sensitivity pressure channel had a system range of 210 bars while the high sensitivity channel had a range of 1000 psi.

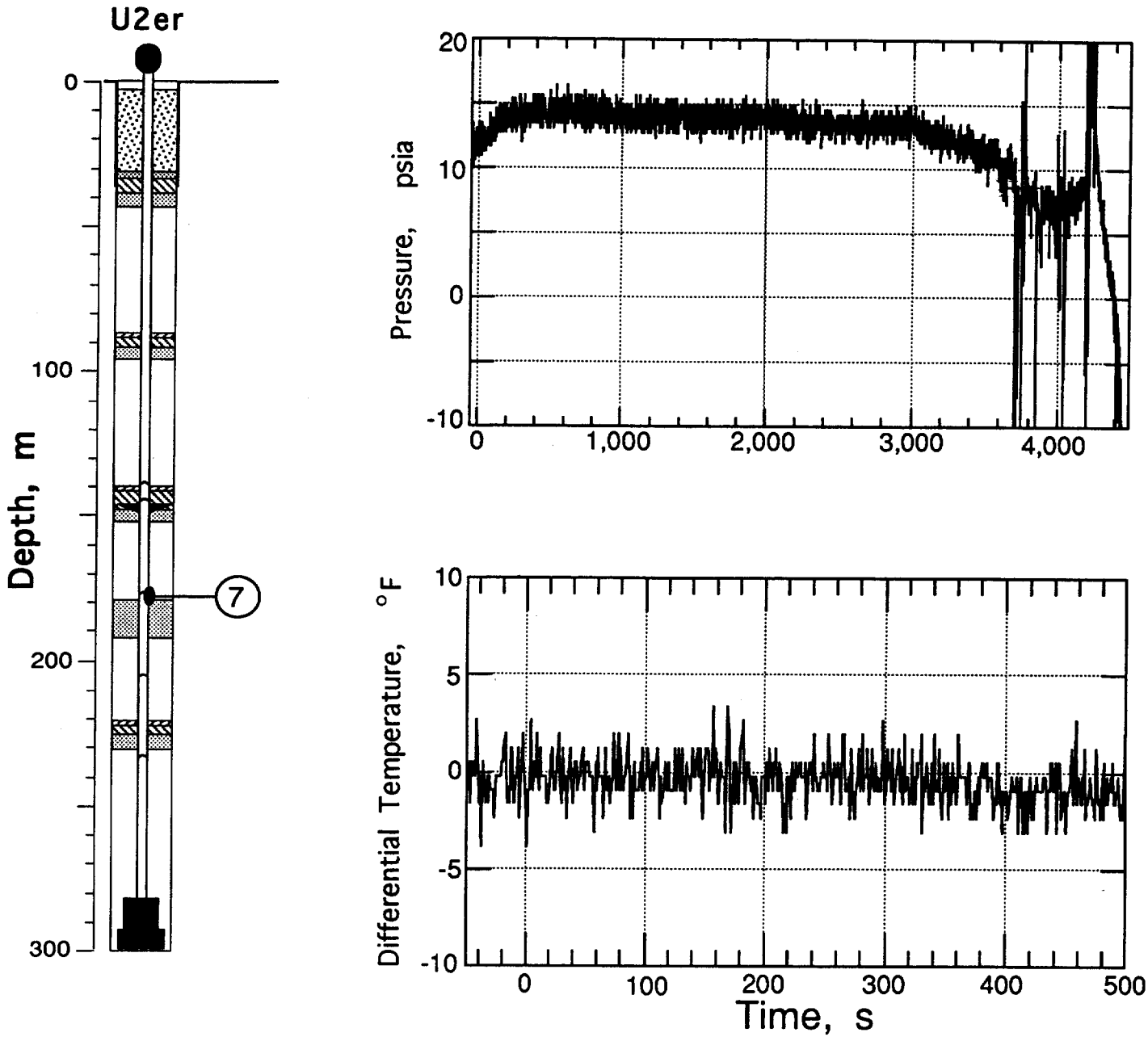

Figure 4.10 Pressure and temperature recorded in the emplacement pipe 1.6 m below the third pressure dome above the diagnostics canister (station 7 at a depth of 178.4 m).

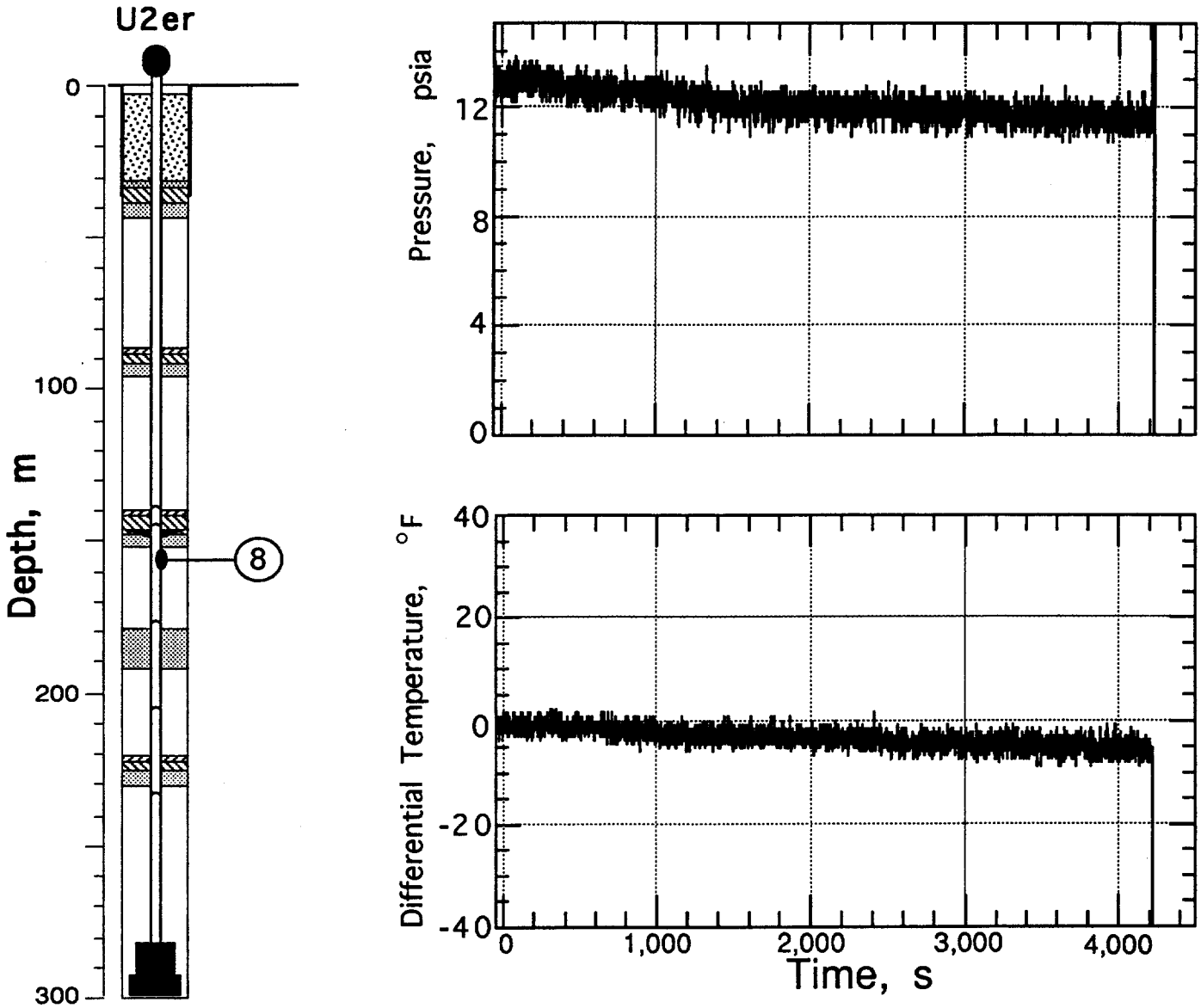

Figure 4.11 Pressure and temperature recorded in the emplacement pipe 10.9 m below the fourth pressure dome above the diagnostics canister (station 8 at a depth of 155.7 m).

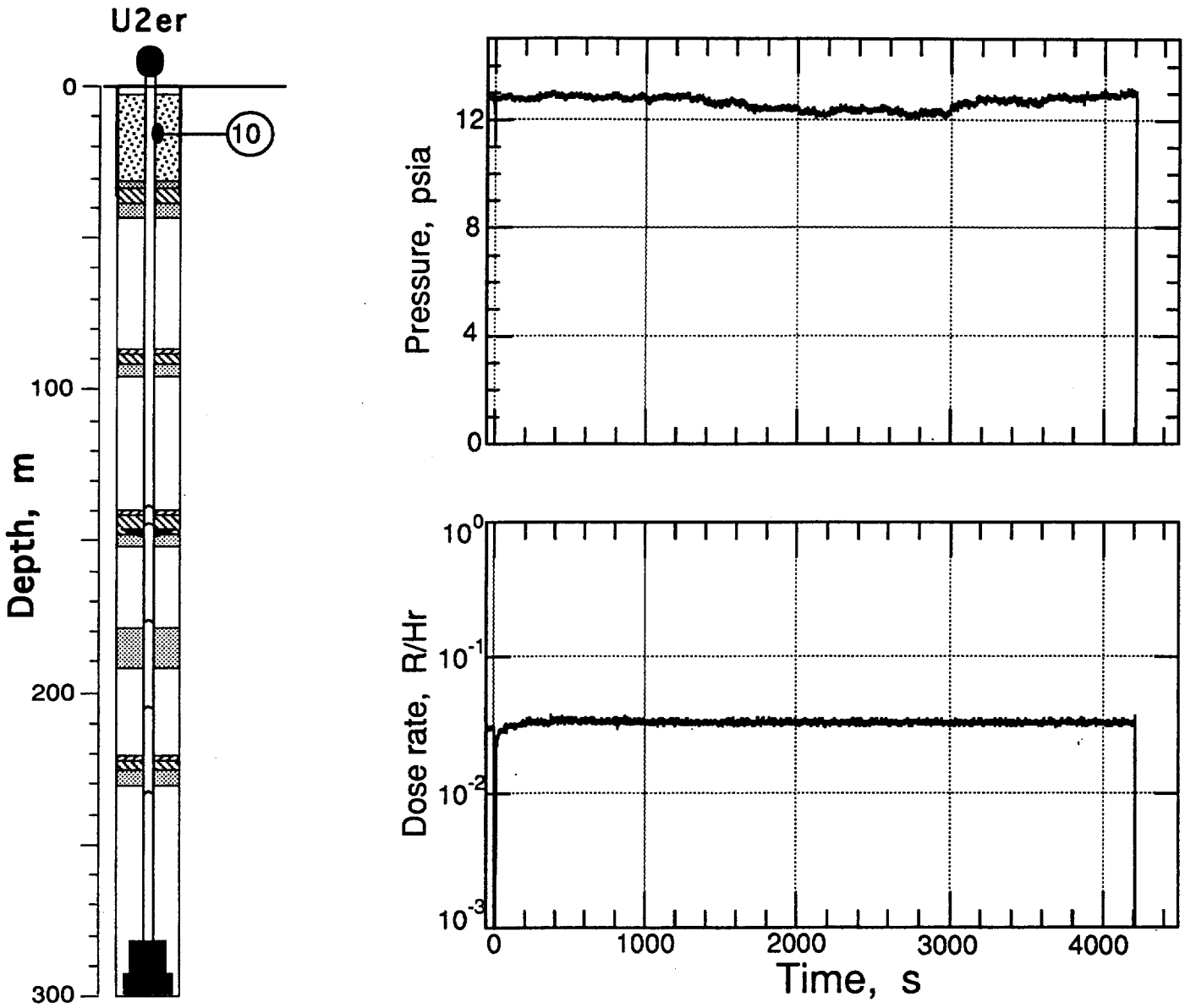

Figure 4.12 Pressure and radiation recorded in the emplacement pipe near its top (station 10 at a depth of 15.2 m).

References

1. Nancy W. Howard and Gayle Pawloski, "U2er Preliminary Site Characteristics Summary", DM 81-28, Lawrence Livermore National Laboratory, Livermore, CA, March 18, 1981.

2. George Kronsbein, "Containment Report for U2er," Holmes & Narver, NTS:A2:81-81, August 25, 1981.

3. LLNL contacts for additional information: R. A. Heinle (CORTEX and SLIFER data)

4. Lee E. Davies, "Special Measurements Final Engineering Report ISLAY, U2er", EG&G, Energy Measurements, Las Vegas, NV, SM:81E-89-31, 18 September 1981.

5. Lee E. Davies, "Special Measurements Physics/Instrumentation Package for ISLAY, U2er, Revision 'B' (final)", EG&G, Energy Measurements, Las Vegas, NV, SM:81E-89-29, 18 September 1981.

Distribution:

LLNL

TID/Brenda Staley (3)	L-658
Test Program Library	L-160
Containment Vault	L-221
Burkhard, N.	L-221
Cooper, W.	L-160
Denny, M.	L-205
Goldwire, H.	L-221
Hannon, W. J.	L-221
Heinle, R. (5)	L-221
Mara, G.	L-149
Moran, M. T.	L-777
Moss, W.	L-200
Pawloski, G.	L-221
Rambo, J.	L-200
Valk, T.	L-154

LANL

Brunish, W.	F-659
Kunkle, T.	F-665
Trent, B.	F-664

Sandia

Bergstresser, T.	MS-1159

BNL/AVO

Brown, T.	A-5
Hatch, M.	A-5
Still, G.	A-5
Stubbs, T.	A-5

BNL/NVO

Bellow, B.	N 13-20
Davies, L.	N 13-20
Moeller, A.	N 13-20
Robinson, R.	N 13-20

Defense Special Weapons Agency

Ristvet, B.

Maxwell Technologies

Peterson, E.

Eastman Cherrington Environment

Keller, C.